Characterization and Development of

potential molecular therapies for retinal photoreceptor disease

BY

AMBARISH S. PAWAR
B.E, University of Mumbai, 2003
M.S., University of Illinois at Chicago, 2007

THESIS

Submitted as partial fulfillment of the requirements
For the Doctor of Philosophy in Bioengineering
in the Graduate College of
University of Illinois at Chicago, 2011

Chicago, Illinois

Defense Committee:

David Pepperberg, Chair and Advisor
John Hetling
Richard Magin
Thomas Royston
Haohua Qian, National Eye Institute (NEI/NIH)

This thesis is dedicated to my parents and friends, without whom this would never have been accomplished.

PREFACE

This thesis presents research that I have conducted in the laboratory of Dr. David R. Pepperberg, in the UIC Department of Ophthalmology and Visual Sciences. The research program in Dr. Pepperberg's laboratory is within the areas of neural and biomolecular engineering. This program has, as its overall objective, the development of new types of molecular structures for ultimate therapeutic application in retinal degenerative diseases that involve deterioration and loss of the retina's native rod and cone photoreceptors. My thesis research has addressed two specialty areas within this lab program. In first of these, I and my colleagues have used electroretinographic and biochemical techniques to better understand the nature of photoreceptor dark adaptation in the *abcr-/-* mouse, a model system for the human retinal degenerative disease known as Stargardt disease. Part 1 of the present thesis is adapted from a published study in which I conducted all of the electrophysiology experiments, in addition to contributing to both the experimental design and the interpretation of data. Part 2 of the thesis reports my work in experiments to construct and test a novel chemical structure representing a prototype anchoring component of the retinal therapeutic structures under development. The experiments I conducted in this second area combined the approaches of fluorescence visualization, ELISA, and electrophysiology relevant to the preparation and performance analysis of the anchoring components, and to the development of a microprobe-based system for presenting test chemical structures to model cell systems.

TABLE OF CONTENTS

TABLE OF CONTENTS (continued)

LIST OF TABLES

LIST OF FIGURES

LIST OF FIGURES (continued)

PAGE

FIGURE

LIST OF ABBREVIATIONS

A2E	*N*-retinylidene-*N*-retinylethanolamine
AMD	Age-related Macular Degeneration
B-d-M-B	B-domain-maleimide-poly(ethylene glycol) 3400-biotin
DMSO	Dimethyl Sulfoxide
DTT	Dithiothreitol
ERG	Electroretinogram
FBS	Fetal Bovine Serum
FCS	Fetal Cow Serum
His6	Hexa-histidene
MR	Mammalian Ringer
N-ret-PE	N-retinylidene-phosphotidylethanolamine
Ni^{2+}	Nickel
Ni^{2+}/NTA	Nickel/ Nickel-nitrilo-triacetic acid
NNP	Nanoscale Neuromodulating platform
Norm DR	Normalized Derived Response
PBS	Phosphate-buffered-saline
PDE	Phosphodiesterase
PE	Phosphotidylethanolamine
PEG	Poly(ethylene glycol)
Qdots	Quantum Dots
RPE	Retinal Pigment Epithelium
SA	Streptavidin
scFv	Single-chain Variable Fragment
TBST	Tris-Buffered Saline Tween-20

SUMMARY

An important goal of the overall research program in Dr. Pepperberg's lab is to study photoreceptor dark adaptation in wildtype and disease mouse models. Specifically, Part I of my thesis involved the study of dark-adaptation in a mouse strain that lacks the photoreceptor protein known as ABCR protein (*abcr-/-* mouse). The ABCR protein is present along the periphery of rod discs in the rod photoreceptors of the retina (described in detail in the Background Section). The ABCR protein plays an important role in the regeneration of rhodopsin (a light sensitive molecule present in rod photoreceptors that is inactive in the dark, but is activated on exposure to light), and hence aids in dark adaptation. Impairment in the activity of the ABCR protein has been associated with Stargardt disease and other photodegenerative diseases in humans. Thus the *abcr-/-* mouse serves as an important animal model for understanding dark-adaptation in patients affected by Stargardt disease.

A paired-flash electroretinography (ERG) technique was used to compare dark-adaptation between wildtype and *abcr-/-* mice. Specifically, our focus was on the recovery of the amplitude of the ERG *a*-wave, which is the electrical response of the photoreceptors in response to light stimulation (described in detail in the Background Section). In 1999, Weng *et al.* compared the ERG *a*-wave recovery in age-matched *abcr-/-* mice and wildtype after illumination that bleached ~45% rhodopsin molecules in the mouse eye. In the study by Weng *et al*. (1999), recovery of the *a*-wave amplitude in *abcr-*/- mice was significantly slower than that of the wildtype mice, indicating a slower dark-adaptation in *abcr-/-* mice as compared to wildtype.

SUMMARY (continued)

In studies of both single rod photocurrents (by suction electrode recording) and the *in vivo* massed rod response (by ERG recording), it has been observed that photoactivation of as little as 100 rhodopsins per rod (i.e., a fractional bleach of 10^{-6}), produces a rod photocurrent response of near-saturating peak amplitude. Thus, a ~45% bleach far exceeds the bleaching range associated with the electrophysiological dynamic range of the rod photoreceptors. Based on this property of the rods, on the previous ERG data obtained with 45% bleaching, and on the established importance of ABCR protein on rod recovery after illumination, we were particularly interested to determine whether *abcr-/-* mice might exhibit a detectable delay in rod recovery at fractional bleaches well below 45%. In the current ERG study, we used paired-flash ERG recording to examine rod *a*-wave recovery among *abcr-/-* and wildtype mice at bleaching extents that extended to relatively young animals (6-12 weeks).

1. BACKGROUND AND AIMS

The human eye contains two primary classes of photoreceptors, known as rods and cones (Fig. 1A). The rods are responsible for low-light vision and cones are responsible for bright-light vision. There are ~120 million rods and ~6-7 million cones in the human retina. Thus, the number of rods in the human retina outnumber the number of cones by a factor of 20 (Kandel *et al.*, 2000).

The outer segments of rod photoreceptors consist of a number of discs stacked up on top of each other as illustrated in Fig. 1B. Each outer segment disc contains a light sensitive molecule called rhodopsin. There are approximately 1000 discs per rod outer segment, and 10^5 rhodopsin molecules per rod disc. In general, each mammalian rod contains approximately 10^8 rhodopsin molecules.

1.1 Phototransduction

Rhodopsin has two components; opsin, which is the protein moiety, and the chromophore 11-*cis*-retinal. The process of phototransduction starts with the absorption of photons by rhodopsin (Hargrave, 1995; Hargrave and Hamm, 1994; Palczewski and Saari, 1997; Rao and Oprian, 1996). The absorption of light by rhodopsin known as photoisomerization, converts the 11-*cis*-retinal to all-*trans* retinal. Photoisomerization alters the conformation of the protein that binds the chromophore leading to the formation of intermediates and eventually metarhodopsin II, the physically active form of rhodopsin that triggers the phototransduction cascade.

Fig. 1: Organization of the retina and structure of rod outer segments and rhodopsin.

(**A**) Diagram showing the organization of the retina with the different cell-types, including the rods and cones, as labeled. (**B**) View of the rod outer segment, which consists of a number of rod-disc stacked up against each other. Mouse rod outer segments have a diameter ~1-1.5 μm and length ~25 μm. Right: Rhodopsin is an intrinsic disc membrane protein, which spans the disc membrane of the rod outer segment. Each outer segment disc contains 10^5 of rhodopsin molecules. Rhodopsin has two main components; opsin, which is the protein moiety and 11-cis-retinal (shown inset), which is the chromophore. *http://webvision.med.utah.edu/*

A

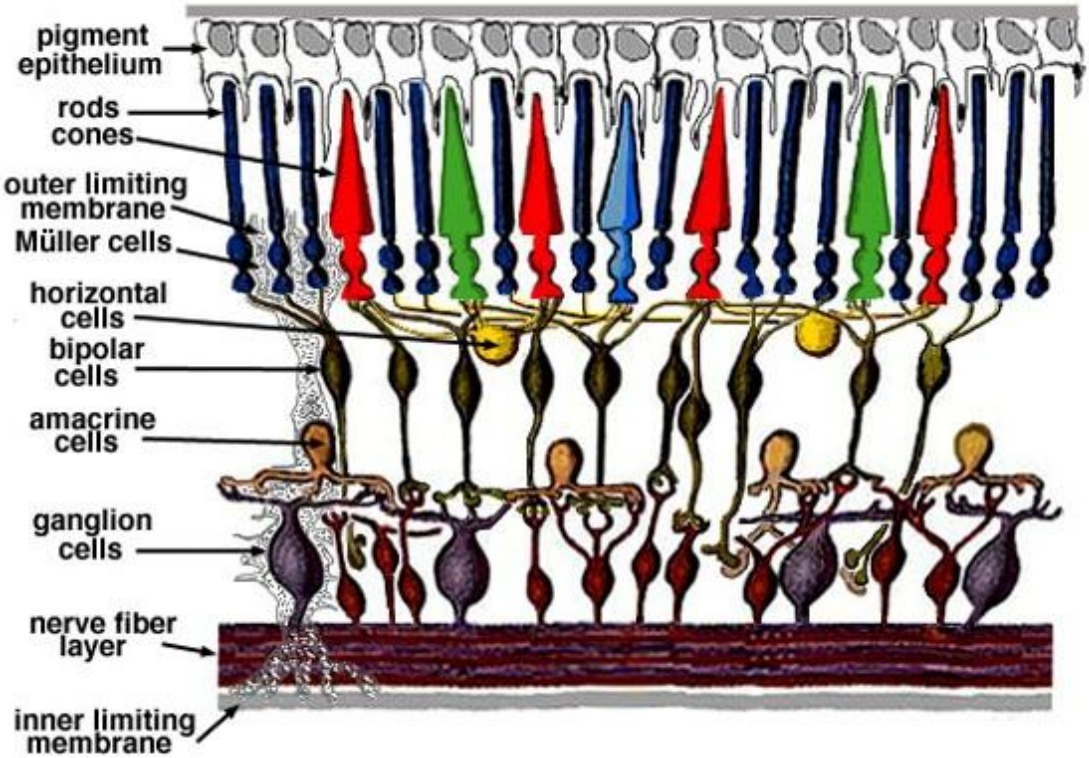
pigment epithelium
rods
cones
outer limiting membrane
Müller cells
horizontal cells
bipolar cells
amacrine cells
ganglion cells
nerve fiber layer
inner limiting membrane

B

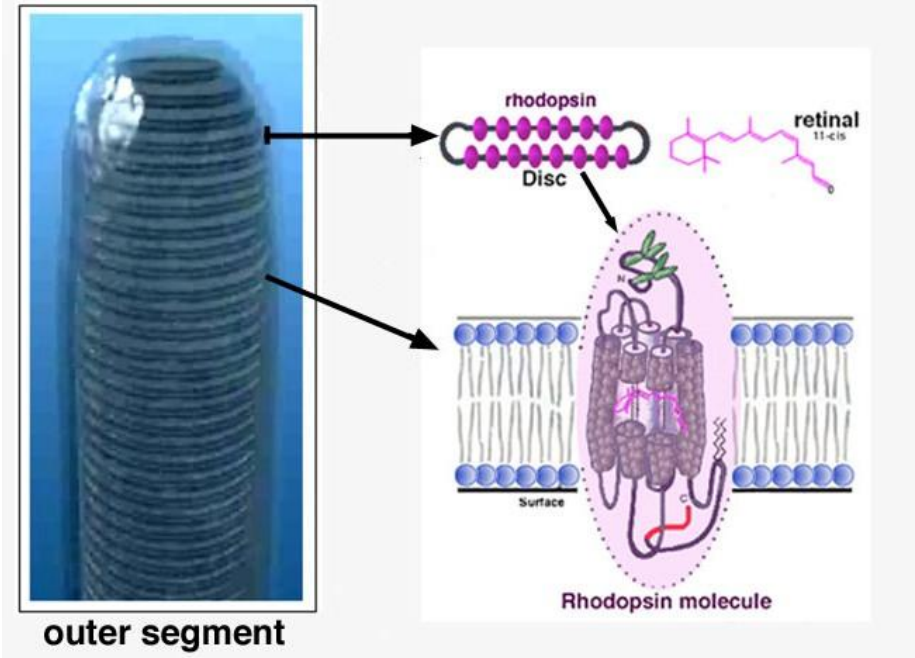
rhodopsin
retinal
Disc
Surface
Rhodopsin molecule
outer segment

Formation of metarhodopsin II causes transducin to bind to it. Transducin binds GTP, which in turn activates a membrane-bound cyclic nucleotide cGMP phosphodiesterase (PDE) by pulling away the inhibitory subunit of phosphodiesterase (Burns and Baylor, 2000). This leads to hydrolysis of cGMP. The plasma membrane of the rod outer segments contain Na^+ channels that are maintained in the open state (in darkness) due to the binding cGMP. Hydrolysis of cGMP (in the presence of light) thus leads to closure of cGMP gated Na^+ channels as a result of which, influx of Na^+ and other cations (Ca^{2+}, which accounts for one seventh of the current that flows through these channels) into the rod outer segment decreases, causing hyperpolarization of rods. Hyperpolarization of rods in turn modulates the rate of release of the neurotransmitter L-glutamate at the synaptic terminals where rods connect to the rod horizontal and bipolar cells of the retina. Release of L-glutamate at the synaptic terminals is regulated by the intracellular concentration of Ca^{2+}. In darkness, where the intracellular potential as well as the intracellular concentration of Ca^{2+} in the rods is highest, release of L-glutamate is the highest. Increasing the amount of light falling on the retina leads to closure of the cGMP-gated channels and thus downregulation of the intracellular concentration of Ca^{2+} and downregulation of the amount of L-glutamate released (Pugh and Lamb, 1993; Yau, 1994). Ca^{2+} is known to inhibit guanylyl cyclase, the enzyme that synthesizes cGMP from GTP. Thus, in the dark, when the Ca^{2+} level is relatively high, guanylyl cyclase is in a partially inhibited state. Under light-adapted conditions, when there is a reduction in the intracellular concentration of Ca^{2+} in rods due to the closure of cGMP-gated channels, the inhibitory effect of Ca^{2+} on guanylyl cyclase is relieved. Thus more cGMP is synthesized and the concentration of cGMP in the rod outer segment increases, leading to the opening of the cGMP gated channels and thus depolarization of the rods (Kandel *et al*., 2000).

Photoreceptor recovery has two very important aspects to it. They are the recovery of membrane current (i.e., the reopening of the cGMP gated Na^+ channels and return of the rod photocurrent to from its hyperpolarized state to baseline or dark-current level) and recovery of the rod sensitivity to further light stimulation (i.e., recovery of rhodopsin to its pre-illumination level such that it becomes sensitive to light again). The recovery of the membrane current response requires the deactivation of intermediates i.e. metarhodopsin II, transducin, phosphodiesterase and the replenishment of cGMP which binds to cGMP-gated plasma membrane channels, and opens the channels.

The shut-down (i.e., deactivation) of the phototransduction cascade starts with the inactivation of metarhodopsin II. Two processes contribute to this. One of them is the phosphorylation of rhodopsin (Kuhn and Dreyer, 1972; Bownds *et al.*, 1972). This increases the binding affinity of arrestin, which is a cytosolic protein, to the phosphorylated rhodopsin. When phosphorylated rhodopsin binds arrestin, transducin is deactivated and can no longer interact with photo-activated rhodopsin (Wilden *et al.*, 1986; Palczewski *et al.*, 1991; Palczewski *et al.*, 1992). Deactivation of transducin leads to inactivation of phosphodiesterase by allowing the release, by transducin, of the two inhibitory γ subunits of phosphodiesterase. Thus, phosphodiesterase is deactivated through re-inhibition by its inhibitory subunits, leading to inactivation of the phototransduction cascade. (Krupnick *et al.*, 1997; Kuhn *et al.*, 1984; Pulvermuller *et al.*, 1997).

1.2 Retinoid Visual Cycle

There are two aspects to the recovery of rhodopsin; recovery of photocurrent through the shutdown of the phototransduction cascade, and regeneration of rhodopsin

to its original light-sensitive state. The amount of rod desensitization produced by rhodopsin bleaching correlates quantitatively with the extent of bleaching. However, the extent of desensitization induced by a given amount of bleach is very large compared to the amount expected merely from the bleached induced reduction in quantum capture by the rods. After bleaching, a reduced rod photocurrent response still persists, but the sensitivity of the rod, i.e. the amount of photoreceptor response produced by a stimulus flash, is much reduced from the sensitivity of the fully dark adapted rod. Rhodopsin can become light sensitive when a fresh molecule of 11-*cis* retinal is provided to opsin and binds at the opsin's chromophore binding site, thereby regenerating the rhodopsin. This provision of 11-*cis* retinal to opsin requires, in turn, the conversion of all-*trans* retinal (rhodopsin bleaching product) to 11-*cis*-retinal. This is achieved through the 'retinoid visual cycle' (McBee *et al.*, 2001; Saari *et al.*, 2000). The all-*trans* retinal has to be released from the opsin before it can be reduced. During the formation of metarhodopsin II all-*trans* retinal is still attached to the opsin. It is here that the chromophore gets eventually dissociated from the opsin and moves into the disc lumen. In the disc lumen, the all-*trans*-retinal combines with PE to form N-ret-PE. After the N-ret-PE moves out of the disc lumen into the rod cytosol, it is converted to all-*trans*-retinol, by an enzyme called all-*trans* retinol dehydrogenase, within the rod outer segments. The chromophore then moves to the retinal pigment epithelium (RPE). The retinal pigment epithelium is a pigmented layer that lines the back of the eye, behind the retina. In the RPE, the all-*trans*-retinol is enzymatically converted to 11-*cis*-retinal, and is transported back to the photoreceptor where recombination with opsin takes place.

1.3 Electroretinography

The electroretinogram (ERG) is a light-induced, multi-component electrical signal recorded from an electrode placed on the corneal surface (Fig. 2A). The ERG is the massed response of different cell types in the retina to a flash of light (Granit, 1933). Two principal components of the ERG are the *a*-wave, which is a flash-induced massed (cumulative) rod photoreceptor current response, i.e., reduction of rod circulating current of the rod photoreceptors in response to light stimulus (Brown and Wiesel (1961), Penn and Hagins (1969, 1972), and the b-wave, which is the response of the ON-bipolar cells (Furakawa and Hanawa, 1955; Sillman *et al.*, 1969a; Noell, 1954; Brown and Watanabe, 1962; Nilsson, 1971; Robson and Frishman, 1998). Other components of the ERG include the *c*-wave (response of the RPE) (Noell, 1954), *d*-wave (response of the off-bipolar cells) and the oscillatory potentials or OPs (response of amacrine cells). In our present study, we were interested in the *a*-wave.

Fig. 2: ERG a-wave and paired-flash ERG

(**A**) Typical ERG showing the a-wave, which is the response of the photoreceptors, and b-wave, which is a response of the ON-bipolar cells. (**B**) A pictorial depiction of the paired-flash technique. Inset shows a typical ERG, with an a-wave, b-wave and oscillatory potentials (OP) as labeled. Intrusion by the b-wave masks the ability of the a-wave to serve as a monitor of the rod photoreceptor current. The paired-flash technique consists of a weak test-flash followed by a bright probe-flash. The graph illustrates the status of rod photoreceptor current amplitude 'A' on the y-axis *vs.* time interval between the test and probe-flash (*t*) on the x-axis. A weak test flash closes some of the cGMP channels, which is indicated by the decrease in the rod photocurrent amplitude. A saturating probe flash certain time interval after the test-flash closes the rest of the cGMP channels and thus titrates the rod photoreceptor current. Details of the paired-flash technique as used in this study have been described in Sec. 4.2

A

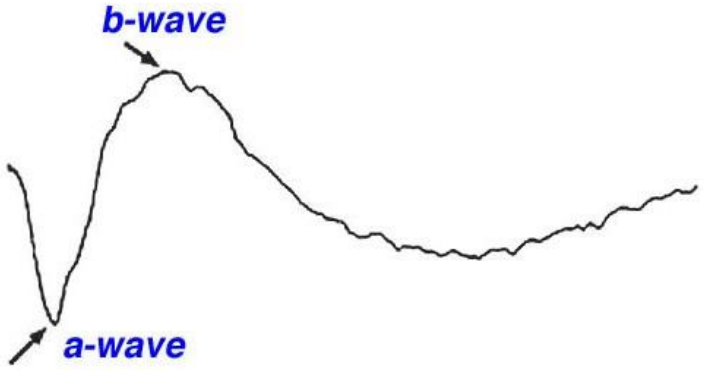
b-wave
a-wave

B

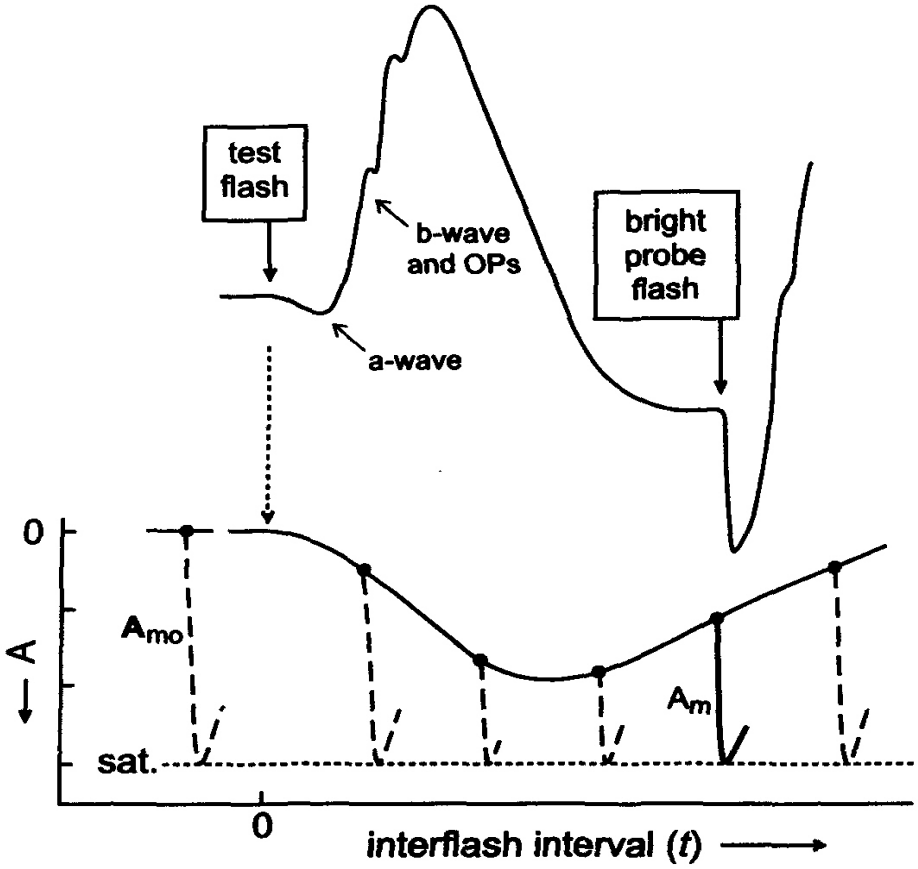
test flash
b-wave and OPs
bright probe flash
a-wave
0
A
A_{mo}
A_m
sat.
0
interflash interval (t)

1.4 *a*-wave and paired-flash ERG

The activation phase of the rod photoreceptors is represented by the ERG *a*-wave (Hood and Birch, 1990; Breton *et al.*, 1994). Previous studies have shown that the time course of the negative-peak *a*-wave is in the range of several hundreds of milliseconds with weak flashes and increases with flash strengths. However, intrusion by the positive-peak *b*-wave and other components of the ERG masks the ability of the *a*-wave to serve as a monitor of the photoreceptor activity. Thus, in the absence of the b-wave, it would have been possible to get information about the photoreceptors from the *a*-wave itself. To overcome this drawback, the paired-flash technique has been used. Instead of using a single flash, in the paired-flash technique, two flashes (a weak test flash followed by a bright saturating probe flash) are used (Birch *et al.* 1995; Lyubarsky & Pugh, 1996; Goto *et al.* 1996; Pepperberg *et al.* 1996, 1997; Robson and Frishman, 1999, Hetling and Pepperberg, 1999, Friedburg *et al.*, 2001)

Thus, the paired-flash technique has a distinct advantage over a single flash. In the paired-flash method, a weak test flash closes some of the cGMP-gated ion channels. A bright probe flash following a defined time interval after the test flash drives the photoreceptor current to saturation, thus closing the remaining open channels, thus titrating the photoreceptor current. The amplitude of the *a*-wave in a paired flash trial is then subtracted from the amplitude of the *a*-wave in a saturating probe flash alone trial (Fig 2B). The resulting value (derived response) represents an approximate value of the real photocurrent response produced by the test-flash.

1.5 ABCR and wildtype

The protein known as ABCA4 (also as ABCR) is a member of the ATP binding cassette subfamily of active transporter proteins present on the rim of the rod and cone outer segment disc membranes. An important step in the retinoid visual cycle is the movement of the all-*trans* retinal from the disc lumen to the rod cytosol and its subsequent conversion to all-*trans*-retinol. The ABCR protein is known to play an important role in this cycle (Mata *et al.*, 2000; Molday *et al.*, 2000; Sun and Nathans, 2001; Ahn J, 2003). In an ATP dependent, energy requiring process, the ABCR protein facilitates the movement of a complex formed between all-*trans* retinal and phosphatidylethanolamine (PE) across the disc membrane to the rod cytosol. The all-*trans* retinal is then enzymatically reduced to all-*trans* retinol in the cytosol of the rod, and the all-*trans* retinol is then transported to the retinal pigment epithelium (RPE) by other mechanisms. The transport of all-*trans* retinal to the RPE is an important step in the rhodopsin cycle which promotes the shut-off of the phototransduction cascade. In the absence of the ABCR protein, there is a build-up of all-*trans* retinal and the chemical product that it forms with phosphatidylethanolamine. In the RPE, this product is metabolized to *N*-retinylidene-*N*-retinylethanolamine (A2E), which is a prominent component of lipofuscin (Eldred and Lasky, 1993; Sakai *et al.*, 1996). Also, in some cases, the all-*trans* retinal can recombine with the opsin in the rod disc membrane to form a product called pseudometarhodopsin II that exhibits small but non-zero activity in excitation of the phototransduction cascade (Hofmann *et al.*, 1992; Jager *et al.*, 1996; Sachs *et al.*, 2000). Accumulation of these products can lead to the prolongation of the phototransduction cascade and tissue damage.

1.6 Rationale and Aims

Photoreceptor dark adaptation in the *abcr-/-* mouse, which lacks ABCR protein, was investigated in a 1999 study by Weng *et al.* The Weng *et al.* (1999) study employed rhodopsin bleaching illumination that photolyzed ~45% of the total rhodopsin. Animals used in the Weng *et al.* (1999) study were in the age-range of 8 weeks to 1 year, but the exact ages of the mice used were not specified. However, a number of issues relevant to photoreceptor recovery in the *abcr-/-* have not been investigated fully. One key question was whether smaller extents of rhodopsin bleaching differentially affects rod recovery in the *abcr-/- vs*. wildtype mice. Thus, the aims of our study were to use the paired-flash ERG technique to compare the *a*-wave responses in *abcr-/-* and two wildtype strains (control strains; discussed in the Methods section) at

Aim 1.1: Fractional bleaching illumination of 10^{-6}, i.e., illumination that bleaches ~10^{2} rhodopsin molecules per rod. This bleaching illumination is within the physiological range of the rod photoreceptor response.

Aim 1.2: Fractional bleach of 3×10^{-5},

Aim 1.3: Illumination that bleaches 3% of the rhodopsin molecules. This bleach, along with Aim 1.2, served as intermediate bleach extents.

Aim 1.4: Illumination that bleaches 30-40% of the rhodopsin, an extent roughly comparable to that used in the Weng *et al.* (1999) study.

In all the above aims, we focused our attention on using relatively younger animals (6 weeks – 2 months), where tissue degeneration in the *abcr-/-* mouse is expected to be less significant.

2. MATERIALS AND METHODS

All animal procedures carried out in this thesis research project were in accordance with the principles embodied in the Statement for the Use of Animals in Ophthalmic and Vision Research established by the Association for Research in Vision and Ophthalmology. Three types of mice were used in these experiments. Breeding pairs of the gene knockout ABCR mice were kindly provided by Dr. Gabriel H. Travis at the University of California at Los Angeles. Two wildtype mice strains *(abcr+/+*) were used as controls. The first wildtype mouse strain was a C57-derived strain that was kindly provided to us by Michael Danciger (Loyola Marymount University, 5 breeding pairs). Similar to the *abcr-/-*, these C57BL/6J mice possess the leucine (leu) variant at amino acid position 450 of the RPE protein RPE65. RPE65 is a protein present in the RPE that promotes the conversion of all-trans retinyl ester to 11-cis retinol and thus plays an important role in the regeneration of 11-cis retinal through the retinoid visual cycle (Moiseyev *et al*., 2005, Redmond *et al*., 2005). These mice will be henceforth termed as C57-leu450. The second wildtype strain was the C57BL/6J mice obtained from Jackson Laboratories (Bar Harbor, ME, USA) (both sexes, 5-16 weeks of age). Unlike the *abcr-/-*, these mice possess the methionine (met) variant at amino acid 450 of the RPE protein RPE65. Previous studies have shown that the leu450 variants of the RPE65 mice (like the *abcr-/-* mice) show greater catalytic activity as compared to the met450 variants, resulting in quicker dark-adaptation (Wenzel *et al*., 2001, Kim *et al*, 2004, Lyubarsky *et al.*, 2005). In light of the evidence that the conversion of all-trans retinyl esters to 11-cis retinol by RPE65 is a critical step in the retinoid visual cycle (Moiseyev *et al*., 2005, Redmond *et al*., 2005) and that rhodopsin regeneration is critical for full dark adaptation of the rods (Pepperberg *et al*., 1978, Cornwall and Fain, 1994),

the comparison of rod recovery in the *abcr-/-* mice with that in control animals possessing both the leu450 and met450 variants of RPE65 was important in the present study and will be henceforth termed as C57-met450.

Procedures used for animal maintenance and (see below) for ERG recording were generally similar to those employed in previous mouse ERG studies conducted in our laboratory (Hetling and Pepperberg, 1999; Silva *et al*., 2001, Kang Derwent *et al*., 2004). All mice were maintained on a light-dark cycle (12h light: 12h dark; ambient illumination of ~2-19 lux). Mice were dark adapted 12 hours prior to the beginning of an experiment. After ~12 hours of dark adaptation, all procedures were carried out under dim red light. The mouse was first anesthetized by intraperitoneal injection of saline solution of ketamine and xylazine (0.15 and 0.01 mg (g body wt)$^{-1}$, respectively). Regular boosts of the same composition of anesthetics (same composition, but typically 1/5 to 1/6 of the initial volume) were subsequently delivered subcutaneously beginning at approximately 40 minutes after the initial dose. The intervals between the boosts were about 18-20 minutes. The pupil was dilated by applying single drops each of 2.5% phenylephrine HCl and 1% tropicamide. The cornea was anesthetized by application of 0.5% proparacaine HCl. The mouse was then placed on its right side on a brass plate. A pad of foam rubber was used for stabilization and spacing of the mouse head position to ensure that the visual axis of the left eye was approximately vertical. The brass plate was in contact with a thermoelectric module which maintained the plate at a temperature of ~ 42-44 °C. This plate temperature maintained the mouse body temperature at ~37.5 - 38.5 °C, as measured by a rectal probe. Lubrication of the corneal surface was achieved by regular addition of an ophthalmic methylcellulose solution at ~ 20 minute intervals. After the conclusion of the experiment, the mouse was allowed to recover from the

anesthesia and was monitored throughout the recovery period. After the recovery the mouse was returned to the university animal care facility. In all experiments, a given mouse was used in a single experiment.

2.1 Instrumentation

Typically, 3 flash sources were used in the experiments. Conditioning and probe flashes were provided by one flash unit (Model 2105-C flash head and 1000VR power pack; Novatron, Inc., Dallas, TX, USA). Half-height duration of the flashes was approximately 1.7 ms. The recharge period of the Novatron flash unit was 2.0 s. Light from the probe flash unit passed through an infrared attenuating filter. Test flashes of half height duration of about 20 µs were generated by a flash unit (Model MVS2020; EG&G Electro-Optics, Salem, MA, USA) modified with a 72 µF, 600 V external capacitor bank. The recharge period for the EG&G flash gun was 0.05 s. Light from this test flash unit passed through neutral density filters and a Wratten 58 filter (peak transmittance near 520 nm, Eastman Kodak Co.). The light from the two flash units was delivered through two fiber optic guides (12 mm diameter), to the inner surface of a hemispheric dome (15 cm). The inner surface of the hemispheric dome was coated with a Kodak White Reflectance Coating. Light was spread over this coating with the help of a convex lens affixed to the exit of each light guide. The mouse was placed with the visual axis of the left eye aligned approximately axially with the dome, in a plane about 2.5 cm below the dome's equatorial plane. The eye received diffuse, essentially full field illumination from the luminous surface. An integrating photometer was used to measure the strengths of the test and probe flashes (Model 1700, equipped with an SED033 silicon photodiode detector, radiance barrel and ZCIE scotopic filter; International Light, Inc., Newburyport, MA, USA). All measurements are reported in units of time-integrated

luminance, scotopic candela s m^{-2} (sc cd-s m^{-2}) of the dome inner surface. Electroretinogram (ERG) signals were recorded using a stainless steel wire electrode placed in gentle contact with the corneal surface. The tip of the wire (0.28 mm) was bent into a hook shape of ~2 mm in diameter. The curved apex was approximately centered on the cornea. The plane defined by the hook and shank was approximately 30 degrees to the equatorial plane. The shank was held stationary by an adjustable x-y-z manipulator. The reference electrode was a stainless steel wire of the same diameter; placed in the mouth of the mouse. A platinum subdermal needle electrode (Model F-E2; AstroMedÏGrass, Inc., West Warwick, RI, USA) used as a ground electrode, this electrode inserted under the skin in the nape of the neck. The recording, reference and the ground electrode were connected to the respective input terminals of a differential AC amplifier (Model 511; AstroMed/Grass). The signal was amplified 1000-fold (bandpass (−6 dB) at 0.1—3000 Hz). Data acquisition and storage employed a Pentium computer equipped with a 3001 A/D board and DT VEE software package (Data Translation, Inc., Marlboro, MA, USA). All data were sampled at 100 kHz and mapped to a voltage range of ±10 V with 12-bit resolution.

2.2 Protocols

In this project ERG experiments were performed on 18 *abcr-/-*, 17 C57-leu450, and 20 C57-met450 mice, the age ranges of which were 23 to 116, 23 to 95, and 23 to 86 days, respectively. Dark-adapted responses consisted of a series of single- and paired-flash measurements that were conducted at the beginning of the experiment. A-wave responses to a bright probe flash of fixed strength (773 scotopic candela seconds per square meter [sc cd-s m^{-2}]) were recorded in single flash trials, to determine the peak

amplitude (A_{peak}) and time-to-peak (t_{peak}) of the responses. The derived rod response to a weak test flash (0.3 sc cd-s m^{-2}) at a fixed post-test-flash time (t = 86 ms) was determined in paired-flash trials, by using a test-probe interval (t_{probe}) of 80 ms, a probe flash of 773 sc cd-s m^{-2}, and a determination time (t_{det}) of 6 ms. (Hetling and Pepperberg, 1999). There was a dark-adaptation period of ≥ 2 minutes between consecutive experimental runs. The normalized amplitude, at t = 86 ms, of the dark-adapted derived response to the weak test flash was obtained from the relation (Hetling and Pepperberg, 1999).

$$\text{Normalized response} = A(t)/A_{moD} = 1 - [A_m(t)/A_{moD}] \qquad (1a)$$

$$t = t_{probe} + t_{det}, \qquad (1b)$$

where $A(t)$ is the derived response amplitude, A_{moD} is the amplitude (at 6 ms) of the response to the probe flash in a probe-alone trial under dark-adapted conditions, and $A_m(t)$ is the amplitude of the probe response in the paired-flash trial.

After completion of the dark-adapted characterization, a bleaching stimulus was delivered, and the time course of recovery of the derived response $A(t)$ to this bleaching light was investigated through analysis of the response to the 773 sc cd-s m^{-2} probe flash. The present study employed four different bleaching stimuli:

(1) The weak test flash (0.3 sc cd-s m^{-2}) used in the dark-adapted characterization (Aim 1.1);

(2) A single bright flash of strength sufficient to produce rod saturation (7.9 sc cd-s m^{-2}) (Aim 1.2) (Hetling and Pepperberg, 1999);

(3) A series of 20 flashes (each of 477 sc cd-s m^{-2}) delivered over a period of approximately 100 seconds [cumulative bleaching energy: (20)*(477 sc cd-s m^{-2}) = 9.5 x 10^3 sc cd-s m^{-2}] (Aim 1.3); and

(4) A 2-minute exposure to intense full-field green light from a microscope illuminator positioned above the eye under investigation (Aim 1.4) (Qtaishat *et al.*, 1999).

The recording electrode was withdrawn during the 2-minute illumination period. In experiments of types 1 and 2, the bleaching light was presented in each experimental run (Hetling and Pepperberg, 1999), and the experiment typically involved two determinations at a given t_{probe}. Some experiments involved the investigation of recovery from both the subsaturating (type 1) and saturating (type 2) bleaching flashes. Unless otherwise indicated, values of A(t) determined after the bleaching illumination were normalized to the dark-adapted probe-alone amplitude A_{moD} determined early in the experiment. For recoveries from the 20-flash and 2-minute bleaching stimuli, the 6-ms determination time t_{det} was negligible and was ignored. The conclusion of the bleaching illumination defined time 0 in each experiment or (in type 1 and type 2 experiments) each experimental run. For the 20-flash and 2-minute bleaching illuminations, the bleaching light was presented only once in the experiment, and the recovery time course was determined by presentations of the probe flash alone at various times. In all four types of experiment, probe responses obtained after the bleaching illumination were analyzed to yield $A_m(t)$, and the derived response A(t) was obtained through equation 1. In experiments of types 3 and 4, both the post-bleach times of measurement and the overall post-bleach period of investigation differed somewhat among experiments. To permit ANOVA of individual sets of recovery data in the type 3 experiments, consecutive values of the determined, normalized derived response. $A(t)/A_{moD}$ were linearly interpolated to yield minute-by-minute values of $A(t)/ A_{moD}$. For sets of recovery data in the type 4 experiments, determined values of $A(t)/ A_{moD}$ were grouped within 3-minute bins to permit ANOVA (see the Results section).

2.3 Bleaching extents

For low extents of rhodopsin bleaching (i.e., those relevant to the present experiments of types 1–3), the fractional bleach B produced by a bleaching stimulus of strength L (in sc cd-s m^{-2}) is approximately given by $B = aL/R_o$, where Ro is the population of rhodopsin molecules in the dark-adapted (i.e., unbleached) rod, and *a* is the number of photoisomerizations (R*) produced by a flash of unit strength. Previous estimates of *a* (based on different experimental approaches) have ranged from 100 R* (sc cd-s $m^{-2})^{-1}$ (Hetling and Pepperberg, 1999) to 490–580 R* (sc cd-s $m^{-2})^{-1}$ (Lyubarsky *et al.*, 2004). If one assumes that Ro = 7 x 10^7 (Lyubarsky *et al.*, 2004) and *a* = 250 R*, the fractional bleaches corresponding with the bleaching illuminations in the present type 1 to 3 experiments (0.3, 7.9, and 9.5 x 10^3 sc cd-s m^{-2}, respectively) are ~10^{-6}, ~3 x 10^{-5}, and ~0.03, respectively. Procedures used to determine the extent of rhodopsin bleaching by the 2-minute illumination (type 4 experiment) followed those described (Kang Derwent *et al.*, 2007 and Qtaishat *et al.*, 1999). The anesthetized mouse was killed by cervical dislocation immediately after the bleach, and the retinas and RPEs were isolated. The retina and RPE of a given eye were extracted by using formaldehyde (for analysis of retinaldehydes) and isopropanol/hexane (for analysis of all-*trans* retinol and retinyl ester) extraction procedures. The extracts were analyzed for molar amounts of 11-*cis* retinal, all-*trans* retinal, all-*trans* retinol, and retinyl ester by using normal-phase high-performance liquid chromatography and standard curves. The difference in molar percents of 11-*cis* retinal measured for the illuminated versus unilluminated eyes was used to determine the percentage of rhodopsin bleached (Kang Derwent *et al.*, 2007 and Qtaishat *et al.*, 1999). The data yielded bleaching extents of 40% ± 11% in the *abcr*-/- mice (*n* = 3; ages of 73, 78, and 78 days); 32% ± 8% in the C57-leu450 mice (*n* = 4; ages of 73, 73, 69, and 69 days); and 31% ± 5% in the C57-met450 mice (*n* = 3; ages of

63, 58, and 63 days). Based on their average values, the following text quotes the extent of bleaching as ~30% to ~40%.

3. RESULTS

3.1 Dark-adapted responses

The waveforms shown in Fig. 3 are the dark-adapted responses in the *abcr-/-*, C57-leu450 and C57-met450 respectively. The characterization of the dark-adapted responses were performed at the beginning of the experiment (See Methods). The larger waveforms labeled PA are the probe-alone response to a bright probe flash (773 sc cd-s m^{-2}), whereas the waveforms labeled 80 are the responses to a test-probe flash with an inter-flash interval of t_{probe}= 80 ms. The PA responses were analyzed for the peak amplitude (A_{peak}) and time-to-peak (t_{peak}). The values for A_{peak} and t_{peak} and the other investigated parameters have been summarized Table 1. Table 1A–C shows, for each of the three investigated strains, the number of experiments and ages of the mice for which determinations of A_{peak} (column 1) and t_{peak} (column 2) were made. Columns 1 and 2 in Table 1D–F show data (means ± SD) obtained for A_{peak} and t_{peak}, respectively, in the *abcr-/-*, C57-leu450, and C57-met450 mice. Peak amplitude of the probe-alone response ranged, on average, from 315 to 369 µV. Between-groups ANOVA showed a significant difference among the three investigated strains for A_{peak} ($F_{2,52}$ = 3.183; P = 0.050); in addition, values of t_{peak} among the strains differed significantly ($F_{2,52}$ = 6.974; P = 0.002. Post-hoc comparisons of A_{peak} and t_{peak} in the *abcr-/-* and C57-leu450 mice indicated a significant difference only for t_{peak} (P = 0.001). In the *abcr-/-* versus C57-met450 mice, there were significant differences in both A_{peak} and t_{peak} (P = 0.015 and P = 0.008, respectively). Between the C57-leu450 and C57-met450 mice, A_{peak} and t_{peak} did not differ significantly. Average values of t_{peak} ranged from 7.10 to 7.64 ms among strains. The response to the test-probe flash at t_{probe}= 80 ms were also analyzed and is presented in Table 1D-F (column 3).

Fig 3: Dark-adapted characterization.
Dark-adapted responses recorded from *abcr-/-* **(A)** C57-leu450 (**B**), and C57-met450 (**C**) mice in single-flash and paired-flash trials. Each illustrated waveform is a single response. Traces labeled PA: responses to the 773 sc cd-s • m^{-2} probe flash presented alone. The A_{peak} and t_{peak} of the probe response were determined as shown in (**A**). Traces labeled 80: probe responses recorded in paired-flash trials with an 80-ms test probe interval.

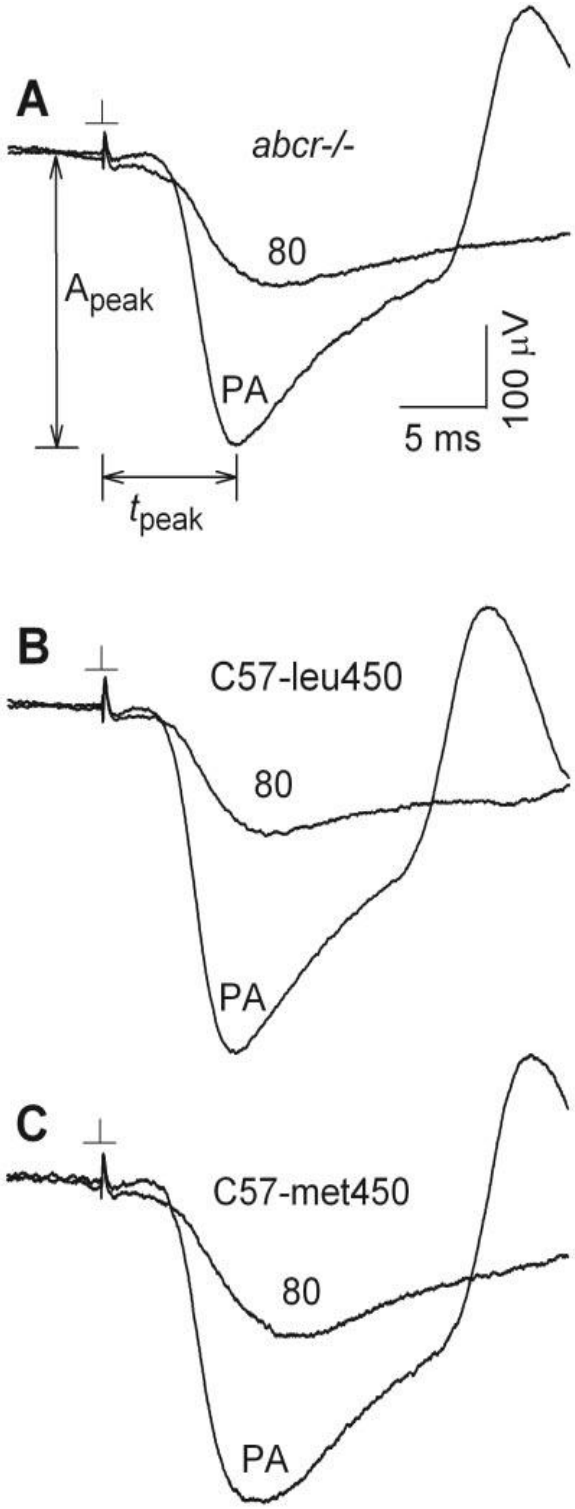
A
abcr-/-
80
Apeak
PA
100 µV
5 ms
tpeak
B
C57-leu450
80
PA
C
C57-met450
80
PA

Table 1: Details of ages of mice, dark-adapted responses and curve-fitting parameters

* A_{peak} and t_{peak}: peak amplitude and time to peak, respectively, of the dark-adapted response to the 773-sc sc cd-s • m^{-2} probe flash; Norm DR: normalized derived response to a 0.3- sc cd-s • m^{-2} test flash at t = 86 ms. Determinations of A_{peak} and t_{peak} within a given experiment are based on data obtained in three presentations of the probe flash. Determinations of Norm DR within a given experiment are based on data obtained in three paired-flash trials.

† Columns 4 –7 indicate, for the four investigated bleaching conditions, the numbers of mice investigated (A–C) and the determinations of recovery parameters (D–F). In D–F, recover kinetics determined with fractional bleaches of ~10^{-6}, ~3 x 10^{-5} and ~0.03 are described in relation to the time constants τ_r, τ_ω, and τ, respectively. These time constants are defined by equations 2, 3, and 4. Recovery kinetics determined with the ~30% to ~40% bleach are described in relation to the slope σ, as defined by equation 5. Values of R^2 in sections D–F denote the goodness of fit of equations 2, 3, 4, or 5 to the aggregate data.

‡ Determinations of slope σ within a given experiment are based on fitting a straight line to ≥ 3 data points obtained within ~12 to ~20 minutes after bleaching

Type of measurement			Dark-Adapted Characteristics *			Approximate Bleach †			
			1	2	3	4	5	6	7
			A_{peak}	t_{peak}	Norm DR	~10^{-6} τ_r	~3×10^{-5} τ_ω	~3% τ	~30% to ~40% Slope (σ)
A	*abcr* $^{-/-}$	No. of mice	18	18	15	3	5	8	4
		Age (days)	55 ± 30	55 ± 30	57 ± 32	40 ± 6	43 ± 6	63 ± 40	58 ± 27
B	C57-leu450	No. of mice	17	17	17	4	3	8	4
		Age (days)	58 ± 26	58 ± 26	58 ± 26	53 ± 26	43 ± 24	61 ± 24	63 ± 36
C	C57-met450	No. of mice	20	20	17	3	5	9	5
		Age (days)	56 ± 19	56 ± 19	58 ± 19	62 ± 3	51 ± 13	50 ± 21	72 ± 14

Determined parameters		Dark-Adapted Characteristics *			~10^{-6}	~3×10^{-5}	~3%	~30% to ~40%
		A_{peak} (μV)	t_{peak} (ms)	Norm DR	τ_r (ms)	τ_ω (ms)	τ (min)	σ (min^{-1}) ‡
D	*abcr* $^{-/-}$	315 ± 60	7.10 ± 0.37	0.65 ± 0.07	319 ± 24	321 ± 39	2.34 ± 0.74	–0.0281 ± 0.0079
					320 (R^2 = 0.95)	315 (R^2 = 0.99)	2.45 (R^2 = 0.96)	–0.0280 (R^2 = 0.95)
E	C57-leu450	340 ± 56	7.64 ± 0.36	0.67 ± 0.04	171 ± 26	362 ± 29	5.36 ± 2.20	–0.0099 ± 0.0068
					181 (R^2 = 0.98)	362 (R^2 = 0.98)	4.95 (R^2 = 0.99)	–0.0079 (R^2 = 0.87)
F	C57-met450	369 ± 79	7.50 ± 0.56	0.65 ± 0.08	213 ± 41	395 ± 39	5.92 ± 2.44	–0.0200 ± 0.0127
					211 (R^2 = 0.99)	392 (R^2 = 0.96)	4.93 (R^2 = 0.97)	–0.0225 (R^2 = 0.98)

The normalized derived responses (Norm DR) are derived responses to a weak test flash (0.3 sc cd-s m^{-2}) and were calculated using equations 1a and 1b (see Methods). As indicated in column 3 of Table 1D–F, the average, normalized derived response amplitudes determined for the *abcr*-/-, C57-leu450, and C57- met450 mice were within a narrow range (0.65– 0.67). Between-groups ANOVA showed no significant difference among strains for the dark-adapted, normalized derived response ($F_{2,46}$ = 0.387; P = 0.681). Post-hoc pair-wise comparisons showed no significant difference between values for the *abcr*-/- versus C57-leu450 mice (P = 0.472). In addition, there was no significant difference between the *abcr*-/- and C57-met450 mice (P = 0.972) or between the C57-leu450 and C57-met450 mice (P = 0.436).

3.2 ~10^{-6} and ~3 x 10^{-5} Fractional Bleaches

The ~10^{-6} fractional bleach was produced by a weak test flash (0.3 sc cd-s m^{-2}). The results of the experiments using the weak test flash are depicted in fig. 4. The strength of the weak test flash was identical with that used in estimated the normalized dark-adapted responses in paired flash trials described above. Fig. 4A shows the representative waveforms for the three strains. The plot of Normalized derived response *vs*. time (ms) has been plotted. Each plot is the average ± SD of multiple experiments. Each data point in the plot represents a paired-flash (test-probe) trial with the corresponding t_{probe}. In this type 1 experiment, the t_{probe} was varied between 80 ms to 500 ms. Probe-alone trials were carried out at regular intervals (~ after every 4 paired flash trials) during the experiment to establish a baseline to which each paired-flash trial

Fig 4: Recovery of rod photoreceptor current after a weak bleaching illumination. Recovery after relatively weak bleaching illumination. (**A**) Bleaching flash of 0.3 sc cd-s • m^{-2} (~10^{-6} fractional bleach). Left: paired-flash data obtained in single representative experiments. Labels indicate values of t_{probe}. Right: aggregate results obtained from three *abcr-/-*, four C57-leu450, and three C57-met450 mice. The curves illustrate the fitting of equation 2 to data obtained with t_{probe} ≥ 200 ms. (**B**) Bleaching flash of 7.9 sc cd-s • m^{-2} (~3 x 10^{-5} fractional bleach): Left: data obtained in single representative experiments. Right: aggregate results obtained from five *abcr-/-*, three C57-leu450, and five C57-met450 mice. The curves illustrate the fitting of equation 3 to the data.

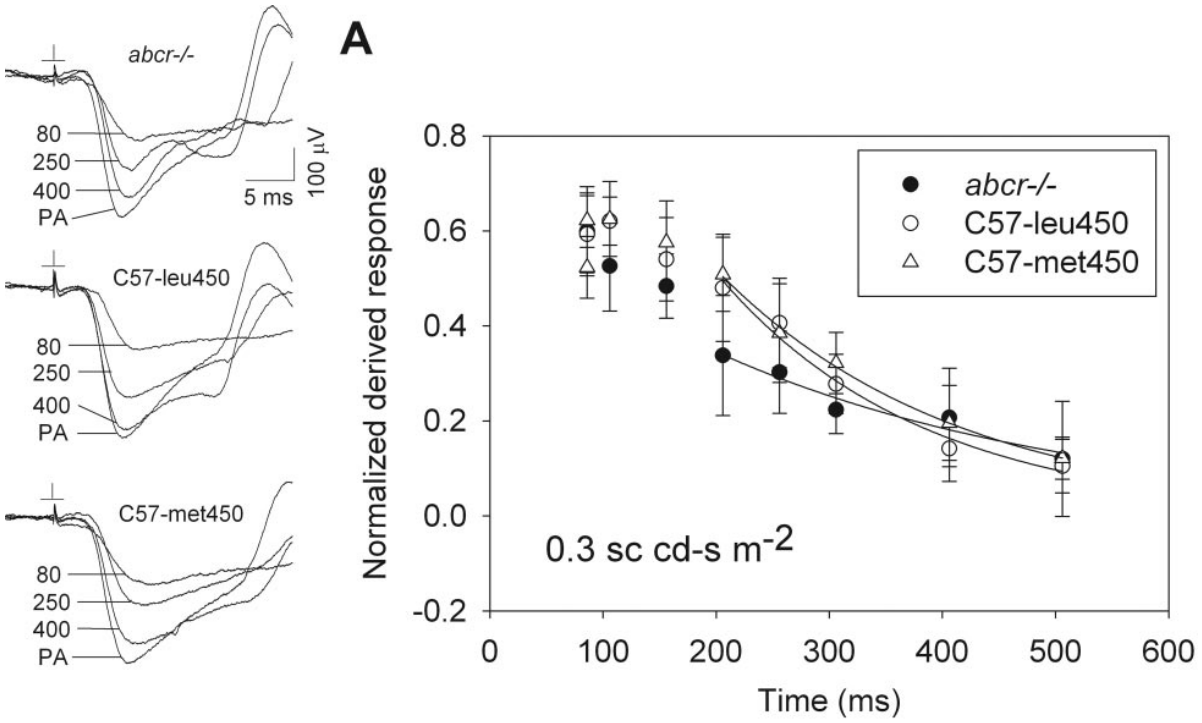
A
abcr-/-
80
250
400
PA
5 ms
100 µV
C57-leu450
80
250
400
PA
C57-met450
80
250
400
PA
Normalized derived response
0.8
0.6
0.4
0.2
0.0
-0.2
0
100
200
300
400
500
600
Time (ms)
abcr-/-
C57-leu450
C57-met450
0.3 sc cd-s m-2

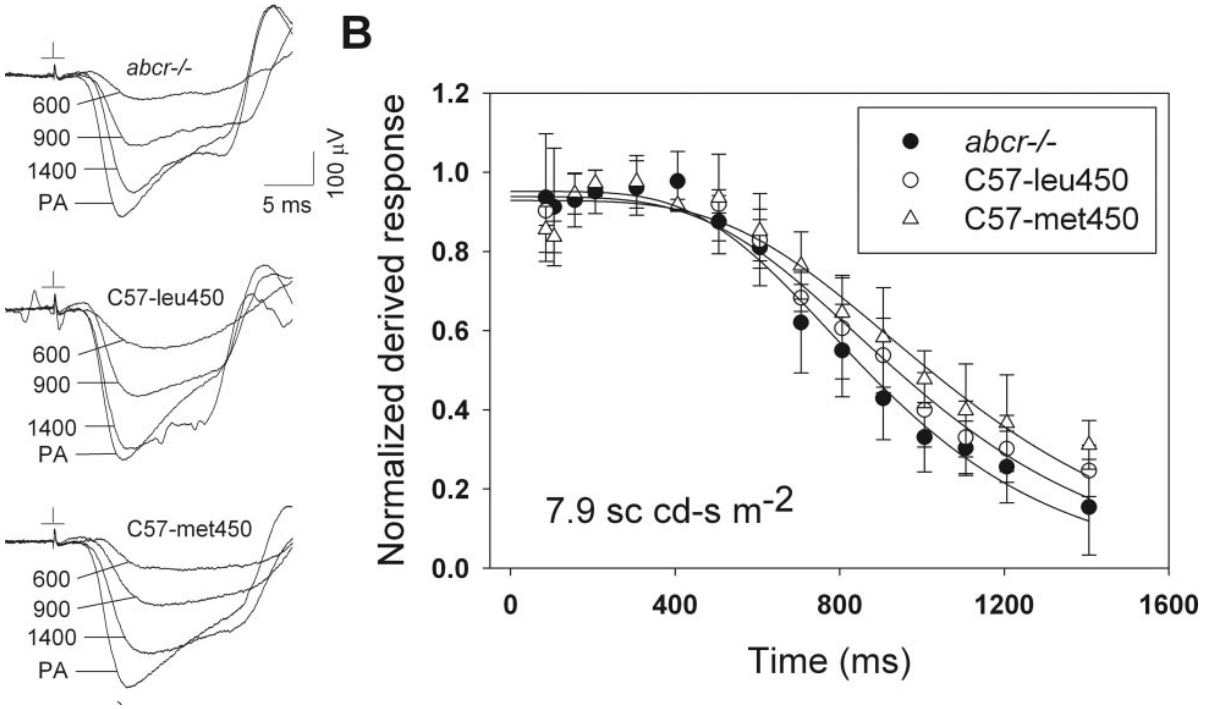
B
abcr-/-
600
900
1400
PA
5 ms
100 µV
C57-leu450
600
900
1400
PA
C57-met450
600
900
1400
PA
Normalized derived response
1.2
1.0
0.8
0.6
0.4
0.2
0.0
0
400
800
1200
1600
Time (ms)
abcr-/-
C57-leu450
C57-met450
7.9 sc cd-s m-2

would be referenced. The baseline probe alone amplitude at each time point during the experiment was estimated using linear interpolation between the bracketing probe-alone responses. The normalized derived responses were then calculated using equations 1a and 1b and have been plotted in fig. 4A. To quantify the time course of recovery of the paired-flash-derived response, we analyzed determinations of the normalized response $A(t)/A_{moD}$ beginning at t_{probe} = 200 ms (i.e., t = 206 ms) in relation to the exponential decay function (curves in Fig. 2A)

$$A(t)/A_{moD} = \eta \exp [- (t - 206)/\tau_r], \qquad (2)$$

where the dimensionless parameter η and the exponential time constant τ_r are free parameters. Determinations of the recovery time constant τ_r in these ~10^{-6} bleach experiments (number of experiments and animal ages shown in column 4 of Table 1A–C) are summarized in column 4 of Table 1D–F. These data are organized to indicate results obtained from the fitting of equation 2, both to data from individual experiments and to the aggregate data set obtained from a given strain. Thus, for example, the column 4 data in Table 1D indicate, for the *abcr*-/- mice, the mean ± SD of τ_r values obtained in individual experiments (upper entry) and the single τ_r value determined from equation 2 fitting to the aggregate data set (lower entry). Accompanying the aggregate best-fit value is the corresponding goodness of fit ($R2$). Among the investigated strains, the average τ_r determined from the individual fits ranged from 171 to 319 ms and corresponded closely with the aggregate fitted values of τ_r. Between-samples ANOVA of τ_r indicated a significant difference ($F_{2,7}$ = 20.517; P = 0.001). Post-hoc pair-wise comparisons of the data showed that τ_r for the *abcr*-/- mice significantly exceeded those for both the C57-leu450 (P=0.001) and C57-met450 (P=0.004) mice. There was no significant difference in τ_r between the C57-leu450 and C57-met450 mice. For the three

investigated strains, η (equation 2) was 0.34 ± 0.07 (*abcr*-/-), 0.51 ± 0.07 (C57-leu450), and 0.50 ± 0.04 (C57-met450).

The results of the 7.9 sc cd-s m^{-2} bleach extent are illustrated in fig. 4B. The experimental protocol used in the experiment was similar to the one used in the experiments that employed the 0.3 sc cd-s m^{-2} weak flash strength described above. However, in the experiments described in fig. 4B, the flash was a bright, saturating probe flash. This flash, of strength sufficient to saturate the rod response (Hetling and Pepperberg, 1999), produced fractional bleach of ~3 x 10^{-5}. To sufficiently study the recovery of the derived response to this bright saturating flash, longer interflash intervals (t_{probe}) were used. In these experiments, the t_{probe} was varied from 80 ms to 1400 ms. Recovery data obtained in these experiments were analyzed in relation to a nested exponential function similar to those used previously (Hetling and Pepperberg, 1999, Kang Derwent *et al.*, 2002)

$$A(t)/A_{moD} = \theta_1\{1 - \exp[- \theta_2 \exp(- t/\tau_\omega)]\}, \qquad (3)$$

where the dimensionless parameters θ_1 and θ_2 and the recovery time constant τ_ω are free parameters. Column 5 of Table 1D–F summarizes the results obtained. The upper entry in each row is the mean ± SD for the recovery time constant τ_ω based on the fitting of equation 3 to individual data sets; the lower entry indicates the value of τ_ω obtained by fitting equation 3 to the

aggregate data set for a given strain. As illustrated in Figure 2B, aggregate recovery data obtained from the three investigated strains exhibited a generally similar pattern, although recovery in the C57-met450 mice was, on average, somewhat slower than that in the *abcr*-/- and C57-leu450 mice. ANOVA of the values of τ_ω (Table 1D–F, column 5) indicated a significant difference ($F_{2,10}$ = 4.808; P = 0.034). Post-hoc pair-wise comparisons showed a significant difference between the *abcr*-/- and C57-met450 mice

(P = 0.011), no significant difference between the *abcr-/-* and C57-leu450 mice, and no significant difference between the C57-leu450 and C57-met450 mice. θ_1 and θ_1 (equation 3) for the three strains were, respectively, 0.96 ± 0.03 and 11.76 ± 4.28 (*abcr-/-*), 0.93 ± 0.02 and 10.67 ± 0.51 (C57-leu450), and 0.92 ± 0.02 and 11.07 ± 3.38 (C57-met450).

3.3 <u>3% bleach</u>

Figure 5 shows the results of experiments from a 3% bleach extent. The experimental protocol used in these experiments differed from that used in the earlier low-bleach experiments. In previous experiments, bleaching flashes were presented in each trial during the experiment (see above section). In the current experiments, the entire bleaching illumination was presented at the beginning of the experiment, after the dark-adapted characterization. Here, the bleaching illumination consisted of a series of 20 bright flashes (of strength 477 sc cd-m s^{-2} each, yielding a cumulative luminance of 9.5 x 10^3 sc cd-s m^{-2}) delivered over an approximately 100-second period. This bleaching illumination produced a fractional bleach of ~0.03. The recovery of the rod response was then analyzed by having a series of probe flashes at specific time intervals after the bleaching illumination. Figures 5A, 5C, and 5E show results from single representative experiments on *abcr-/-*, C57-leu450, and C57-met450 mice, respectively. Figures 5B, 5D, and 5F show aggregate results obtained in eight experiments on the *abcr-/-* mice, eight on the C57-leu450 mice, and nine on the C57-met450 mice (Table 1A–C, column 6). In these experiments, the normalized derived response determined after the bleaching illumination declined toward the prebleach baseline and in a number of cases exhibited an overshoot (i.e., an amplitude that exceeded the dark-adapted amplitude,

Fig. 5: Recovery after the ~ 3% bleach.
(**A**, **C**, **E**) Recovery data obtained in single experiments on the *abcr-/-*, C57-leu450, and C57-met450 mice, respectively. Insets: representative responses to the probe flash. Dashed curve: simple exponential function fitted to the data obtained from the time of conclusion of the bleaching light (time 0) to the apparent plateau of recovery. (**B**, **D**, **F**) Aggregate data obtained in groups of experiments on *abcr-/-*, C57-leu450, and C57-met450 mice, respectively. In cases for which data obtained at different values of t_{probe} were binned, the abscissa value and horizontal error bar of the illustrated data point represent the mean ± SD of the binned t_{probe} values. Vertical arrows: conclusion of the period over which data were analyzed in relation to the exponential function.

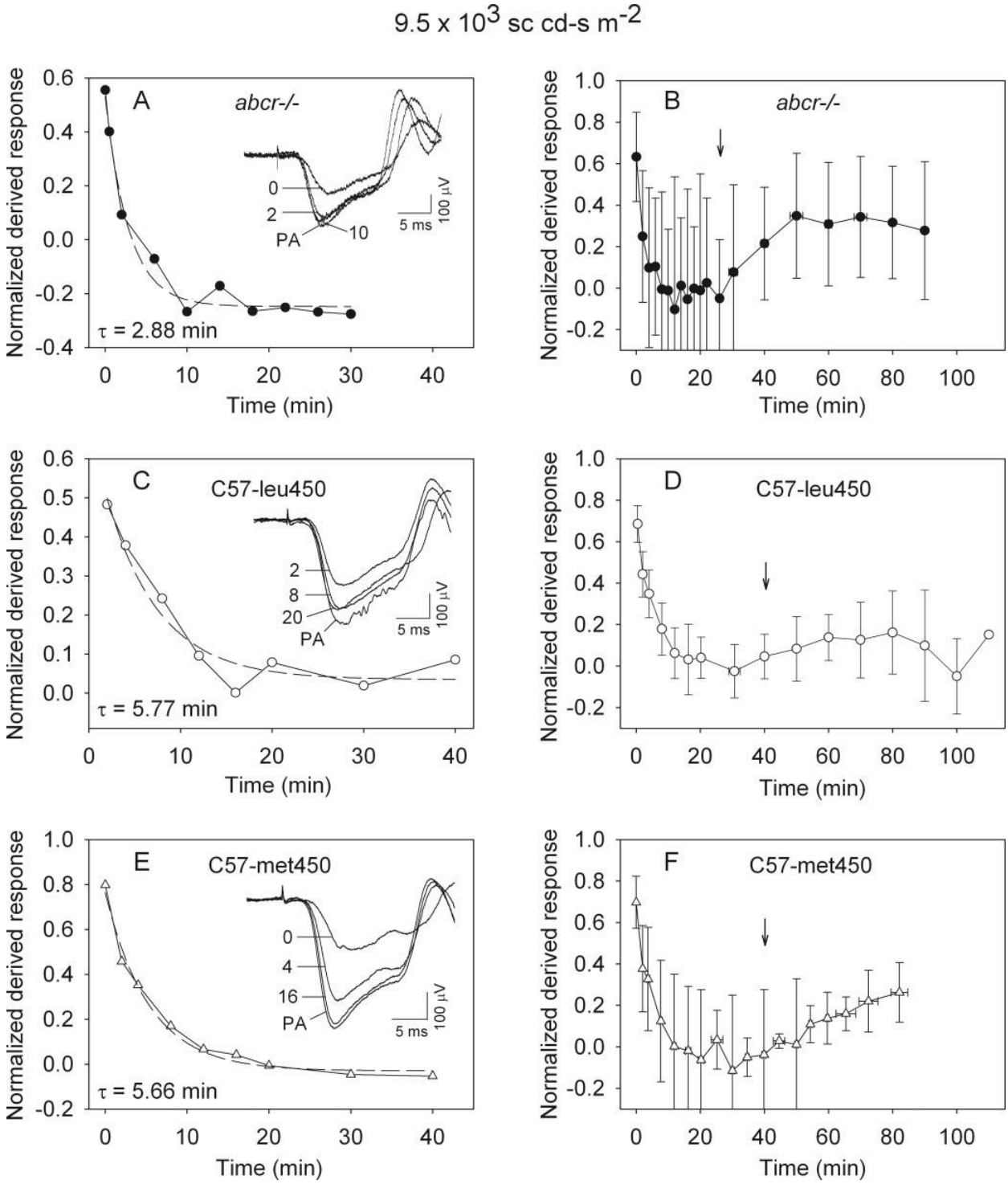
9.5 x 10^3 sc cd-s m^-2
A
abcr-/-
0
2
PA
10
5 ms
100 µV
τ = 2.88 min
Normalized derived response
Time (min)
B
abcr-/-
C
C57-leu450
2
8
20
PA
τ = 5.77 min
D
C57-leu450
E
C57-met450
0
4
16
PA
τ = 5.66 min
F
C57-met450

A_{moD}). A similar overshoot in the post-bleach recovery of wild-type rods has been reported (Mata *et al.*, 2001 and Xu *et al.*, 2005). To quantify the results obtained, data collected in each experiment (which typically differed in post-bleach times of determination of the derived response) were linearly interpolated to yield values of $A(t)/A_{moD}$ at post-bleach times of 2, 3, . . . , 30 minutes and (for a subset of the data set) at times 31, 32, . . . , 60 minutes. Repeated-measures ANOVA demonstrated a significant interaction between strains as a function of time for the interval of 2–30 minutes ($F_{56,616} = 3.934$; $P = 0.001$). Post-hoc tests showed a significant difference between the *abcr-/-* and C57- leu450 mice and between the *abcr-/-* and C57-met450 mice, but no significant difference between the C57-leu450 and C57- met450 mice. Unlike the case of the 2- to 30-minute interval, repeated-measures ANOVA indicated no significant difference among the investigated strains for the 31- to 60-minute interval. The recovery time course in these ~3% bleach experiments was further characterized by determinations of a characteristic time constant, τ. In the first of two methods used, data obtained in a single given experiment were analyzed by fitting a simple exponential function,

$$A(t)/A_{moD} = \alpha + \beta \exp(-t/\tau), \qquad (4)$$

where α, β, and τ are free parameters, to recovery data obtained between time 0 (i.e., the time of conclusion of the bleaching illumination) and post-bleach time T. The value of T was chosen based on visual inspection of the data, and corresponded with the time of completion of a visually apparent plateau in the derived response amplitude. Among experiments, values of the selected period T were, respectively, 29.75 ± 10.28 (*abcr-/-*), 42.50 ± 8.86 (C57-leu450), and 40.78 ± 14.65 (C57-met450) minutes. Overall results obtained for the recovery time constant τ are shown in the upper entries in column 6 of

Table 1D–F. The average τ determined for the *abcr-/-* mice (2.34 minutes) was substantially less than that determined for the C57-leu450 and C57-met450 mice (5.36 and 5.92 minutes, respectively). ANOVA of these determinations of τ indicated a significant difference between strains ($F_{2,22}$ = 7.144; P = 0.004). Furthermore, post-hoc comparisons between the strains indicated a significant difference between the *abcr-/-* and C57-leu450 mice (P = 0.008) and between the *abcr-/-* and C57-met450 mice (P = 0.002). There was no significant difference between the C57-leu450 and C57-met450 mice. The second of the two analysis methods involved the fitting of equation 4 to aggregate data obtained from a given strain (Figs. 5B, 5D, 5F). Vertical arrows in Figures 5B, 5D, and 5F indicate the conclusions of the post-bleach periods used for this analysis of aggregate data, and lower entries in column 6 of Table 1D–F show the values of τ obtained. These aggregate-fit values of τ corresponded closely with the average values determined by fitting to the individual data sets.

Aggregate data obtained from all three strains (Figs. 5B, 5D, 5F) exhibited an upward trend of the derived response in the later phase of the experiments (i.e., a positive-directed trend that opposed the downward-directed recovery process). This upward-directed process, if of sufficient magnitude, might be anticipated to skew determination of (i.e., lead to underestimation of) the recovery time constant τ. However, ANOVA of the values of the excursion τ of the simple exponential function fitted to individual data sets (equation 4; values of β: 0.68 ± 0.26 for *abcr-/-*; 0.74 ± 0.17 for C57-leu450; and 0.77 ± 0.27 for C57-met450) showed no significant differences ($F_{2,22}$ = 0.252; P = 0.779), and post-hoc pair-wise comparisons indicated no significant differences. In addition, aggregate data for the *y*-intercept of this fitted exponential

function [i.e., for the time 0 value, given by the sum (α + β)] were similar among strains (0.66 ± 0.22 for *abcr-/-*; 0.74 ± 0.10 for C57-leu450; and 0.68 ± 0.12 for C57-met450). Thus, although the basis of the opposing process remains unclear, the similarities of the excursion β and of the *y*-intercept (α + β) among strains suggest that this process operates in similar fashion among strains and does not account for the relatively fast recovery determined for the *abcr-/-*

3.4 ~30% - 40% Bleach

The protocol used in the ~30-40% bleach experiments was similar to the one used in the ~3% bleach extent experiments described in the previous section. The 2-minute bleaching illumination was done at the beginning of the experiment, and the rod response recovery was analyzed by a series of bright probe flashes, similar to previous experiments.

Fig. 6 shows overall results obtained in experiments with the 2-minute illumination that bleached ~30% to ~40% of the rhodopsin. Figure 4A shows aggregate results obtained from the investigated strains over periods that ranged up to 100–110 minutes after bleaching. As illustrated by Figure 6A, recovery in *abcr-/-* mice was, on average, faster than those in the C57-leu450 and C57-met450 mice. The initial ~12 to ~20 minutes of recovery determined in the investigated strains was further analyzed by determining the slope of a straight line

$$A(t)/A_{moD} = \psi + \sigma t, \qquad (5)$$

where the slope (in units of inverse time) and the dimensionless intercept are free parameters fitted to the data obtained over the initial ~12- to ~20-minute post-bleach

period. Figures 6B–G illustrate results obtained in representative single experiments on *abcr-/-* (Figs. 6B, 6C), C57-leu450 (Figs. 6D, 6E), and C57-met450 (Figs. 6F, 6G) mice, and data for the determinations of slope are summarized in column 7 of Table 1D–F. ANOVA of the values of the slope indicated no significant differences among the investigated strains ($F_{2,10}$ =3.420; P = 0.074). However, post-hoc pair-wise comparisons showed that slopes determined for the *abcr-/-* mice differed significantly from those of the C57-leu450 mice (P = 0.026). There was no significant difference between the *abcr-/-* and C57-met450 mice or between the C57-leu450 and C57-met450 mice. For the three investigated strains, values of the *y*-intercept of the fitted linear functions were 0.88 ± 0.12 (*abcr-/-*), 0.92 ± 0.08 (C57-leu450), and 0.97 ± 0.04 (C57-met450). ANOVA of the values of yielded no significant differences among strains ($F_{2,10}$ = 1.516; P = 0.266), and post-hoc pair-wise comparisons also indicated no significant differences between strains.

Fig 6: Recovery after the ~30% to ~40% bleach.
(**A**) Aggregate data obtained from four *abcr-/-*, four C57-leu450, and five C57-met450 mice. Inset: data illustrated on a faster time scale. (**B**–**G**) Data obtained in representative single experiments on *abcr-/-* (**B**, **C**), C57-leu450 (**D**, **E**), and C57-met450 (**F**, **G**) mice over the first ~12 to ~20 minutes after the conclusion of the bleaching illumination. Each panel illustrates the fitting of a straight line to the data. Insets: paired-flash data obtained in representative single experiments. Labels indicate the post-bleach time, in minutes.

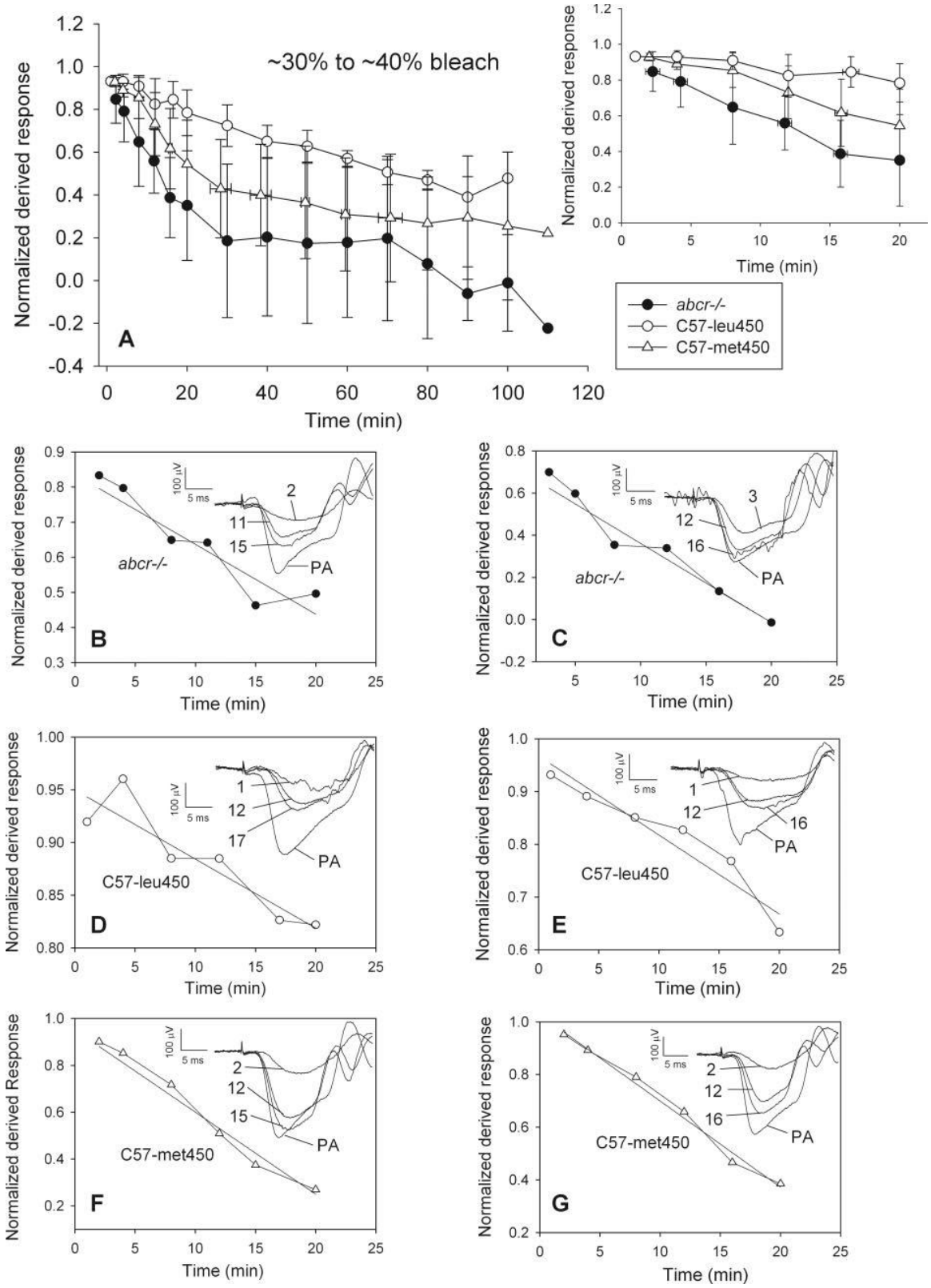
~30% to ~40% bleach
Normalized derived response
Time (min)
A
abcr-/-
C57-leu450
C57-met450
B
C
D
E
F
G
100 µV
5 ms
PA
Normalized derived Response

4. DISCUSSION

The study just described involved comparison of the recovery of the rod photoreceptor response in *abcr-/-*, C57-leu450 and C57-met450 at four different bleach levels, ranging from ~10^{-6} to ~30%-40%. The most striking result in this study was that, based on the values of the exponential time constants, the *abcr-/-* exhibited a significantly faster recovery of the rod response as compared to the controls at the 3% bleach level (fig. 4 and Table 1D-F, column 6). At the ~30%-40% bleaching extent, the *abcr-/-* rod response recovery significantly exceeded that of the C57-leu450 and was on average faster than the C57-met450 (albeit not significantly) (fig. 6 and Table 1D-F, column 7). The differences that were observed in the rod response recovery were based on analysis of the normalized derived response following bleaching illumination. However, there was no significant difference between the strains in the dark-adapted normalized derived response (Table 1D-F, column 3). Thus the differences observed in the rod response recovery at the different bleach conditions cannot be attributed to differences among the investigated strains in pupil size, other preretinal factors, or absorptivity (i.e., amount) of rhodopsin in the rods. That is, such differences would be expected to have produced differences in the dark-adapted, derived rod response to a weak test flash, yet these determinations of weak-flash sensitivity were similar among the *abcr-/-* mice and controls. Thus the significantly faster recovery kinetics observed in the *abcr-/-* mice under the different bleach conditions must reflect an intrinsically rapid process of post-bleach recovery in *abcr-/-* rods.

It is important to note that the results observed in this study differ from the results reported by Weng *et al*. (1999). In their study, at a ~45% bleach level, the recovery kinetics of the *abcr-/-* was significantly slower than that of the wildtype mice. The highest bleaching extent used in our study (~30%-40%) is lower but comparable to that of Weng *et al*. (1999). In our study the *abcr-/-* are significantly faster than the C57-leu450 and faster on average than the C57-met450. Another important point to note in light of these observed differences in the two studies is, that in our study at the ~3% bleach level, the *abcr-/-* demonstrated a significantly faster rate of recovery of the rod photoreceptor current than both the wildtype strains There contrasting results (especially at the ~30%-40% bleach level) could be attributed to two factors; the age of the mice, or the specific wildtype strain used in the Weng *et al*., (1999) study, both of which are unknown.

Two strains of wildtype mice were used in the present study; the pigmented C57-derived lines possessing the leu450 and the met450 variants of the RPE65, the isomerohydrolase of the retinoid visual cycle that promotes the conversion of all-*trans* retinyl ester to 11-*cis* retinol in the RPE (Moiseyev *et al*., 2005, Redmond *et al*., 2005). Previous studies have shown that the leu450 and the met450 variants of the RPE65 mice are known to differ in the rate of isomerhydrolase activity (Wenzel *et al*., 2001, Kim *et al*., 2004, Lyubarsky *et al*., 2005). The isomerhydrolase reaction is also a critical step in the retinoid visual cycle (Moiseyev *et al*., 2005, Redmond *et al*., 2005) and is important for rhodopsin regeneration for full rod dark adaptation (Pepperberg *et al*., 1978, Cornwall and Fain 1994). For these reasons, the comparison of rod recovery in the *abcr-/-* mice with that in control animals possessing both the leu450 and met450 variants of RPE65 was important in the present study. Interestingly, these two wild-type strains exhibited remarkably similar rod recovery properties under the present

experimental conditions. In particular, there were no significant differences among data obtained from the C57-leu450 and the C57-met450 after ~3% bleaching or during the initial ~12- to ~20-minute period after ~30% to ~40% bleaching. These findings imply that occurrence of the leu450 variant of RPE65 in *abcr*-/- mice does not underlie the observed relatively rapid recovery of the *abcr*-/- rod response after the more extensive bleaches used here. Significant differences in rod recovery kinetics in albino mice possessing the leu450 versus met450 variant of RPE65 have been reported by Nusinowitz *et al*. (2003). Specifically, these investigators compared ERG *a*-wave recovery in BALB/c mice, which possess the leu450 variant, with that in c2J mice, which possess the met450 variant. For bleaching illuminations of 3.61 and 3.97 log sc td-s, the exponential time constant describing recovery in the BALB/c was, respectively, approximately 48% and 21% faster than in c2J mice. Furthermore, after ~80% to ~90% bleaching, recovery of the ERG b-wave proceeded more rapidly in the BALB/c mice.

The fast recovery of post-bleach rods in *abcr-/-* mice raises interesting questions relevant to the processing of all-*trans* retinal and the contribution of the ABCR protein in the retinoid visual cycle, as compared to wildtype mice. Previous biochemical experiments indicate that ABCR's facilitation of all-*trans* retinal movement across the disc membrane contributes to the post-bleach processing of all-*trans* retinal in the visual cycle. For example, Weng *et al*. (1999) found that the amount of all-*trans* retinal per eye in *abcr*-/- mice at up to 1 hour after 45% bleach significantly exceeded that in wild-type controls. However, the magnitude of this increase, on average up to ~30 picomoles per eye (Fig. 3C Weng *et al*.) represents only a small fraction of the decrease in rhodopsin produced by the 45% bleach (Figs. 3A, 3B in Weng *et al*., 1999). Thus, ABCR deficiency under the conditions investigated by Weng *et al*. (1999) corresponds with a relatively

small, albeit significant, prolongation of all-*trans* retinal clearance. Interestingly, the rod outer segments of *abcr*-/- mice contain an abnormally high level of phosphatidylethanolamine (PE), the lipid that combines with all-*trans* retinal to form *N*-ret-PE. A high PE level in (presumably, the disc membranes of) *abcr*-/- rods conceivably could underlie the present observation of relatively fast recovery kinetics in *abcr*-/- mice. For example, the abnormally large amount of PE in *abcr*-/- disc membranes (the luminal surface, the cytosolic surface, or both; see also Wu and Hubbell, 1993) might promote, by mass action, the sequestering of all-*trans* retinal as *N*-ret-PE at a rate considerably exceeding that in wild-type rods, thereby accelerating response recovery relative to the wildtype. Alternatively, the high level of PE in the *abcr*-/- rod, by binding 11-*cis* retinal arriving from the RPE through operation of the visual cycle, might localize 11-*cis* retinal to the vicinity of opsin and thereby promote rhodopsin regeneration (Sun *et al*., 1998). A further possibility derives from the finding that ABCR itself can bind 11-*cis* retinal (Sun *et al*., 1998). That is, the ABCR of wild-type rods, a major protein of the disc rims, might delay recovery relative to *abcr*-/- by *competing* with opsin for 11-*cis* retinal and thereby slowing rhodopsin regeneration.

Thus, the results in the current experiments indicate that the presence of the ABCR protein (in wildtype mice) delays rather than accelerate dark-adaptation, as compared mice lacking the ABCR protein. This is perhaps a puzzling outcome, in that one might hypothesize that in the absence of ABCR, there would be delayed clearance of all-*trans* retinal from the rod disc lumen and thus prolongation of the retinoid cycle as indicated in the Weng *et al.*, (1999) study. That is, in terms of photoreceptor evolution, it would seem detrimental to have processes that slow down dark adaptation. The seeming paradox is resolved, however, if the primary physiological role of the ABCR-

mediated reaction is to promote clearance, from the disc, of *minute, residual amounts* of all-*trans* retinal that other mechanisms, such as thermal diffusion across the disc membrane, cannot achieve. That is, the ABCR mediated action might not be responsible for the removal of bulk or the major portion of all-*trans* retinal and MII-like complexes of all-*trans* retinal and opsin from the disc. Rather, the role of ABCR might be the removal of trace amounts of all-trans retinal from the disc and thus oppose the build-up over the lifetime of a rod disc (Young and Bok, 1969), of retinoid based compound that would otherwise be transferred to the RPE and there accumulate as A2E and other retinoid based components of lipofuscin (Sparrow and Boulton, 2005). On this hypothesis, the slower rod recovery observed in normal rods upon the bleach-induced elevation of all-*trans* retinal in the disc lumen represents a cost, or tradeoff, associated with the presence of a system (ABCR) that can clear tiny remaining amounts of all-*trans* retinal. Beyond its consistency with the observed modest difference in post-bleach all-*trans* retinal levels in ABCR-deficient versus wild-type rods (Weng *et al*., 1999), this hypothesis is consistent with the finding that abnormal A2E build-up in *abcr-/-* mice amounts, on average, to only several tens of picomoles per eye (~21 picomoles per eye over 4 to 5 months, Weng *et al*., 1999; ~30 picomoles per eye over 8 to 9 months, Kim *et al*., 2004), a molar quantity small by comparison with, for example, the amount of 11-*cis* retinal present as rhodopsin chromophore in fully dark-adapted rods (Qtaishat *et al*.,1999, Saari *et al*., 1998). The hypothesis is also consistent with the near-normal course of rod recovery frequently observed in human subjects with Stargardt disease and an ABCA4 (i.e., ABCR) mutation (Kang Derwent *et al*., 2004, Cideciyan *et al*., 2004), and with the prolongation, in these subjects, of primarily the final, tail phase of psychophysically measured dark adaptation after major bleaching of rhodopsin (Fig. 9 in

Kang Derwent *et al*., 2004). More recent studies (Sullivan, 2008) point out that despite the occurrence of an increasing amount of A2E with increasing age in the *abcr-/-* mouse, no retinal degeneration ensues. A double knockout mouse (*abcr-/-* and rod trans-retinol dehydrogenase knockout) that causes a large and rapid accumulation of A2E, formation of drusen and photoreceptor degeneration might represent a better model for AMD and Stargardt disease (Maeda et al., 2008) as compared to *abcr-/-.* A recent study by Blakeley et al. (2011), using isolated retinas and single rods and a combination of fluorescence imaging and high performance liquid chromatography of retina extracts, found that the formation of all-*trans* retinol is independent of the ABCR protein in *abcr-/-* mice. These recent results confirm our findings, that under the conditions of low-medium bleaches (upto ~40%), the recovery of rod photoreceptor current in *abcr-/-* mice is not slower (and in many cases faster) as compared to recovery in wildtype mice.

References

1. Ahn J, Beharry S, Molday LL, Molday RS (2003). Functional interaction between the two halves of the photoreceptor-specific ATP binding cassette protein ABCR (ABCA4): evidence for a non-exchangeable ADP in the first nucleotide binding domain. *J Biol Chem*. **278**, 39600–39608.
2. Baylor, D.A., Lamb, T.D., Yau, K.W. (1979). Responses of retinal rods to single photons.

   J Physiol. **288**, 613-34.
3. Birch, D. G., Hood, D. C., Nusinowitz, S. & Pepperberg, D. R. (1995). Abnormal activation and inactivation mechanisms of rod transduction in patients with autosomal dominant retinitis pigmentosa and the pro-23-his mutation. *Investigative Ophthalmology and Visual Science* **36**, 1603—1614.
4. Bownds, D., Dawes, J., Miller ,J., Stahlman, M. (1972). Phosphorylation of frog photoreceptor membranes induced by light. *Nature New Biol* **237**, 125–127.
5. Breton, M. E., Schueller, A. W., Lamb, T. D. & Pugh, E. N. Jr. (1994). Analysis of ERG a-wave amplification and kinetics in terms of the G-protein cascade of phototransduction. Investigative Ophthalmology and Visual Science **35(1),** 295-309
6. Brown, K. T. & Watanabe, K. (1962). Isolation and identification of a receptor potential from the pure cone fovea of the monkey retina. *Nature* **193**, 958-960.
7. Brown, K. T. & Wiesel, T. N. (1961). Localization of origins of electroretinogram components by intraretinal recording in the intact cat eye. *Journal of Physiology* **158**, 257—280.

8. Brown, K.T., Watanabe, K., Murakami, M. (1965).The early and late receptor potentials of monkey cones and rods. *Cold Spring Harbor Symp Quant Biol* **30**, 457-482.
9. Burns, M.E., Baylor, D.A. (2001). Activation, deactivation, and adaptation in vertebrate photoreceptor cells. *Annu Rev Neurosci*. **24**, 779-805.
10. Cornwall, M.C., Fain, G.L. (1994). Bleached pigment activates transduction in isolated rods of the salamander retina. *J Physiol.* **480(2),** 261-79.
11. Cornwall, M.C., Fein, A., MacNichol, E.F. Jr. (1990). Cellular mechanisms that underlie bleaching and background adaptation. *J. Gen. Physiol*. **96**:345-72.
12. Cideciyan, A. V., Aleman, T. S., Swider, M.,Schwartz, S. B., Steinberg, J. D., Brucker, A. J., Maguire, A. M., Benett, J., Stone, E.M., Jacobson, S. G. (2004). Mutations in *ABCA4* result in accumulation of lipofuscin before slowing of the retinoid cycle: a reappraisal of the human disease sequence. *Hum Mol Genet*. **13**:525-534
13. Eldred, G. E., Lasky, M. R. (1993). Retinal age pigments generated by self-assembling lysosomotropic detergents. *Nature (London)* **361,** 724–726.
14. Friedburg, C., Thomas, M.M., Lamb, T.D. (2001). Time course of the flash response of dark- and light-adapted human rod photoreceptors derived from the electroretinogram. *J Physiol.* **534(1),** 217-42.
15. Furakawa, T. and Hanawa, I. (1955). Effects of some common cations on electroretinogram of the toad. *Japanese Journal of Physiology* **5**, 289-300.
16. Goto, Y., Peachey, N. S., Ziroli, N. E., Seiple, W. H., Gryczan, C., Pepperberg, D. R. & Naash, M. I. (1996). Rod phototransduction in transgenic mice expressing a mutant opsin gene. *Journal of the Optical Society of America A* **13**, 577-585.

17. Granit, R. (1933). The components of the retinal action potential in mammals and their relation to the discharge in the optic nerve. *Journal of Physiology* **77**, 207—239.
18. Hargrave, P. A. and Hamm, H.E. (1994). Regulation of visual transduction. In:*Regulation of Cellular Signal Transduction Pathways by Desensitization and Amplification*, edited by Sibley DR and Houslay MD. New York: Wiley, pp. 25–67
19. Hargrave, P.A. (1995). Future directions for rhodopsin structure and function studies. *Behav Brain Sci* **18**, 403–414.
20. Hetling, J. R. and Pepperberg, D. R. (1999). Sensitivity and kinetics of mouse rod flash responses determined in vivo from paired-flash electroretinograms. *J Physiol.* **516**, 593-609
21. Hofmann, K.P., Pulvermuller, A., Buczylko, J., Van Hooser, P., Palczewski, K. (1992). The role of arrestin and retinoids in the regeneration pathway of rhodopsin. *J Biol Chem*. **267(22)**, 15701-15706.
22. Hood, D. C. & Birch, D. G. (1990). A quantitative measure of the electrical activity of human rod photoreceptors using electroretinography. *Visual Neuroscience* **5**, 379—387.
23. Jager, S., Palczewski, K., Hofmann, K.P. (1996). Opsin/all-*trans*-retinal complex activates transducin by different mechanisms than photolyzed rhodopsin. *Biochemistry* **35(9)**, 2901-2908.
24. Kang Derwent, J.J., Derlacki, D.J., Hetling, J. R., Fishman, G. A., Birch, D. G., Grover, S., Stone, E. M., Pepperberg, D. R. (2004). Dark adaptation of rod photoreceptors in normal subjects, and in patients with Stargardt disease and an *ABCA4* mutation. *Invest Ophthalmol Vis Sci*. **45**:2447–2456.

25. Kandel, E. R.; Schwartz, J.H.; Jessell, T.M. (2000). *Principles of Neural Science* (4th ed.). New York: McGraw-Hill. pp. 507–513. ISBN 0-8385-7701-6.

26. Kim, S. R., Fishkin, N., Kong, J., Nakanishi, K., Allikmets, R., Sparrow, J. R. (2004). Rpe65 Leu450Met variant is associated with reduced levels of the retinal pigment epithelium lipofuscin fluorophores A2E and iso- A2E. *Proc Natl Acad Sci USA*. **101**:11668–11672.

27. Kraft, T. W., Schneeweis, D. M. & Schnapf, J. L. (1993). Visual transduction in human rod photoreceptors. *Journal of Physiology* **464**, 747—765.

28. Krupnick, J. G., Gurevich, V. V., Benovic J. L. (1997). Mechanism of quenching of phototransduction. *J Biol Chem* **272**: 18125–18131.

29. Kuhn, H. and Dreyer, W. J. (1972). Light dependent phosphorylation of rhodopsin by ATP. *FEBS Lett* **20**, 1–6, 1972.

30. Kuhn, H., Hall, S. W., Wilden, U. (1984). Light-induced binding of 48-kDa protein to photoreceptor membranes is highly enhanced by phosphorylation of rhodopsin. *FEBS Lett* **176**: 473–478.

31. Lyubarsky, A. L. & Pugh, E. N. Jr. (1996). Recovery phase of the murine rod photoresponse reconstructed from electroretinographic recordings. *Journal of Neuroscience* **16**, 563- 571.

32. Lyubarsky, A.L., Daniele, L.L., Pugh, E.N. Jr. (2004). From candelas to photoisomerizations in the mouse eye by rhodopsin bleaching in situ and the light-rearing dependence of the major components of the mouse ERG. *Vision Res.* **44(28)**, 3235-3251.

33. Lyubarsky, A. L., Savchenko, A. B., Morocco, S. B., Daniele, L. L., Redmond, T. M., Pugh, E. N. Jr. (2005) Mole quantity of RPE65 and its productivity in the

generation of 11-*cis*-retinal from retinyl esters in the living mouse eye. *Biochemistry* **44**:9880–9888.

34. Maeda, A., Maeda, T., Golczak, M., Palczewski, K., 2008. Retinopathy in mice induced by disrupted all-trans-retinal clearance. *J. Biol. Chem.* **283**, 26684–26693
35. Mata, N.L., Weng, J., Travis, G.H. (2000). Biosynthesis of a major lipofuscin fluorophore in mice and humans with ABCR-mediated retinal and macular degeneration. *Proc Natl Acad Sci USA*. **2000(97)**, 7154–7159.
36. McBee, J. K., Palczewski K., Baehr W., Pepperberg, D. R. (2001). Confronting complexity; the interlink of phototransduction and retinoid metabolism in the vertebrate retina. *Prog Retin Eye Res* **20(4),** 469-529.
37. Moiseyev, G., Chen, Y., Takahashi, Y., Wu, B. X., Ma, J. (2005). RPE65 is the isomerohydrolase in the retinoid visual cycle. *Proc Natl Acad Sci USA*. **102**:12413–12418.
38. Nakatani, K., Tamura, T. & Yau, K.-W. (1991). Light adaptation in retinal rods of the rabbit and two other nonprimate mammals. *J Gen Physiol.* **97(3),** 413-35.
39. Noell, W. K. (1954). The origin of the electroretinogram. *American Journal of Ophthalmology* **38**, 78-90.
40. Nusinowitz, S., Nguyen, L., Radu, R., Kashani, Z., Farber, D., Danciger, M. (2003). Electroretinographic evidence for altered phototransduction gain and slowed recovery from photobleaches in albino mice with a MET450 variant in RPE65. *Exp Eye Res*. **77**:627_638

41. Palczewski, K., Pulvermiller, A**,** Buczylko, J., and Hofmann, K. P. (1991) Phosphorylated rhodopsin and heparin induce similar conformational changes in arrestin. *J Biol Chem.* **266(28),** 18649-54.

42. Palczewski, K., Rispoli, G., and Detwiler, P. B. (1992). The influence of arrestin (48K protein) and rhodopsin kinase on visual transduction. *Neuron* **8(1),** 117-26.

43. Palczewski, K. and Saari, J.C. (1997). Activation and inactivation steps in the visual transduction pathway. *Curr Opin Neurobiol* **7**: 500–504.

44. Penn, R. D. & Hagins, W. A. (1969). Signal transmission along retinal rods and the origin of the electroretinographic *a*-wave. *Nature* **223**, 201—205.

45. Pepperberg, D. R., Brown, P. K., Lurie, M., Dowling, J. E. (1978). Visual pigment and photoreceptor sensitivity in the isolated skate retina. *J Gen Physiol*. **71**:369-396.

46. Pepperberg, D. R., Birch, D. G., Hofmann, K. P. & Hood, D. C. (1996). Recovery kinetics of human rod phototransduction inferred from the two-branched *a*-wave saturation function. *Journal of the Optical Society of America A* **13**, 586—600.

47. Pepperberg, D. R., Birch, D. G. & Hood, D. C. (1997). Photoresponses of human rods in vivo derived from paired-flash electroretinograms. *Visual Neuroscience* **14**, 73—82.

48. Pugh Jr, E.N., Lamb, T.D. (1993) Amplification and kinetics of the activation steps in phototransduction. *Biochem Biophys Acta* **1141,** 111-149.

49. Pulvermuller A., Maretzki, D., Rudnicka-Nawrot, M., Smith, W. C., Palczewski, K., and Hofmann, K. P. (1997). Functional differences in the interaction of arrestin and its splice variant, p44, with rhodopsin. *Biochemistry* **36**: 9253–9260.

50. Qtaishat, N. M., Okajima, T-I. L., Li, S., Naash, M. I., Pepperberg, D. R. (1999). Retinoid kinetics in eye tissues of VPP transgenic mice and their normal littermates. *Invest Ophthalmol Vis Sci*. **40**:1040–1049.

51. Rao, V. R., and Oprian, D. D. (1996). Activating mutations of rhodopsin and other G protein-coupled receptors. *Annu Rev Biophys Biomol Struct* **25**: 287–314.

52. Redmond, T. M., Poliakov, E., Yu, S., Tsai, J.-Y., Lu, Z., Gentleman, S. (2005). Mutation of key residues of RPE65 abolishes its enzymatic role as isomerohydrolase in the visual cycle. *Proc Natl Acad Sci USA*. **102**:13658–13663.

53. Robson, J. G. & Frishman, L. J. (1996). Photoreceptor and bipolar cell contributions to the cat electroretinogram: a kinetic model for the early part of the flash response. *Journal of the Optical Society of America A* **13**, 613-622.

54. Robson, J. G. & Frishman, L. J. (1999). Dissecting the dark-adapted electroretinogram.
Doc Ophthalmol. **95(3-4),** 187-215.

55. Saari, J. C., Garwin, G. G., Van Hooser, J. P., Palczewski, K. (1998). Reduction of all-*trans*-retinal limits regeneration of visual pigment in mice. *Vision Res*. **38**:1325–1333.

56. Sakai, N., Decatur, J., Nakanishi, K., Eldred, G. (1996). Ocular Age Pigment "A2-E": An Unprecedented Pyridinium Bisretinoid *J. Am. Chem. Soc.* **118**, 1559–1560.

57. Sillman, A. J., Ito, H. & Tomita, T. (1969a). Studies on the mass receptor potential of the isolated frog retina. I. General properties of the response. *Vision Research* **9**, 1435-1442.

58. Silva G. A., Hetling, J. R., Pepperberg, D.R. (2001). Dynamic and steady-state light adaptation of mouse photoreceptors in vivo. *J. Physiol* **534**, 203-216

59. Sokolov, M., Lyubarsky, A. L., Strissel, K. J., Savchenko, A. B., Govardovskii, V. I.,Pugh, E. N., Jr., Arshavsky, V. Y. (2002). Massive Light-Driven Translocation of Transducin between the Two Major Compartments of Rod Cells: A Novel Mechanism of Light Adaptation. *Neuron* **34**, 95-106.

60. Sparrow, J. R., Boulton, M. (2005). RPE lipofuscin and its role in retinal pathobiology. *Exp Eye Res*. **80**:595-606.

61. Sullivan, J. M. (2009). Focus on Molecules: ABCA4 (ABCR) – An import-directed photoreceptor retinoid flippase. *Exp Eye Res*. **89**, 602-603

62. Sun, H., Nathans, J. (2001). Mechanistic studies of ABCR, the ABC transporter in photoreceptor outer segments responsible for autosomal recessive Stargardt disease. *J Bioenerg Biomembr*. **33**, 523–530.

63. Wenzel, A., Reme,´ C. E., Williams, T. P., Hafezi, F., Grimm, C. (2001). The Rpe65 Leu450Met variation increases retinal resistance against light-induced degeneration by slowing rhodopsin regeneration. *J Neurosci*. **21**:53-58.

64. Wilden, U., Hall, S. W., and Kuhn, H. (1986). Phosphodiesterase activation by photoexcited rhodopsin is quenched when rhodopsin is phosphorylated and binds the intrinsic 48-kDa protein of rod outer segments. *Proc Natl Acad Sci U S A.* **83(5),** 1174-1178.

65. Wu, G., Hubbell, W. L. (1993). Phospholipid asymmetry and transmembrane diffusion in photoreceptor disc membranes. *Biochemistry*. **32**:879–888.

66. Yau, K-W (1994) Phototransduction mechanism in retinal rods and cones. *Invest Ophthalmol Vis Sci* **35,** 9-32.

67. Young, R. W., Bok, D. (1969). Participation of the retinal pigment epithelium in the rod outer segment renewal process. *J Cell Biology*. **42**:392–403

PART II

SUMMARY

In retinal degenerative diseases like age-related macular degeneration (AMD), there is a loss of photoreceptors and subsequent blindness. However, inner retinal neurons that synapse with the photoreceptors are thought in many cases to be intact and capable of function. Part II of this thesis project is a component of an overall research program that is aimed at developing a type of bioengineered molecular structure (termed a “nanoscale neuromodulating platform”, or “NNP”) that can restore vision lost in AMD. The NNP devices are light sensitive molecular structures that when injected into the eye, will bind to extra-cellular domains of postsynaptic membrane receptors on specific cells of the inner retina. In response to light, there will be a change in the conformation of the NNPs, thus modifying (activating or inhibiting) the function of the receptor.

My role in the overall research program has concerned the testing and delivery of test NNP “anchor” and “linker” components being developed by the project’s research team. The anchor component will allow the NNPs to bind to post-synaptic membrane receptors. Two membrane receptor types that are sensitive to the neurotransmitter gamma-aminobutyric acid (GABA, which is an important inhibitory neurotransmitter found in the vertebrate central nervous system) were used as test systems in this thesis project; the $GABA_C$ receptor and the $GABA_A$ receptor. For the $GABA_C$ receptors, two types of anchoring systems have been developed: a polyclonal antibody ($GABA_C$ Ab-*N*14) directed against a specific amino acid segment of the *N*-terminal extracellular

SUMMARY (continued)

domain region of the $GABA_C$ receptor; and a scFv (single-chain variable fragment) with anti-$GABA_C$ activity that has been developed using phage display technology. For the $GABA_A$ receptor, a commercially available antibody ($GABA_A$-Ab) was used as an anchoring system. The “linker”, or interfacing component used here was the B-domain, which was common to both receptor test systems. The B-domain is a shorter chain segment of a larger Protein A, which is a type of surface protein found in the cell wall of the *Staphylococcus aureus* bacteria and has high binding affinity to antibodies, like the $GABA_C$ and $GABA_A$ antibodies mentioned above. The B-domain served as a scaffold to which the other components of the NNP, like the “photosensor” and “effector” can be attached. In my project, I have tested protein structures consisting of the $GABA_A$ antibody attached to the B-domain and the $GABA_C$ antibody bound to the B-domain in electrophysiological and fluorescence visualization studies.

The second aspect of Part II of my thesis project has concerned the delivery of test protein structures or complexes (described above) to $GABA_C$-receptor expressing cells. The objective here was to permit the focal application of tiny quantities of NNP-like test structures to the receptor-expressing cell surface under conditions that allow electrical recording of the effects of this presentation. In Part II of the thesis, we have functionalized commercially available streptavidin (which is a protein purified from the bacterium *Streptomyces avidinii)* micron-sized beads with a quantum dot compound (henceforth identified as the 50:50 compound) that has multiple poly(ethylene glycol) (PEG) chains (~150), half of which are terminated with muscimol, which is a $GABA_C$ receptor agonist and the other half with biotin, which enables attachment to the

SUMMARY (continued)

streptavidin beads through the Streptavidin-biotin interaction. Individual functionalized beads were held at the tip of glass micro-pipettes (tip diameter ~1-2 µm) through gentle suction. With the aid of a micro-manipulator, such a microprobe was used to present the muscimol terminated 50:50 compound functionalized on the beads, to the $GABA_C$ receptors expressed on a model cell system (neuroblastoma cells) held under patch clamp, to record the electrophysiological effects of binding of the muscimol to the $GABA_C$-receptors.

1. AIMS

Aim 2.1: Testing and assembly of the protein complexes consisting of $GABA_C$ Ab-*N*14 and B-domain *in-vitro*.

The first protein construct under development employed a polyclonal antibody for anchoring and the attached scaffold protein B-domain. A second such construct used a monoclonal antibody (the scFv). Aim 2.1 involved assembly of the above-mentioned constructs *in vitro* and also testing, through fluorescence visualization, binding of the protein complexes to $GABA_C$ receptor expressing neuroblastoma cells. This involved tagging the anchor complex with a fluorophore and testing for fluorescently labeled target cells by fluorescence microscopy. This investigation further involved studying the effect of $GABA_C$ receptor binding of the protein complex on the electrophysiological responses of the neuroblastoma cells. Anchoring the molecular device of the kind under development in the project must preserve much (and ideally, essentially all) of the electrophysiological activity of the target receptor. It was therefore important to test whether the binding of the protein complex to the $GABA_C$ receptors modulates or changes the response properties of the receptors.

Aim 2.2: Testing the microprobe technology

This aim was to develop a microscale probe delivery system that can achieve focal and efficient delivery of the protein complex to a model mammalian cell line ($GABA_C$-expressing neuroblastoma cells). Aim 2.1 experiments above, involved the delivery of solubilized protein complex to $GABA_C$-expressing target cells by inclusion of the protein complex in the solution bathing (perfusing) the cell. However, the limited amount of the

sample of protein complex (i.e., the availability typically of only tiny quantities of this NNP test component), together with possible solubility issues of these protein complex preparations in aqueous medium, encouraged a focal, direct presentation of the type that was developed in this aim of the thesis work.

Thus, a population of commercially available streptavidin (SA) and Nickel (Ni^{2+}) beads were first functionalized with the protein complex described in Aim 2.1. Single functionalized beads were then held at the tip of glass micropipettes (with tip diameter of 1-3 μm) through gentle suction. A micro-manipulator with nanometer (~40 nm) precision was employed to guide and position the microprobes in close proximity (gently touching) to the surface of $GABA_C$-receptor expressing neuroblastoma cells. The electrophysiological effect of the binding of the protein complex (bound to the surface of the spherical bead) to the $GABA_C$ receptors on the target cells was studied through whole cell patch clamp technique (see Section 3.4 below).

Aim 2.3: Testing the binding of the protein complex consisting of the $GABA_A$-Ab: B-domain to mouse retinal slices

Another system tested in this thesis project was the use of a commercially available $GABA_A$ antibody as an anchoring system. In this aim, a protein complex consisting of this primary $GABA_A$-Ab coupled with the scaffold protein B-domain and a fluorophore was tested for its binding to $GABA_A$ receptors on mouse retinal slices.

These three aims and their relation to the overall project are summarized in Fig. 7.

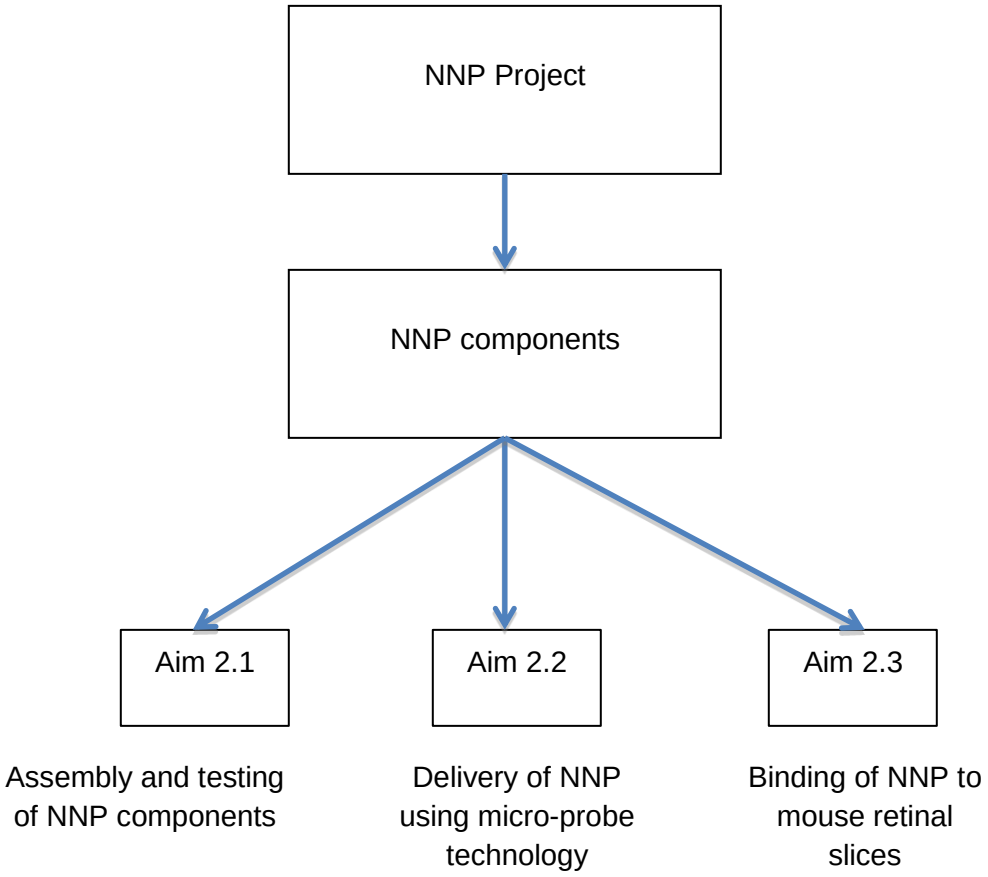

Fig. 7: **General outline of the overall NNP thesis project.**
The NNP project consists of the several NNP components that were tested and have been described in detail in the accompanying text. The overall project consisted of three Aims; Aim 2.1 involves the *in-vitro* assembly and testing of the NNP components. Aim 2.2 concerned the delivery of candidate NNP structures to test mammalian cell systems using the microprobe technology. Aim 2.3 involved testing the binding of the candidate anchor components to isolated mouse retinal slices.

2. BACKGROUND

2.1 General background

In close collaboration with colleagues in other laboratories at UIC and at other institutions, our laboratory is conducting fundamental research on biomedical molecular structures that can interface with specific post-synaptic receptor proteins on the inner retinal neurons. The overall goal of this project is development of a new type of molecular therapy for photoreceptor degenerative diseases such as age-related macular degeneration (AMD). In AMD, the photoreceptors are a primary target of the disease, and disease progression leads to gradual photoreceptor deterioration and hence blindness (Fine *et al.*, 2000, Zarbin, 2004). However, in many cases, retinal neurons "downstream" from the photoreceptors, i.e. bipolar cells and ganglion cells of the retina, remain intact and potentially capable of function. Visual processing in the retina depends on electrical and chemical synaptic transmission, and thus on postsynaptic receptor proteins present on different postsynaptic cell types in both outer and inner layers of the retina. One approach being used by many groups is the electronic retinal prosthesis. This type of a retinal prosthesis consists of a camera, which captures images and then processes and converts the image into electrical impulses that can stimulate the ganglion cells (Humayun *et al*., 2009). These electrical impulses are then transmitted through the optic nerve to the brain, which perceives the light and dark spots corresponding to the electrode stimulation, which in turn correspond to the captured images (Humayun *et al*., 1996, Rizzo *et al*., 2003). Other groups are designing methods for delivering neurotransmitters (such as L-glutamate, a native neurotransmitter) to the retinal neurons using microfluidic technology (Finlayson and Iezzi, 2010).

Such a prosthesis employs a controlled delivery of neurotransmitters through an array of micro-pump like devices, to the retina at different points in space and time. Some of the challenges facing an electronic retinal prosthesis includes; pixel density and electrode sizes such that maximum information, or maximum resolution can be provided by the stimulating array such that the brain can understand and utilize all the information, inter-electrode distance (in case of closely spaced high density electrode array) to reduce electrode cross-talk, and optimization of the distance between electrodes and the cells in order to avoid the need to adjust the stimulating signal intensity in each electrode (Palanker *et al*., 2005).

A number of different chemical strategies are being pursued by our group, and by other investigators (Gorostiza *et. al.*, 2007; Szobota *et al.*, 2007; Gorostiza and Isacoff, 2008), to allow light to control ion-channel types of postsynaptic membrane receptors of inner retinal cells. A very different approach to remedy the loss of photoreceptor function is one involving the use of stem cells (or retinal progenitor cells) (MacLaren *et al*., 2006), which can integrate and differentiate into rod photoreceptors and form synaptic connections with host cells, and at least partially restore visual function in photoreceptor-impaired experimental animals. In other studies, light sensitive photo-proteins such as channelrhodopsin-2, which is a rhodopsin-like protein with intrinsic channel activity (Nagel *et al.*, 2003) derived from green algae, have been extensively investigated in studies. Roska and colleagues have demonstrated that expression of channelrhodopsin-2 in ON bipolar cells in mice that have degenerated photoreceptors, evoke light sensitive spiking activity in the downstream ganglion cells (Lagali *et al.*, 2008). Deisseroth and colleagues have developed transgenic mice that express channelrhodopsins in specific neuronal types. Channelrhodopsins are light-sensitive,

cation permeable ion channels, whose photocurrents can be initiated and terminated with different wavelengths of light (Berndt *et al*., 2009; Zhao *et al*., 2008). Such a light-sensitive channelrhodopsin based mouse model is useful for studying *in-vivo* light-induced activation and neural circuit mapping (Arenkiel *et al*., 2007; Wang et al., 2007). Other approaches have been used to generate light sensitive K^+ selective ion channels (Banghart *et al*., 2004) and light sensitive ionotropic glutamate receptors (Volgraf *et al*., 2006). The common theme of both of these latter types of studies is to create a genetically engineered ion channel (for e.g., a ionotropic glutamate receptor iGluR) with a surface-exposed cysteine residue. The presence of a cysteine residue that is accessible on a receptor surface enables a compound containing a maleimide reactive group to specifically bind to the receptor. Use of an azobenzene photoswitch on the compound renders the entire structure (the genetically modified iGluR with the maleimide containing bound compound) light sensitive. The other end of the structure (the non-maleimide end) was terminated with a receptor ligand. The light-induced isomerization of the azobenzene photoswitch between the *cis* and *trans* states regulates access of a ligand-mimicking component of the cysteine-attached structure to a binding site on the target protein, thereby regulating the target channel's physiological activity.

The above-cited previous studies utilizing cysteine-modified target protein or channelrhodopsin in the target neuron necessarily involve genetic engineering of the cell, and thus, the possibility of complications (side effects) associated with the cell's expression of these non-native proteins. Considered in this context, it would therefore be highly desirable to have a receptor-specific molecular device that is workable with the native receptor (or other target protein) of the cell that one seeks to make light-sensitive. The focus of our research is to construct and design such devices (NNPs, as defined

above). The main components of this molecular device are an effector component, which is a neurotransmitter mimic of the $GABA_A$ receptor (like propofol, which is a $GABA_A$ receptor agonist) or the $GABA_C$ receptor (like muscimol), a photosensor component (like azobenzene) that can absorb light and cause a conformational change in response to light, and an anchoring system that can tether the molecular structure to a site present on the membrane receptor. This molecular structure will eventually be used as a therapy, where the physician will inject the device into the vitreous of the eye and the device will find its target receptor by diffusing through the retina to reach its targeted membrane protein.

The primary focus of current experiments in our project is the $GABA_C$ and $GABA_A$ receptor, types of postsynaptic membrane receptors that respond to the native neurotransmitter γ-aminobutyric acid (GABA). $GABA_C$ receptors are abundantly found in vertebrate retina and other tissues of the central nervous system (Sivilotti and Nistri, 1991; Albrecht *et al*., 1997; Enz and Cutting, 1999). Specifically, they are present on retinal bipolar cells (Qian and Dowling 1995; Qian, *et al*., 1997), rod-driven horizontal cells in the white perch (Qian and Dowling 1993), cone driven horizontal cells of the catfish (Dong *et al*., 1994; Kaneda *et al*., 1997) and amphibian ganglion cells (Zhang and Slaughter,1995). GABAA receptors are distributed throughout the mammalian brain, including the cerebral cortex, hippocampus, basal ganglia, thalamus and the brain stem (Young and Chu, 1990). In the retina, $GABA_A$ receptors are found on the axons of the ganglion cells of primates (Hughes *et al.,* 1989), ganglion cells and amacrine cells in the cat retina (Hughes *et al*, 1991), dendrites and axons of bipolar cells in macaques (Vardi and Sterling, 1994). These receptors are thought to play important roles in passing visual information from the photoreceptors to the higher centers of the brain. In our

project, we are focusing on developing NNPs that will attach to the $GABA_C$ and $GABA_A$ receptors and render them sensitive to light. Visualization and electrophysiology studies are being conducted to study the effect of the binding of NNPs on the $GABA_C$ and $GABA_A$ receptors expressed on model cell systems.

$GABA_C$ and GABAA receptors are ligand-gated inhibitory chloride channels. The GABA-induced currents of the $GABA_C$ receptor are mediated by chloride ions. Binding of the GABA ligand in the binding pocket of the receptor leads to a conformational change of the protein and a consequent opening of the ion channel. In the case of the $GABA_C$ receptor, the ion channel remains open and exhibits relatively little desensitization (a state in which the neurotransmitter remains bound to the binding pocket of the receptor, but the ion channel is closed) as long as GABA remains bound in the receptor's ligand binding pocket. Removal of the GABA ligand leads to channel closure and brings the current back to baseline. However, the $GABA_A$ receptor does undergo desensitization. $GABA_C$ and $GABA_A$ receptors are pentameric in structure, i.e., they have five subunits. Native $GABA_C$ receptors consist of ρ1, ρ2 and/or ρ3 subunits (Amin and Weiss 1996). However, it is well established that ρ1 subunits can assemble to form fully functional homomeric receptors, and this relatively simple system is serving as our model for study (neuroblastoma cells engineered to stably express ρ1 $GABA_C$ receptors). Native $GABA_A$ receptors in the retina and the brain can be formed from the following subunits; α (6 types, α1-6), β (3 types, β1-3), γ (3 types, γ1-3), δ, ε, π and θ (McKernan and Whiting, 1996).

As noted above, the ultimate NNP device will be designed for introduction into the eye and will be capable of diffusing to the ultimate target sites of the inner neurons of the retina. However, in most cases, the candidate anchoring structures are available in

only tiny quantities and are being tested in the model cells (neuroblastoma cell line, see below). It is desirable to have available a delivery system that permits focal presentation of test anchor component to the target cell surface where the target receptors are being expressed. In a conventional system of the type used in experiments to date, treatment of the target cells with a test sample such as a protein involves dispersal of the sample in the perfusing aqueous medium that bathes the cell. However, in such treatments, a considerable portion of the investigated sample is lost by wash-out of the perfusate. To achieve presentation of the test sample to the target cell with minimal consumption and minimal loss of material, we have developed a bead-micropipette based probe system with a suitable chemical functionalization of the bead surface that will attach the protein structure and in controlled manner deliver the protein to $GABA_C$ receptors on the neuroblastoma cells. Experiments using such a bead based microprobe system will be discussed in the Results section.

2.2 Polyclonal and monoclonal antibody

Aim 2.1 concerns the assembly and testing of a polyclonal and a monoclonal antibody. A polyclonal antibodies are a mixture of different antibodies obtained from a diverse population of immune cells that have specificity for different epitopes on an antigen and a monoclonal antibodies are highly purified antibodies obtained from identical immune cells and specific to a single epitope on an antigen. $GABA_C$ antibodies based NNP anchoring systems on $GABA_C$ receptor-expressing neuroblastoma cells. There are two main purposes here: to confirm the binding of the above-mentioned protein complexes on $GABA_C$-receptor-expressing neuroblastoma cells using

fluorescence visualization, and to determine the effects of binding of the protein complexes on the electrophysiological responses of the $GABA_C$-receptor-expressing target cells. In these experiments, the prepared test components were tested by dissolving them in physiological saline (Ringer solution) and presenting the supplemented solution to $GABA_C$-expressing cells and then visualizing them in a fluorescence microscope or by recording GABA-elicited membrane currents from treated *vs.* untreated cells.

The first objective in the development of the NNPs was to have an anchoring system on the $GABA_C$ receptors. Dr. Helène Gussin and other colleagues in our project have developed a polyclonal antibody in the guinea pig, against a 14-mer peptide located in the *N*-terminal extracellular domain region of the human ρ1 $GABA_C$ receptor. This guinea pig antibody ($GABA_C$ Ab-*N*14) has a high specificity for the extracellular domain of the $GABA_C$ receptor (Gussin *et al*., 2011), and is a principal candidate for use as an anchoring system.

A related but distinct type of anchor, also under development in the project, is one based on a type of monoclonal antibody termed a single-chain variable fragment (scFv). Such an scFv based monoclonal antibody system is a better defined system as compared to the polyclonal antibody ($GABA_C$ Ab-*N*14) which by itself is a mixture of proteins. A monoclonal antibody system is more amenable for conjugation and addition of different residues (cysteine, biotin) as compared to a polyclonal antibody. Thus, although a working polyclonal antibody is available, it would be desirable to have an scFv-based monoclonal antibody that has good binding and does not destroy the electrophysiological responses of $GABA_C$ receptors expressed on neuroblastoma cells. My role to date in this line of study was the electrophysiological testing of candidate

scFv's in preparations of $GABA_C$-expressing neuroblastoma cells. scFv's reactive with $GABA_C$ Ab-*N*14 were selected by phage display technology and prepared by Drs. Adnan Memic and Brian Kay (Dept. of Biological Sciences, UIC). In phage display technology, a heterogeneous mixture of bacteriophages (called a phage library; bacteriophages are a broad class of viruses that infect bacteria) each displaying a different peptide on its surface, are tested for binding to a target peptide (for e.g., our $GABA_C$ Ab-*N*14 peptide). We can then "capture" phages displaying peptides that can specifically bind to the target peptides from a large phage library displaying many different peptide structures. Thus, a phage library was screened for binding to the $GABA_C$ Ab-*N*14 peptide. Following four rounds of phage-display selection of this library using the $GABA_C$ Ab-*N*14 peptide as a target, five scFv binders (i.e. antibody fragments (peptides) that bound specifically to $GABA_C$ Ab-*N*14) were identified (termed Pep1, Pep7, Pep8, Pep11 and Pep12). Soluble forms of these scFv's were then generated by Drs. Kay and Memic. Section 4.1.3 below describes experiments involving the testing of scFv's.

2.3 B-domain

In addition to an anchor system suitable for the $GABA_C$ receptor (see above section), the desired NNP device requires an interfacing component, or linker, which not only has a strong binding affinity for the $GABA_C$ Ab-*N*14 and the scFvs, but also serves as a scaffold to which the photosensor and the effector can be attached. One such component is Protein A. Protein A is a well-studied protein produced by *S. aureus* bacteria (Boyle and Reis, 1987). It has played an important part in biochemical research due to its ability to bind to immunoglobulins. It can bind to the Fc region (the part of the

tail region of the antibody that interacts with receptors and complement proteins) of IgG antibodies through interaction with the heavy chains of the antibodies. Protein A, when immobilized on a solid support, can act as an efficient and reliable immunochemical agent for purification and detection of IgG antibodies (Uhlen *et al*., 1992; Nord *et al*., 1997; Nygren and Skerra, 2004). An engineered shorter chain segment of Protein A, known as B-domain, is a three-helix, 59 amino acid chain segment that, like Protein A, binds to the Fc portion of IgGs. The advantage of using B-domain over Protein A is that the B-domain is a smaller component, and at the same time is highly soluble and thermally stable like Protein A (Nilsson *et al*., 1987; Braisted and Wells, 1996). The B-domain thus captures key properties of Protein A structure and suggests its use as a scaffold. In our work, the B-domain has been modified by attachment of a hexa-histidine (his6) tag. Histidine is an amino acid that can form coordination complexes with a transition metal like Nickel (Ni^{2+}). The nitrogen atoms of the imidazole moiety of histidine are the most frequent side chain donor groups that bind to a central Ni^{2+} to form coordination complexes. This property enables chelation of histidine with Ni^{2+} coated surfaces and makes possible the attachment of the B-domain to Ni^{2+}-coated plates for study in ELISA-type assays (section 4.1), as well as binding of the protein complex through the His6 tag, to Ni^{2+}- beads. Because histidine contains an imidazole moiety, free imidazole has the ability to detach his6-tagged proteins from a Ni^{2+}-coated surface, by mimicking the imidazole groups of histidine. Thus the Ni^{2+}-his6 binding is reversible, in that once bound, the his6 can be detached from the Ni^{2+} by addition of imidazole. The B-domain we are investigating has also been engineered to contain a terminating cysteine residue, which enables attachment of other chain linkers to the B-domain via a maleimide, a cysteine reactive group. In current experiments, we have attached a

fluorescence-tagged maleimide compound (maleimide-Alexa, where Alexa is a fluorophore, or a fluorescent molecule) to the cysteine of the B-domain. This derivatization of the B-domain with Alexa has enabled fluorescence visualization of the B-domain itself and of the protein complex consisting of B-domain and antibody through the Alexa fluorophore. Another investigated derivative of the B-domain was a maleimide-terminated poly(ethylene glycol) 3400 (PEG3400) chain containing a distally terminating biotin group. (In PEG3400, 3400 refers to the molecular weight in daltons; the average length of commercially obtained PEG3400 is approximately 77 PEG units). The reason for including a PEG chain here is the added flexibility in terms of chain length. The B-domain-maleimide-poly(ethylene glycol) 3400-biotin (henceforth termed B-d-M-B) was used in a group of experiments described later in the text. We also employed a FITC (fluorescein isothiocyanate, a derivative of fluorescein, which is an organic compound used as a dye for fluorescent labeling) labeled form of the B-domain; this was prepared by our colleague Dr. Nasser Qtaishat. In this form of the B-domain, FITC molecules (potentially 4-6) can be conjugated to lysine residues of the B-domain protein, yielding a stable and highly fluorescent FITC-labeled B-domain. Thus we have three forms of the B-domain; the B-domain by itself, the B-d-M-B and the FITC-B-domain.

The three different anchoring systems and the several forms of the B-domain used in this project are depicted in the flowchart in Fig. 8.

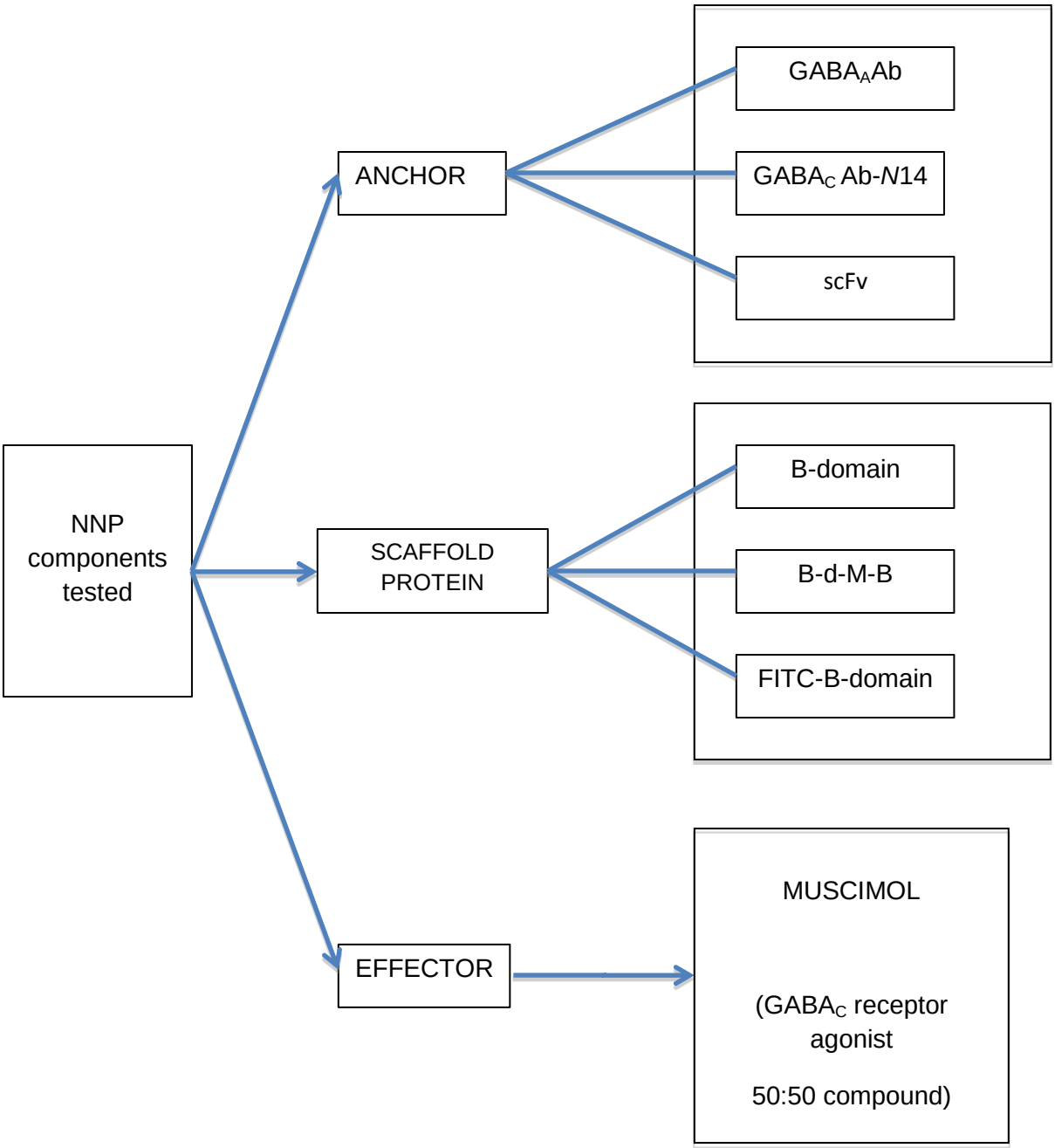

Fig. 8: **The several components of the NNP used in this project.**
Three main components were tested: the anchor, scaffold protein and effector. The anchor consists of the GABA$_A$-Ab, specific to the GABA$_A$ receptor, the polyclonal GABA$_C$ Ab-*N*14 antibody and monoclonal antibody scFv that is specific to the GABA$_C$ receptor. The scaffold protein used was the B-domain, in several forms, the important ones being; the B-domain by itself, the B-domain-maleimide-PEG3400-biotin (B-d-M-B) and the FITC-B-domain. The effector component tested this thesis project was muscimol, a GABA$_C$ receptor agonist. Muscimol was present in the form of the 50:50 compound and was tested in the micro-probe patch-clamp electrophysiology experiments on neuroblastoma cells.

2.4 Patch-Clamp recording

The electrophysiology experiments of Aims 2.1 and 2.2 involve the recording of membrane currents from intact cells. The technology of whole-cell patch-clamp, developed originally by Neher and Sakmann (1976), is widely used to the study membrane receptor physiology including $GABA_C$ receptors (see below) (Hamill *et al*., 1981; Cahalan and Neher, 1992; Jurkat-Rott and Lehmann-Horn, 2004; Wong *et al.*, 2005). The following text briefly summarizes the principle of this technique. The patch-clamp technique consists of a glass micropipette with a tip diameter of ~1 µm pressed against the cell membrane. The hollow glass pipette is filled with a salt solution resembling that found in the intracellular fluid. A metal electrode within the glass micropipette is in contact with the pipette solution. The micropipette tip is advanced (by micromanipulator) to make contact with the cell's surface membrane (plasma membrane). Gentle suction is applied to the micropipette via a port on the shank of the micropipette. This allows formation of an extremely tight seal (giga-ohm seal) between the pipette tip and the membrane. This seal lowers the electronic noise, which otherwise would interfere with the needed measurements of very small currents (range of picoamperes). Once a tight seal is formed, more suction is applied to the micropipette. This ruptures the patch of cell membrane immediately beneath the pipette tip, and allows the metal electrode to measure the currents due to the opening and closing of the cell's ion channels in response to stimulation (in our case, the $GABA_C$ receptor agonist GABA). This metal electrode is connected to an amplifier that measures the current through the ion channels of the cell.

2.5 Interactions (SA-biotin, Ni^{2+}-his)

In the original plan for the thesis discussed in the preliminary report, the plan was to develop microprobes, which have the ability to deliver tiny amounts of protein complex (described above) directly to the cell surface. The aim here was to use custom micro-machined silicon microprobes (in collaboration with Dr. Laxman Saggere and colleagues in the UIC Department of Mechanical and Industrial Engineering) and functionalize them with either nickel-nitrilo-triacetic acid (Ni^{2+}/NTA) or with streptavidin (SA) (in collaboration with Dr. David Thompson and colleagues in the Department of Chemistry at Purdue University). We hypothesized that the above-mentioned functionalization would enable attachment of a B-domain-containing protein complex to the tip of the probe. In the case of Ni^{2+}/NTA functionalization, binding to the probe surface would be through the histidine (his) tag of the B-domain. In the case of SA functionalization of the probe, binding would occur via the biotin label of biotin-functionalized B-domain (B-d-M-B). Presentation of the functionalizing protein to the cell surface would enable the study of specific interactions of the protein complex with the $GABA_C$ receptors on the surface of the neuroblastoma cells. The rationale for using such a preparation is described below.

This proposed approach followed those of previous studies employing chemical modification of probe surfaces to make these surfaces sensitive to specific molecular interactions. Chemically modified probe tips have been used in atomic force microscopy (AFM) to image and measure interactions between specific types of target molecules supported on surfaces (Van der Vegte and Hadziioannou, 1997; Noy *et al*., 1995; Noy *et al*., 1998). Using chemically functionalized probes, it is possible to measure interaction forces of receptor-ligand pairs at single- molecule levels (Allen *et al*., 2003; Zlatanova *et al*., 2000; Janshoff *et al*., 2000; Hugel and Seitz, 2001). In particular, Schmitt *et al.* have

modified AFM tips with nitrilo-triacetic acid (NTA) (Picaud *et al*., 1998). NTA contains negatively charged carboxyl groups that can form a complex with positively charged Ni^{2+} ions (Schmitt *et al*., 2000). Such a Ni^{2+}/NTA complex has the ability to bind hexa-histidine- (His6-) tagged proteins or peptides (Fig.3). An important advance in this technology was provided by Hinterdorfer *et al.*, who used spacer molecules such as PEG chains. The inclusion of the PEG component provides advantages in flexibility, mobility and orientation of the distal (i.e., reactive) end of the functionalizing molecule on the probe tip, and thus facilitates the study of specific molecular interactions between the functionalizing molecule and the target surface (Hinterdorfer *et al*., 1996). Using a long-chain PEG molecule along with the Ni^{2+}/NTA-his6 system greatly improved the binding properties of the his6-tag to the PEG-Ni^{2+}/NTA functionalized probes.

In another study, Kang *et al*. (2007) grafted NTA-PEG derivatives on silica surfaces to test the ability of the modified surfaces to capture his6-tagged structures through the Ni^{+2}/NTA chelation (Kang *et al*., 2007). This study showed that a Ni^{2+}/NTA modified silica surfaces are capable of efficiently immobilizing his6-biotin/Streptavidin-AlexaFluor555 structures through interactions between the His6-tag and the Ni^{2+}/NTA-PEG (Fig. 9). In recent studies, multi-walled carbon nanotubes functionalized with his6-tagged protein have been used for solid phase extraction of Cu^{2+} and Ni^{2+}. Using his6 functionalization enhanced the selectivity of the carbon nanotubes in solid-phase extraction of metal ions (Liu *et al*., 2009).

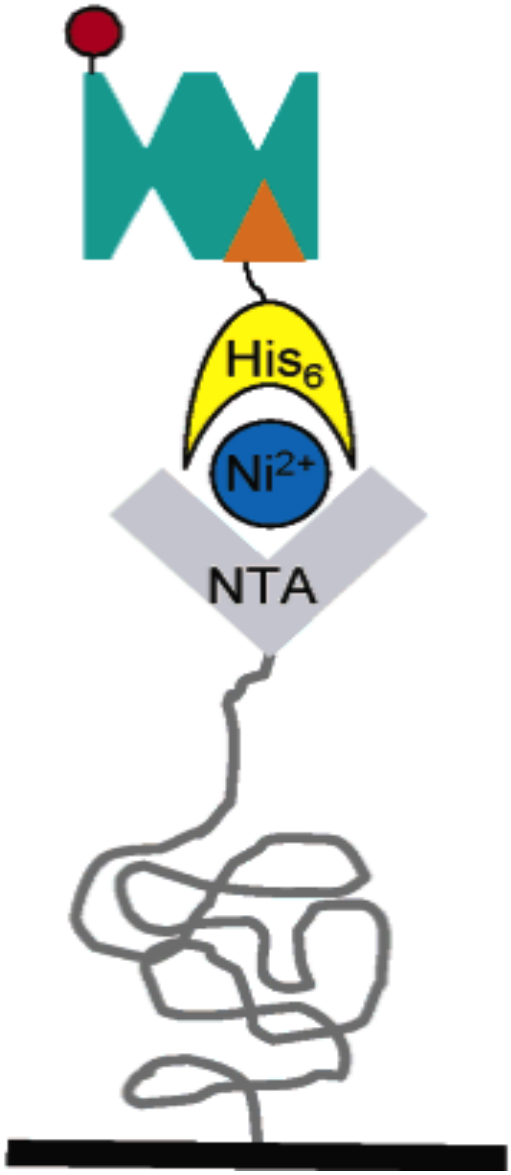

Fig. 9: An example of attachment of a protein to a surface through a Ni^{2+}/NTA interaction. Ni^{2+}/NTA/PEG modified silica surface is capable of capturing a His6 tagged protein structure through specific interactions between the Ni^{2+}/NTA and the His6 tag of the attached protein. The protein structure is represented by the color green (Kang *et al*., 2007).

As one of the major aims of this project (Aim 2.2), the proposal was to develop a silicon probe structure of micrometer tip dimensions, i.e., of size smaller than the diameter of the model cell (neuroblastoma cell) on which the experiments are being conducted. The tip of the probe was to be coated with a Ni^{2+}/NTA complex similar to that described above. Dr. David Thompson and his colleagues at Purdue University collaborated with our research group to prepare the silicon probes that will contain the needed Ni^{2+}/NTA coating.

The main purpose of these probe type of experiments was to achieve a focal delivery of the protein complex on the neuroblastoma cells. By positioning the probe tip immediately adjacent to the cell surface, we sought to prevent diffusion of the protein complex into the bulk solution, and thus avoid wasting of the precious protein. By using a high concentration of the protein complex on the probe tip, we intended to achieve robust binding of the protein complex to the cells within a several-min period. This short incubation time resulting from the high concentration and close proximity of the complex to the cells was to enable patch-clamp recording from a single cell both before and after binding of the protein complex. However, before proceeding to the use of micro-scale probe tips, it was necessary to ascertain the suitability of a silicon-based surface preparation that was functionalized with Ni^{2+}/NTA, capable of attaching the his6-tagged protein complex, and capable of releasing the protein complex upon treatment with imidazole. As a preliminary test system to develop and evaluate these needed features, we used ~5 mm x 5 mm silicon surfaces that, because of their large size, are relatively easy to handle and to analyze through fluorescence visualization. The goal was to demonstrate the workability of these functionalized “macro” silicon surfaces, and then later focus on the micron-sized silicon probes.

The average diameter of a neuroblastoma cell is ~10 µm. Each $GABA_C$-expressing neuroblastoma cell is expected (based on previous electrophysiological studies) to express tens of thousands of $GABA_C$ receptors on the surface of the cell. Each individual channel (i.e., each petameric receptor, with outer diameter ~8 nm) contributes to the total current produced by the cell as measured by the patch-clamp setup, in response to stimulation. It is desirable to have a tip dimension that is large enough to stimulate a sufficient population of $GABA_C$ receptor, such that a measurable response can be detected. Thus, we anticipated the use of probes with tip diameter in the range of 6-7 µm. A tip diameter of this size will not cover the entire cell, but we anticipated that it would allow activation of a population of $GABA_C$ receptors sufficient to produce a robust response

However, after repeated attempts in which we tried to measure the presence of Ni^{2+}/NTA on the silicon surfaces with the aid fluorescence microscopy, we did not find any evidence of successfully functionalization of macro-silicon surfaces (square surfaces with ~5 mm x 5 mm sides) with Ni^{2+}/NTA. The inability to detect the presence of the Ni^{2+}/NTA on the silicon surface through optical detection methods could be attributed to two possible reasons: either that there was no Ni^{2+}/NTA bound to the silicon surface, or the resolution of the measurement procedure was insufficient to detect minute molar concentration of Ni^{2+}/NTA present on the silicon surface. Use of other optical methods, specifically fluorescence confocal microscopy, was similarly unsuccessful. This difficulty presented a major hurdle in the plans of preparing custom micro-machined silicon probes, which would then be functionalized with Ni^{2+}/NTA and SA. To overcome these problems, we turned our attention to using commercially available Ni^{2+} and SA-beads.

2.6 Bead based microprobes

Instead of using micron-sized silicon surfaces that are functionalized with Ni^{2+}/NTA and SA and then bound with the protein complex of interest, we decided to use commercially available micron-sized beads.

Accordingly, streptavidin (SA-) coated beads of diameter 2.8 μm and 7.9 μm were obtained from Solulink. These beads can bind biotinylated (having a terminating biotin) protein structures through the biotin-SA interaction. By using B-d-M-B based protein complex bound to the beads, we anticipated the feasibility of capturing individual beads at the orifice of a hollow glass micropipette to achieve a probe-like assembly. This type of probe assembly could then be used to present the protein of interest to $GABA_C$ receptor-expressing cells to study the interaction of minute amounts of protein with a population of receptors present on the neuroblastoma cell surface.

Similarly, nickel-coated beads were obtained from Millipore Inc. (Billerica, MA). These beads were ~10 μm in diameter. They contain an outer coating of Ni^{2+} ions, which can bind his6 tagged proteins (like the his6-tagged B-domain). In the case of the SA-beads, once the SA-biotin bond is formed, it cannot be disrupted. The advantage of using the Ni^{2+}-beads over SA-beads is that the binding of the Ni^{2+}-his-tag is reversible. Addition of imidazole can disrupt the Ni^{2+}-his-tag bond, thus releasing the protein. Thus, a Ni^{2+}-bead preparation can be used for delivering a protein structure to the $GABA_C$ receptors expressed on the neuroblastoma cells. Individual protein structure functionalized Ni^{2+}-beads will be attached to the tip of glass micro-pipettes and with the help of the micro-manipulator, presented to $GABA_C$ receptors present on the surface of neuroblastoma cells.

3. METHODS

3.1 ELISA

The enzyme-linked immunoabsorbent assay (ELISA) method was used to prepare protein complexes and multiple forms of the B-domain (described later in the thesis report). Specifically, Ni^{2+}-coated 96 well plates were used to in the ELISA preparation. The his6 tag of the B-domain enables binding to nickel-coated plates through the Ni^{2+}- his6 interaction. Preparation of the protein complex on Ni^{2+} plates is done through sequential addition of individual components of the complex to the plates. A detailed description of the use of the 96-well Ni^{2+} plates is described further in Sec. 4.1.1 of Results. For example, as described earlier in the report, it was desirable to have a biotin on the B-domain to enable the binding of the B-domain to SA-coated beads as well as SA-conjugated fluorophores (through a strong non-covalent streptavidin-biotin interaction. Thus the B-d-M-B that was used in several experiments was prepared on Ni^{2+}-coated 96-well ELISA plates. Briefly, 200 µM of B-domain was added to Ni^{2+} plates and incubated at 4°C overnight. Several wells (duplicates) were used to prepare the protein complex and each well held 100 µl of solution. The concentration of the B-domain was chosen such that it completely saturated all of the Ni^{2+} binding sites available in a single well of the 96-well plate. This was done by using a concentration (in terms of moles) of the B-domain that was 2-5X the available his6-binding Ni^{2+} sites per well on the 96-well plate. The plates were then washed three times with 200 µl Tris-Buffered Saline Tween-20 (TBST). The sulfur of a thiol group of cysteine of a single B-domain molecule can bind to the cysteine of another B-domain through a disulfide bond. This yields solutions where the B-domain molecules are in a dimer form (two B-domain

molecules bound to each other) rather than being in a monomer form, which is undesirable. To avoid such a scenario, the plate containing the B-domain was then treated with the reducing agent dithiothreitol (DTT) for 40 min at 37°C, to disrupt the disulfide bonds that form between the cysteines of B-domain, thus yielding a monomer form of the B-domain. The plates were washed four times with TBST. The maleimide-PEG3400-biotin at 2 mg/ml was then added to the plates and allowed to incubate for 2 hr at room temperature. After 2 hours, an elution buffer (20 mM sodium phosphate, 0.5 M sodium chloride and 500 mM imidazole, pH 7.4) was added to the plates to release the biotinylated protein complex from the Ni^{2+} plates. The protein complex collected from all of the wells was divided into two 1.5 ml tubes. About 2/3 of the solution (~140 µl) from each tube was dialyzed overnight in 3500 Da cut-off dialysis cassettes (Thermo Scientific, Waltham, MA) to filter out the imidazole contained in the elution buffer. The solution, which was now about 1 ml was then added to concentrators (3500 Da cut-off) and concentrated until the remaining solution was ~200 µl. The solution was collected and a protein assay was conducted to calculate the concentration of the final protein complex. Concentrations of the final protein complex were in the range of ~2-20 µM for different preparation days.

3.2 Bead Preparation

Two types of beads were used in this thesis project; streptavidin-coated magnetic beads (SA-beads) and nickel coated magnetic beads (Ni^{2+}-beads). SA-beads of diameter 2.8 µm and 7.9 µm were obtained from Solulink (San Diego, CA) and Bang's Labs (Fisher, IN), respectively. Unless otherwise noted, the beads were packaged in 1

mg/ml vials and were stored at 4°C. The binding capacities of the beads were defined for a certain population/volume of beads rather than a single bead. Thus, even though the 7.9 μm beads have a larger surface area per bead, because of their size, there are more 2.8 μm beads in a given volume as compared to the 7.9 μm beads in the same volume. For this reason, the binding capacity of the 2.8 μm beads is quoted to be larger than that of the 7.9 μm beads.

The binding of the protein complex to the SA-beads is through the SA-biotin interaction. To enable the binding of the protein complex to the SA-beads, we used the B-d-M-b. For the bead-probe visualization and electrophysiology experiments we used the 50:50 compound, which has multiple biotin-tags (see Summary). In all cases, unless mentioned otherwise, we began with 10-20 μl bead solution per sample (from a vial containing 1 ml bead solution). From the available information on beads, the binding capacity (in terms of moles) for 10 μl of bead solution was calculated. In all cases, the concentrations in moles of the B-d-M-b and the 50: 50 compound to be incubated with 10 μl of beads were, respectively ~1-2 and ~50-100 times the binding capacity (in moles) of the beads. The amount of excess of the protein (in terms of moles) that was used for binding to the beads was dictated by the concentration of the stock solutions for the respective proteins. For example the concentration used for the 7.9 μm SA-beads was 10 mg/ml. We used 20 μl of beads per sample, which is equivalent to 200 ng of beads. The binding capacity of the beads was calculated by the manufacturer to be 0.061 μg per mg of bead solution. Biotin-FITC which has a molecular weight of 831 Da (or 831 g/mol) was used as the target compound by the manufacturer in their calculations of bead binding capacity. Using these specifications (binding capacity of 0.061 μg per mg of

bead solution, and 831 g/mol protein molecular weight), the binding capacity of 1 ml of bead solution was calculated to be 0.073 nmol/mg, or 0.015 pmol/200 ng (as mentioned above, we used 20 μl of beads per sample, which equates to 200 ng of beads per sample). Thus the binding capacity of 20 μl of beads was 0.015 pmol. The concentration of the stock solution of the 50:50 compound was 520 nM. We diluted the stock to ~5 nM to add to the beads, which equals 1.25 pmol of the 50:50 compound, which is 83X the binding capacity of the 7.9 μm SA-beads.

Bead preparation involved a standard protocol provided by the manufacturer. Briefly, before the addition of the B-d-M-b, the beads were first washed once with 1 ml of TBST. Washing of the beads involved addition of the TBST into the vial containing the beads. The vial was then placed in a special magnetic holder, which enabled the accumulation of the beads along the wall of the vial close to the magnet. The TBST was then removed, and 1 ml of fresh solution was added to the vial for further washing. The next step involved incubation of the beads in 1ml of casein (blocker casein in Tris-buffered-saline, Thermo Scientific, Rockford, IL) for 30 min to prevent non-specific binding of the protein complex (e.g., B-d-M-b bound to the $GABA_C$ Ab-*N*14 and a fluorescent secondary antibody) on the beads. The beads were then washed twice with TBST. The specific concentration of B-d-M-b was prepared in phosphate-buffered-saline (PBS) to yield 250 μl of total solution, which was added to the vial containing the casein blocked beads. The beads were incubated with the B-d-M-b for 1 hr. After 1 hr, the beads were washed 3 times with TBST. The beads were then incubated with the $GABA_C$ Ab-*N*14. The concentration in moles of the $GABA_C$ Ab-*N*14 was chosen to exceed the concentration of the B-d-M-B by ~10-100 times. The beads were then washed 3 times with TBST and then incubated for 1 hr with a secondary antibody with fluorescence Cy5

tag (excitation – 650 nm and emission – 670 nm) (experiment described in Section 4.2.1). The beads were washed 4 times with TBST and resuspended in ~250 μl of PBS. We then placed 100 μl of the bead solution in glass bottom cell-culture dishes (MatTek Corp, Ashland, MA, 35 mm, poly-d-lysine coated) for imaging in a fluorescence microscope.

The Ni^{2+}-beads used in this study were ~10 μm in diameter and were obtained from Millipore Inc., Billerica, MA. The B-domain can bind directly to the Ni^{2+}-beads through the his6 tag present on the B-domain. The procedure for binding of the protein complex onto the Ni^{2+}-beads was similar to the one used for the SA-beads. However, the wash buffer used in these experiments, as specified by the manufacturer, was different from the SA-bead experiments. Instead of PBS, the wash buffer contained 50 mM sodium phosphate, 300 mM sodium chloride and 5 mM imidazole at pH 8. The low concentration of imidazole was used in the buffer to prevent non-specific binding of the protein complexes on the Ni^{2+}-beads. For attaching a protein complex containing the B-domain, $GABA_C$ Ab-*N*14 and a 2°Cy5 to the Ni^{2+} beads is described here briefly (for detailed experimental results, see Section 4.3.1). The binding capacity for the Ni^{2+}-beads was quoted by the manufacturer to be 200-600 µg of protein for 200 µl of bead solution. However, in our experiments, we used 10 µl of bead solution, which equates to 30 µg binding capacity, as specified by the manufacturer. The calculations of the protein binding capacity of the Ni^{2+} beads were performed by the manufacturer using a 50 kDa (or 50,000 g/mol) his6-tagged antibody. Thus the binding capacity of his6-tagged proteins on 10 µl of bead solution comes out to be ~0.6 nmol. (30 µg/50 kg/mol = 0.6 nmol). Since we have a limited quantity of B-domain that we can use per experiment, we used 0.8 nmol (higher than the calculated capacity of ~0.6 nmol) of B-domain to bind

to the Ni^{2+}-beads. The beads were first washed with the 500 µl of wash buffer and then blocked with 1 ml casein. A magnetic holder was used to collect the beads on the wall of the tube. The casein was then pipetted out carefully without affecting the collected Ni^{2+}-beads. After removal of the casein, the tube was taken out of the magnetic holder and the wash buffer was added for washing purposes. Using this method, the beads were washed twice with the wash buffer. The $GABA_C$ Ab-*N*14 antibody was added at a concentration of 1.6 nM, which was in excess of the concentration of the B-domain used in the prior step. After 1 hr, the beads were washed three times with the wash-buffer and then incubated with 2°Cy5 (Abcam, Cambridge, MA) for 1 hour. After washing with the wash buffer three times, the beads were suspended in 200 µl of wash buffer. 100 µl of the beads were then added to a glass-bottom dish and visualized in a fluorescence microscope.

3.3 Electrophysiology

In all of the electrophysiology experiments in this thesis project, we have used the neuroblastoma cell line. The neuroblastoma cells were stably transfected to express human ρ1 $GABA_C$ (SHp5-human ρ1) receptors and were a gift from Dr. David S. Weiss (University of Texas Health Science Center at San Antonio). This is a well-established and well-studied mammalian cancer cell line in which ρ1 subunits can assemble to form fully functional homomeric $GABA_C$ receptors, and this relatively simple system has been used in this project for electrophysiology and visualization studies.

The whole cell patch clamp technique (Neher and Sakmann 1976, Wong *et al.*, 2005) was used in to study the electrophysiological responses of the cells to chemical (in

perfusion and probe studies, described in the Results section) stimuli. The perfusion system consisted of a series of tubes (10-12) connected through rubber tubing to a manifold. The manifold was mounted on a stage that was used to position the tip of the manifold in close proximity of the neuroblastoma cells. The flow of chemicals took place under gravity. All the tubes passed through a controller (H-S Systems) that was programmed to switch different tubes (or reservoirs) at pre-defined time intervals depending on the design of the experiment. At the end of an experiment, all of the tubes were washed with water to prevent contamination and bacterial growth.

Depending on the type of experiment, the cells were prepared either on the afternoon one day prior to the experiment (for visualization studies), or on the morning of the same day of the experiment (for electrophysiology experiments). For visualization experiments, cells were prepared one day earlier to allow a high density of cells to be present at the on the glass bottom dish. In visualization studies, each cell dish goes through a series of washes (~12-15 total washes in a single experiment), during which some cells are lost. The washes are necessary to ensure the removal of components of the protein complex ($GABA_C$ Ab-*N*14, B-domain, fluorophore) that did not bind to the cells during incubation, and thus prevent contamination. To ensure that we have enough cells left for visualization at the end of the experiment, it is desirable to have a high density of $GABA_C$ receptor expressing neuroblastoma cells in visualization experiments. For electrophysiology, each dish is washed just three times at the beginning of the experiment. Also, for patch clamp recording, it is advantageous to have single isolated cells (rather than cells clustered together) for ease of patch clamping.

The neuroblastoma cells expressing the $GABA_C$ receptors are stored in liquid nitrogen in growth medium (4.5 g/L glucose, L-glutamine and sodium pyruvate, 10% fetal

bovine Serum, Mediatech, Herndon, VA) plus 10% serum, + penicillin streptomycin mix that is supplemented with 10% dimethyl sulfoxide (DMSO, a solvent). The cells are first washed once with PBS and then resuspended using 1 ml of commercially obtained Trypsin (Mediatech, Herndon, VA). Expressing cell medium (as mentioned above, without the supplemented 10% DMSO) is then added to the flask, and about 1.5 ml of cell suspension is then added to either glass-bottom dishes (for visualization experiments) or 35 mm plastic cell culture dishes (Falcon, Lincoln Park, NJ, for electrophysiology). The cells are incubated in the dishes in the presence of growth medium at 37°C to allow them to adhere to the bottom of the dishes. Once the cells bind to the bottom of the dish, they are ready for an experiment either the next day for visualization or the same day for electrophysiology.

3.4 Microscopy

Visualization studies were conducted using either on a fluorescence microscope (Zeiss Axiovert100M inverted microscope) or a confocal microscope (Leica confocal laser scanning TCS SP2 AOBS microscope system). For visualizing the neuroblastoma cells, the fluorescence microscope was used in all cases. The beads had a tendency to non-specifically fluoresce at all excitation and emission wavelengths (autofluorescence) on the confocal microscope and in all wavelength regions except the Cy5 region (650 nm excitation, 670 nm emission). Accordingly all bead visualization studies were done on the fluorescence microscope using a fluorophore with peak emission in the 650 nm-670 nm wavelengths.

All visualization studies were done on cells or beads that were respectively attached and suspended in glass bottom dishes. The reason for using glass bottom dishes as opposed to regular plastic dishes is that plastic tends to autofluoresce on both the fluorescence and confocal microscope. The experimental protocols are described in detail in the Results section.

3.5 Image Analysis

Analysis was performed on images obtained from the confocal and the fluorescence microscopes noted above. Briefly, images were analyzed by selecting regions of interest (ROIs) in the fluorescent images. ROIs were areas that were randomly selected to contain 1-6 beads from the overall population present in the image of interest. The regions were selected by freely drawing an enclosed line around the beads of interest, ensuring that the beads selected for analysis were in correct focus. Analyzing the image in Metamorph (Sunnyvale, CA) yielded statistics on the pixels present in the ROI, for e.g., maximum pixel value and average pixel value. The maximum pixel value in that ROI was selected as a desired parameter for analysis, since this value always corresponded to a finite non-zero area on the brightest bead present in the ROI. The minimum pixel value was always zero because a given ROI in all cases contained background areas (which in all cases corresponded to zero pixel brightness).

4. EXPERIMENTS AND RESULTS

4.1 Preparation and testing of anchor binding

Section 4.1 describes experiments in which we prepared and tested the protein complex containing the B-domain and the $GABA_C$ Ab-*N*14 *in-vitro*. As described in the Methods section, protein complexes that were used in the project were prepared using Ni^{2+}-coated plates. Section 4.1.1 describes in detail the preparation of the protein complex on the 96-well Ni^{2+}-coated plates.

4.1.1 ELISA testing of antibody B-domain complex

Aim 2.1 concerns the preparation and testing of the polyclonal antibody ($GABA_C$ Ab-*N*14) and B-domain based protein complex. The objective of the experiments described in section 4.1 is to determine whether we can form the protein complex *in-vitro* on the Ni^{2+}-coated plates (Aim 2.1). Fig. 10 describes the experiments in a flowchart form.

The ultimate protein complex prepared in this study contained the B-domain (in its several forms, described in the later sections) and the $GABA_C$ Ab-*N*14 antibody. The aim of this experiment was to determine the binding interaction *in-vitro* of these two components of the complex (Branch Q1, box 1 in Fig. 10). Demonstration of an *in-vitro* interaction of the two components was viewed as a key objective preceding testing of the B-domain and the $GABA_C$ Ab-*N*14 on the $GABA_C$ receptor expressing neuroblastoma cells. To address Aim 2.1, preliminary experiments were done on 96-well nickel plates where different conditions were used to construct the complex. The Ni^{2+}-

Fig. 10: A detailed description of Aim 2.1 of the project

The experiments described in Aim 2.1 were organized to address three questions, shown here as Q1, Q2 and Q3. These questions were: Q1: To test whether we can bind the B-domain to the $GABA_C$ Ab-*N*14 in-vitro on ELISA plates. Q2: To test if the monoclonal antibody (scFv) can bind to the $GABA_C$ receptor on the neuroblastoma (NB) cells and the electrophysiological effect of binding of the scFv to the receptor. Q3: To test if the NNP containing $GABA_C$ Ab-*N*14 and B-domain (in its several forms, described in the accompanying text) can bind to the $GABA_C$ receptors expressing neuroblastoma cell system. All the experiments represented by the boxes have been described in detail in the text in the Experiments and Results section. The boxes were numbered 1-6 to allow easy referencing of each experiment described in the text to its corresponding box in this flowchart. Text in these boxes shows, in shorthand form, the protein complexes that were tested in each experiment as well as the type of experiment (e.g. ELISA, electrophysiology, visualization). In the 'double-labeling' box, the arrows indicate that the 2°Cy5 was attached directly to the $GABA_C$ Ab-*N*14 antibody.

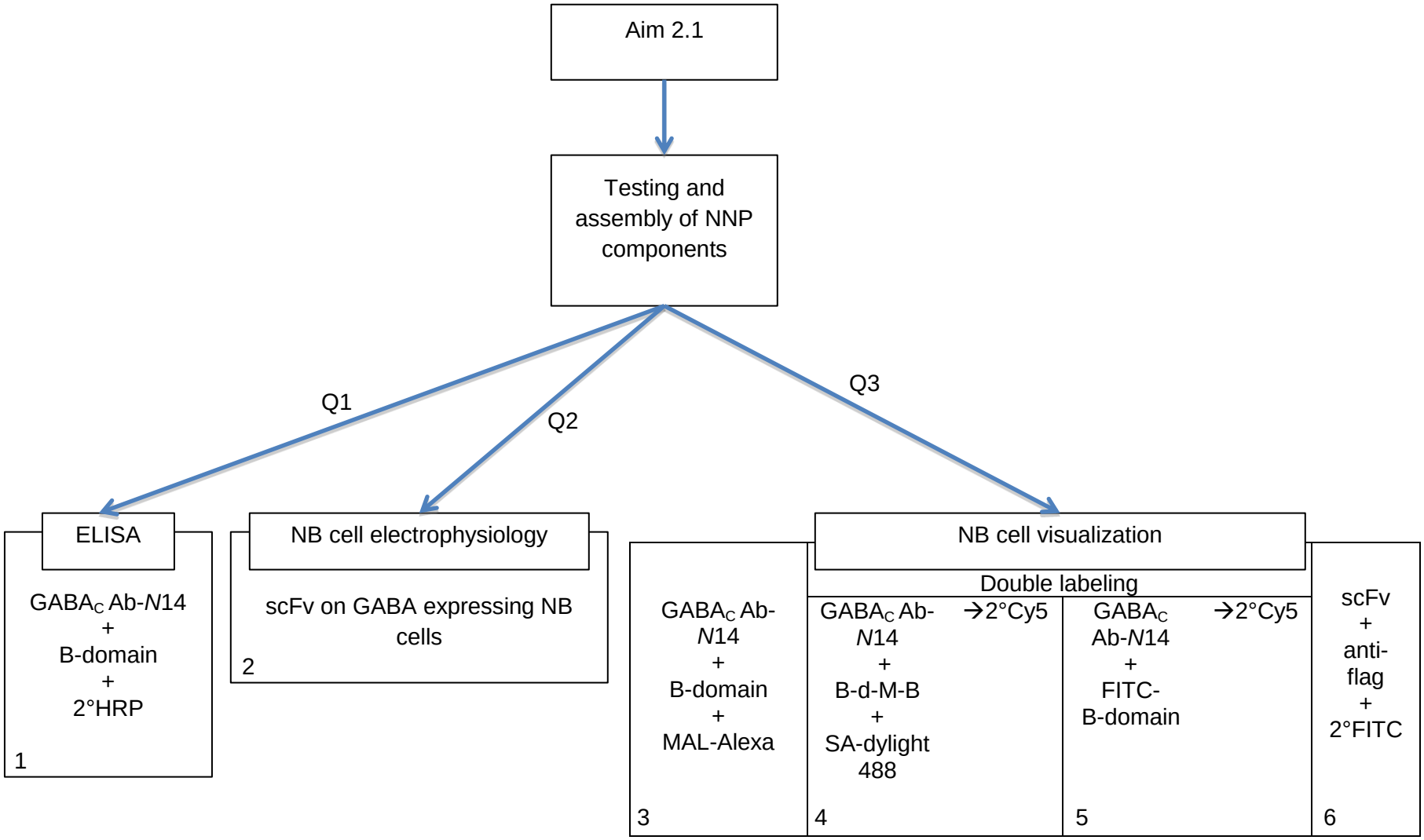
Aim 2.1
Testing and assembly of NNP components
Q1
Q2
Q3
ELISA
GABA$_C$ Ab-*N*14 + B-domain + 2°HRP
1
NB cell electrophysiology
scFv on GABA expressing NB cells
2
NB cell visualization
Double labeling
GABA$_C$ Ab-*N*14 + B-domain + MAL-Alexa
3
GABA$_C$ Ab-*N*14 + B-d-M-B + SA-dylight 488
→2°Cy5
4
GABA$_C$ Ab-*N*14 + FITC-B-domain
→2°Cy5
5
scFv + anti-flag + 2°FITC
6

terminated form of B-domain used in this experiment allowed the attachment of the B-domain to the Ni^{2+}-plate and subsequent tethering of the remaining protein complex on the plate. Here, the Ni^{2+}-plate acted as a capture agent for the his6-tag of the B-domain.

We added the B-domain at a concentrations varying from 0.0001-10uM and allowed it to incubate overnight at 4°C. The $GABA_C$ Ab-*N*14 was allowed to incubate on the Ni^{2+}-plate for 2 hr at room temperature. The secondary antibody used in this experiment was goat anti-guinea pig horseradish peroxidase (Goat-anti-GP-HRP), which was incubated on the Ni^{2+}-plate for 2 hr at room temperature. The substrate of the HRP was then added, allowing the generation product that provides an amplified read-out of the binding of the HRP-tagged secondary antibody (HRP is an enzyme that in the presence of a substrate, emits light that can be detected using spectrophotometric methods. The HRP substrate reaction is highly sensitive and can be used to detect small amounts of specific proteins in a reaction). The development of the product dye was followed for a period of 40 min. The increase in absorbance values after the addition of the substrate was measured with a plate reader (TECAN). Thus, the overall complex was as follows; Ni^{2+}: B-domain: $GABA_C$ Ab-*N*14: Goat-anti-GP-HRP

Two controls were used in this experiment: one with the $GABA_C$ Ab-*N*14 excluded, and the other with both the B-domain and the secondary HRP antibody excluded from the complex. The results of this experiment are shown in Fig. 11. In previous experiments (data not shown), we had determined that $GABA_C$ Ab-*N*14 dilutions of 1/2000 and 1/5000 (representing final concentrations of 0.8 nM and 0.32 nM respectively) are suitable conditions for the formation of the protein complex. In this

Fig 11: **Testing attachment of the $GABA_C$Ab-*N*14 to the B-domain *in-vitro* in an ELISA experiment**

Panels A and B show the rise in the absorbance values *vs.* time in min, for a protein complex that was attached to 96-well Ni^{2+}-coated ELISA plates. The protein complex contained the B-domain, $GABA_C$ Ab-*N*14 and a secondary goat-anti-guinea pig (GP) HRP. Panels A and B used dilutions of 1/2000 and 1/5000 of the $GABA_C$ Ab-*N*14 respectively. In both experiments, the concentration of the B-domain was varied between 0.0001-10 µM. Predictably, there is a marked difference in the data obtained with 10 µM B-domain by comparison with the other concentrations investigated.

A

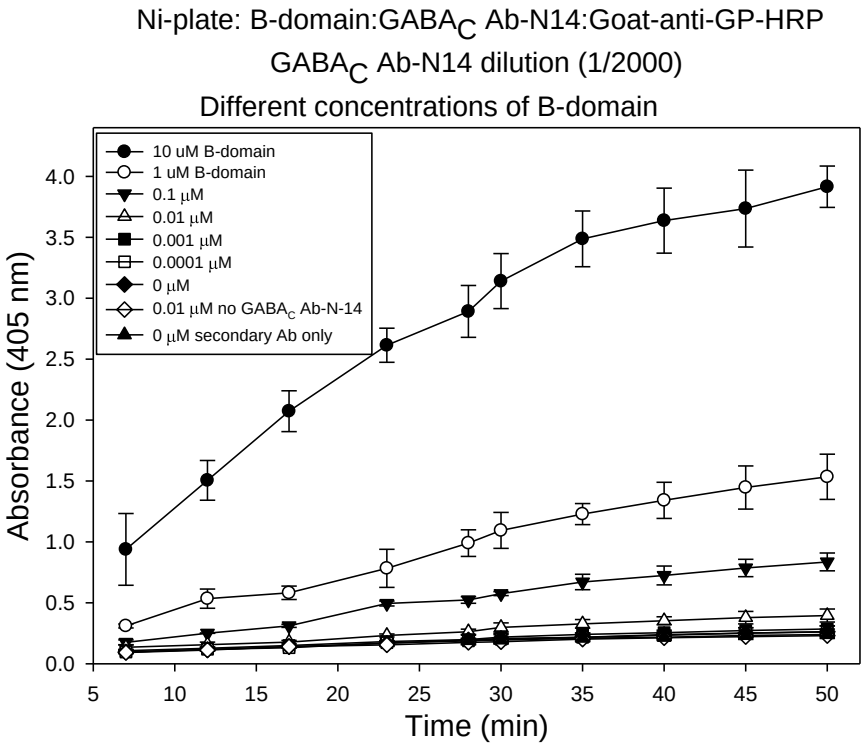
Ni-plate: B-domain:GABA$_C$ Ab-N14:Goat-anti-GP-HRP
GABA$_C$ Ab-N14 dilution (1/2000)
Different concentrations of B-domain
10 uM B-domain
1 uM B-domain
0.1 μM
0.01 μM
0.001 μM
0.0001 μM
0 μM
0.01 μM no GABA$_C$ Ab-N-14
0 μM secondary Ab only
Absorbance (405 nm)
Time (min)

B

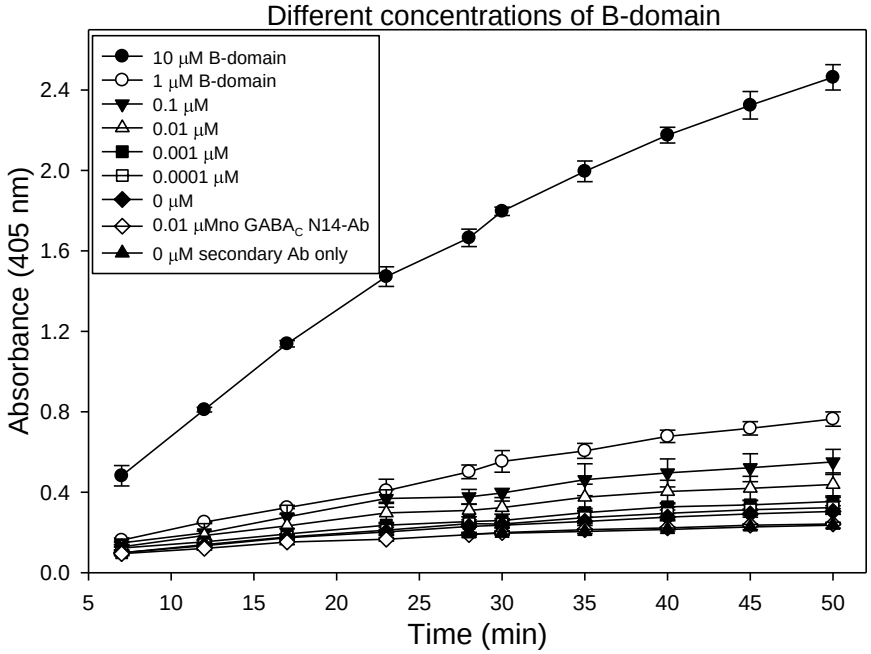
Ni-plate: B-domain:GABA$_C$ N14-Ab:Goat-anti-GP-HRP
GABA$_C$ N14-Ab dilution (1/5000)
Different concentrations of B-domain
10 μM B-domain
1 μM B-domain
0.1 μM
0.01 μM
0.001 μM
0.0001 μM
0 μM
0.01 μMno GABA$_C$ N14-Ab
0 μM secondary Ab only
Absorbance (405 nm)
Time (min)

experiment, we used these two dilutions of 1/2000 and 1/5000 to test whether these two conditions are suitable for the binding of the B-domain to the $GABA_C$ Ab-*N*14. The results of the experiment at the $GABA_C$ Ab-*N*14 dilutions of 1/2000 and 1/5000 are shown in Fig. 11 Panel A and right Panel B, respectively. The X-axis in both figures indicates the periods of incubation of the preparations following the addition of HRP substrate; the Y-axis shows the absolute absorbance values as measured at a wavelength of 405 nm. The different symbols represent the concentrations of the B-domain tested in this experiment. We were interested in following the absorbance time course in order to determine the incubation period that would provide an accurate and stable reading of the absorbance, as well as to compare the behavior of the absorbance curves for different concentrations of the B-domain. For all of the investigated conditions, the Fig. 11 data show a clear dependence of HRP product development on the amount of complex present, and a clear time-dependence of the development of HRP reaction product for a given sample. In particular, data obtained with the higher concentrations of the B-domain exhibited higher absorbance values and a steeper rising phase. The absorbance values for the formation of complex were the highest for a B-domain concentration of 10 μM. Also, the absolute absorbance values were higher for a $GABA_C$ Ab-*N*14 dilution of 1/2000, as seen in Panel A. The controls (♦, ◊, ▲) showed very low absorbance values, close to baseline, giving further indication of the dependence of HRP product generation on the presence of the entire protein complex in the samples. Overall, this experiment shows direct evidence of the formation of the entire aforementioned complex on the Ni^{2+}-plate.

4.1.2. Visualization testing of the $GABA_C$ Ab-*N*14 B-domain complex on the neuroblastoma cells

The experiment in Section 4.1.1 demonstrated the binding of the $GABA_C$ Ab-*N*14 to the B-domain, which can in turn bind to the Ni^{2+}-plate. The experiments described in section 4.1.2 also address Aim 2.1 of this study. The objectives of the experiments described in this section determine whether the complex containing the B-domain and the $GABA_C$ Ab-*N*14 can bind to the neuroblastoma cells system through visualization studies using a fluorescence tag (Fig. 10, Branch Q3 - box 3).

To address this question, we performed visualization experiments on the complex, in which maleimide-Alexa (Invitrogen, Carlsbad, CA, excitation wavelength: 488 nm, emission wavelength: 520 nm) was used as a fluorescent tag to detect the presence of the complex on the cells in a fluorescent microscope. The maleimide group attaches to the cysteine of the B-domain and also serves as a linker to attach the other components of the protein structure (like a PEG chain terminated with biotin, like the B-d-M-B). The complex was first constructed on a Ni^{2+}-plate. The B-domain at a concentration of 4 µM was incubated overnight at 4°C on the plate. The capacity of the Ni^{2+}-plates was ~3 µM (as specified by the manufacturer). Thus the concentration of the B-domain was more than the saturating capacity of the Ni^{2+}-plates. This concentration was also chosen based on the results of the previous experiment as explained in Aim 2.1 above. The B-domain was then treated with the reducing agent dithiothreitol (DTT) for 40 min at 37°C, to disrupt the disulfide bonds that form between the cysteines of B-domain, thus yielding a monomer form of the B-domain. Maleimide-Alexa at a concentration of 20X the concentration of B-domain was then incubated for 2 hr at room

temperature on the Ni^{2+}-plate. The $GABA_C$ Ab-*N*14 at a ~1/100 dilution was then incubated on the Ni^{2+}-plate at room temperature for 2 hr. In the previous Ni^{2+}-plate experiments as described for Aim 2.1 above, dilutions of the $GABA_C$ Ab-*N*14 used were 1/2000 and 1/5000. However, in previous visualization experiments conducted with the complex on the neuroblastoma cells, a $GABA_C$ Ab-*N*14 concentration of 1/2000 did not yield a strong fluorescence signal. For this reason, we increased the amount of the $GABA_C$ Ab-*N*14 to ensure that we had sufficient antibody on the $GABA_C$ receptors to produce a detectable fluorescence signal. Once the complex was present on the Ni^{2+}-plate, we added imidazole, which releases the his6-tagged B-domain from Ni^{2+} chelation. The collected sample of protein was then dialyzed to remove the imidazole after which the sample was concentrated. The resulting concentration of the protein complex was then measured by protein assay and then added onto the neuroblastoma cells. Before adding the complex to the neuroblastoma cells, the cells were blocked with 3% fetal bovine serum (FBS) to prevent non-specific binding of the complex on the cells. This experiment included a positive control that consisted of $GABA_C$ Ab-*N*14 and a FITC-labeled secondary anti-guinea pig antibody (Anti-GP 2° FITC, excitation wavelength – 488 nm, emission wavelength – 520 nm), which were added sequentially to the neuroblastoma cells. Serving as negative controls were (i) a sample that omitted the $GABA_C$ Ab-*N*14 primary antibody, and (ii) a sample that omitted the B-domain. These four cell preparations (sample; positive control; and the two negative controls) were then visualized under a fluorescence microscope. The positive control yielded a bright fluorescence signal on the cells, reflecting the binding of the $GABA_C$ Ab-*N*14 and 2° FITC at the $GABA_C$ receptors of the neuroblastoma cells (data not shown). However, the sample preparation, as well as the negative controls, produced a negligible signal, very

close to background. An obvious possible explanation of the absence of robust signal from the sample preparation is that the complex does not bind to the $GABA_C$ receptors on the cells in the above conditions. However, the negative finding is consistent also with another possible explanation, one that concerns the specific labeling of the sample complex. That is, the positive control that produced a bright fluorescence signal contained ~5 copies of FITC on the secondary antibody and multiple secondary antibodies per primary $GABA_C$ Ab-*N*14 and thus multiple copies of fluorophore per copy of protein complex. By contrast, the sample preparation in this experiment, for which the fluorescence label was provided by the maleimide-Alexa joined to the B-domain, contained only one copy of fluorophore (Alexa-) per protein complex. Thus, the absence of robust binding signal for the sample preparation may have resulted from this relatively low specific labeling of the test protein complex.

To address the problem of insufficient brightness of the maleimide-Alexa, experiments were done in which 2°FITC was used as the fluorophore. These experiments thus involved a tertiary complex consisting of the B-domain, the $GABA_C$ Ab-*N*14 and the 2°FITC. In these experiments using the tertiary complex, the complex was prepared in solution, and not on the Ni^{2+}-plate. Here, the B-domain (concentration of 1 μM) was prepared in mammalian Ringer, and was mixed with the $GABA_C$ Ab-*N*14 at a dilution of 1/1000 (similar to the dilution used to prepare the positive control in the experiment addressing Aim 2.1 above). This mixture was then allowed to incubate overnight at 4°C. This mixture was then added to the cells (which were pre-blocked with 3% FBS) and allowed to incubate for 1 hr at room temperature. The 2° FITC was then incubated with the cells for another 1 hr. Again the FITC-labeled secondary antibody (2° FITC) was added at a dilution of 1/1000, similar to that used in the positive control for

experiments in Aim 2.1 above. The positive control was the same as that used in the experiment above, with the $GABA_C$ Ab-*N*14 and 2°FITC. The negative control was the tertiary complex excluding the $GABA_C$ Ab-*N*14. These three preparations were examined in a fluorescence microscope. Bright fluorescence was observed on the cells for both the sample and positive control, whereas the negative control was close to background. However, because in this experiment the 2° FITC was attached to the $GABA_C$ Ab-*N*14, the experiment did not provide direct reporting from the B-domain, and does not establish whether the B-domain was present when the tertiary complex bound to the cells.

Further experiments were done in an attempt to label the protein complex containing the $GABA_C$ Ab-*N*14 and B-domain with different preparations. One preparation included a double-labeling experiment that used the $GABA_C$ Ab-*N*14, B-d-M-B with a streptavidin-dylight (SA-dylight, Pierce, Rockford, IL) as the fluorescence tag against the B-d-M-B and a 2°Cy5 against the $GABA_C$ Ab-*N*14. We also used the FITC-B-domain in the double-labeling experiments described in the later section. Thus, the protein complex consisted of the FITC-B-domain, $GABA_C$ Ab-*N*14 and a 2°Cy5 against the $GABA_C$ Ab-*N*14 primary antibody. All of these preparations failed to exhibit robust fluorescence of the fluorophore tagged B-domain (the SA-dylight in the first preparation, and the FITC-B-domain in the second, as described above). These experiments have been described in the Results Sec. 4.3.2 and 4.3.4.

The negative result just noted was in contrast to the results obtained by our lab colleagues in which a similar protein complex ($GABA_C$ Ab-*N*14, B-domain with a fluorophore specific to the B-domain) was tested on $GABA_C$ receptors expressed on an

Xenopus oocyte system. In these experiments, robust fluorescence was observed, which confirmed the presence of the B-domain and hence the binding of the protein complex to the $GABA_C$ receptors on the oocytes. Thus, the hurdles we faced in binding the protein complex to the neuroblastoma cells could be specific to the neuroblastoma cells. It is possible that the binding of the $GABA_C$ Ab-*N*14 to the $GABA_C$-receptors on the neuroblastoma cells produces steric hindrance that prevents the B-domain from binding to the antibody. However, this possibility seems unlikely considering that the $GABA_C$ Ab-*N*14 – B-domain reaction has been demonstrated on the *Xenopus* oocyte and other experimental preparations tested in the lab. Another reason could be (as mentioned above) that there are a low number of fluorophore copies per B-domain to yield a substantial fluorescence comparable to the positive control or above background. Thus, it is possible that the neuroblastoma cells expressing the $GABA_C$ receptors are not a workable cell system to study the binding activity of the protein complex as compared to the *Xenopus* oocytes system.

4.1.3. <u>Electrophysiological testing of scFv peptides</u>

Another approach for developing an anchoring system described in Aim 2.1 is the use of monoclonal antibodies, or scFv's. Such an scFv based monoclonal antibody system is a better defined system as compared to the polyclonal antibody ($GABA_C$ Ab-*N*14) which by itself is a mixture of proteins. A monoclonal antibody system is more amenable for conjugation and addition of different residues (cysteine, biotin) as compared to a polyclonal antibody. Thus although we have a working polyclonal antibody, it would be desirable to have an scFv-based monoclonal antibody that has good binding and does not destroy the electrophysiological responses of $GABA_C$

receptors expressed on neuroblastoma cells. My role in this line of study was the electrophysiological testing of the candidate scFv's in preparations of $GABA_C$-expressing neuroblastoma cells. scFv's reactive with $GABA_C$ Ab-*N*14 were selected by phage display technology and prepared by Drs. Adnan Memic and Brian Kay (Dept. of Biological Sciences, UIC). In phage display technology, a population of bacteriophages (called a phage library, where phages are any number of viruses that infect bacteria), each displaying a different peptide on its surface, are tested for binding to a target peptide (for eg. our $GABA_C$ Ab-*N*14 peptide). We can then "capture" phages displaying peptides that can specifically bind to the target peptides from a large phage library displaying many different peptide structures. Thus, a phage library was screened for binding to the $GABA_C$ Ab-*N*14 peptide. Following four rounds of phage-display selection of this library using the $GABA_C$ Ab-*N*14 peptide as a target, five scFv binders (i.e. antibody fragments (peptides) that bound specifically to $GABA_C$ Ab-*N*14) were identified (termed Pep1, Pep7, Pep8, Pep11 and Pep12). Soluble forms of these scFv's were then generated by Drs. Kay and Memic. These soluble scFvs were tested by visualization for binding to ρ1-expressing neuroblastoma cells (Fig. 10, branch Q3 - box 6), and their effect on receptor function was evaluated by electrophysiology (Fig. 10, branch Q2 - box 2).

A total of 13 dishes of neuroblastoma cells were used. Eleven of those were cells expressing the $GABA_C$ receptors, while two of the dishes contained non-$GABA_C$-expressing cells. Specific treatments of these preparations were as follows. Four dishes (Dishes 1-4) containing the neuroblastoma cells were used for electrophysiology. Dishes 1-3 were treated with three different concentrations of the scFvs: 1 μM, 100 nM

or 10 nM to get an estimate of the concentration of scFv that can yield a robust detectable fluorescence signal. Dish 4, which was not treated with scFv, served as a control preparation. The treatment of the nine preparations analyzed by visualization (fluorescence microscopy) were as follows. Dishes 5-7 were treated with 3 different concentrations of the scFvs: 1 µM, 100 nM or 10 nM. Dishes 8-10 were treated with the same concentrations of the scFvs as described above (1 µM, 100 nM or 10 nM) and were also tested for competitive binding with the same three concentrations of the $GABA_C$ Ab-*N*14 (1 µM, 100 nM or 10 nM). Dish 11, which was a control, was treated with FITC-labeled, anti-FLAG secondary antibody only, i.e., there was no treatment with scFv. Dish 12 contained non-$GABA_C$-expressing control cells treated with 1 µM scFv. Dish 13 contained non-$GABA_C$-expressing control cells and was treated with 100 nM scFv.

The 13 dishes containing the neuroblastoma cells were first washed twice with mammalian Ringer (MR). The cells were then blocked for 30 min in 3% fetal calf serum (FCS) prepared in mammalian Ringer. After 30 min, the cells were again washed with MR. All dishes except Dish 4 and Dish 11 were then treated with the 3 concentrations of scFvs (1 µM, 100 nM and 10 nM) diluted in 1% FCS prepared in mammalian Ringer, for 1 hr. Dish 4 was then used in the patch-clamp setup to study the electrophysiological responses of the scFv-untreated neuroblastoma cells. The other dishes were then washed 4 times with MR. Electrophysiology was performed on Dishes 1-3. The remaining dishes were then treated with the anti-FLAG, FITC-labeled secondary antibody diluted to 1/100 in MR along with 1% FCS. The duration of the incubation was 1 hour in darkness. After 1 hour, the cells were washed 5 times with MR.

Fig. 12: Representative data from the electrophysiological experiments conducted on scFv treated $GABA_C$ expressing neuroblastoma cells.
Panels A and B plot the mean ± SD of the peak amplitudes of GABA-elicited responses recorded from untreated and 1 µM concentration pep12 treated neuroblastoma cells respectively. The x-axis represents cell numbers; the y-axis shows the mean ± SD of the absolute peak amplitude per cell. Black bars and grey bars are peak amplitude responses to 3 µM and 1 µM GABA, respectively. Each pair of black and grey bars represents data obtained from the same cell. Note the difference in y-axis scales of these panels.

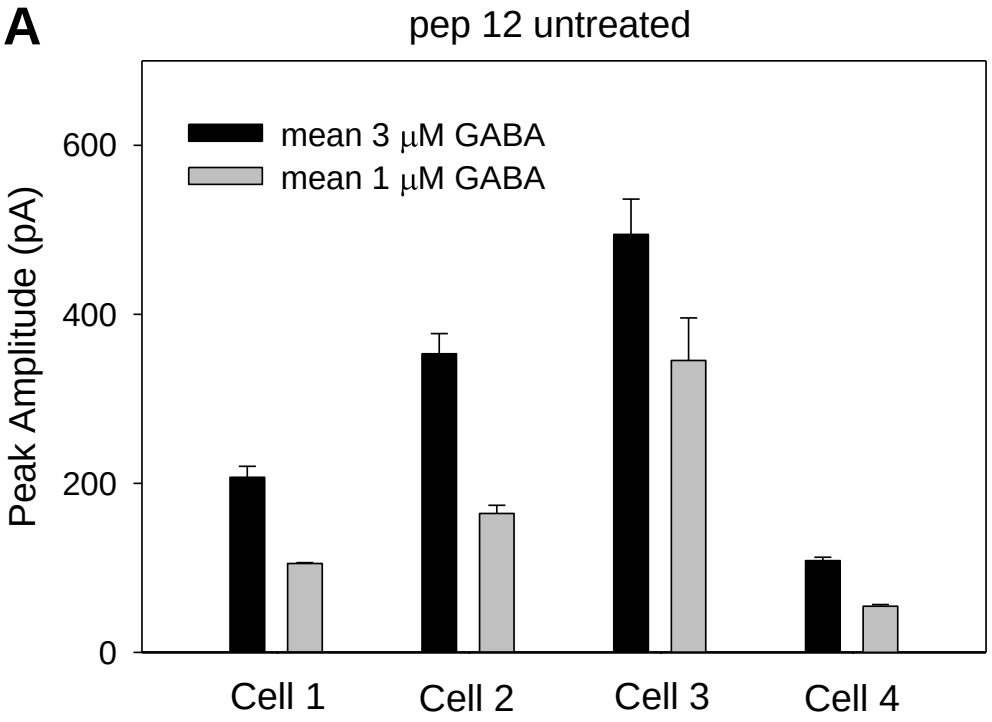
A
pep 12 untreated
mean 3 μM GABA
mean 1 μM GABA
Peak Amplitude (pA)
600
400
200
0
Cell 1
Cell 2
Cell 3
Cell 4

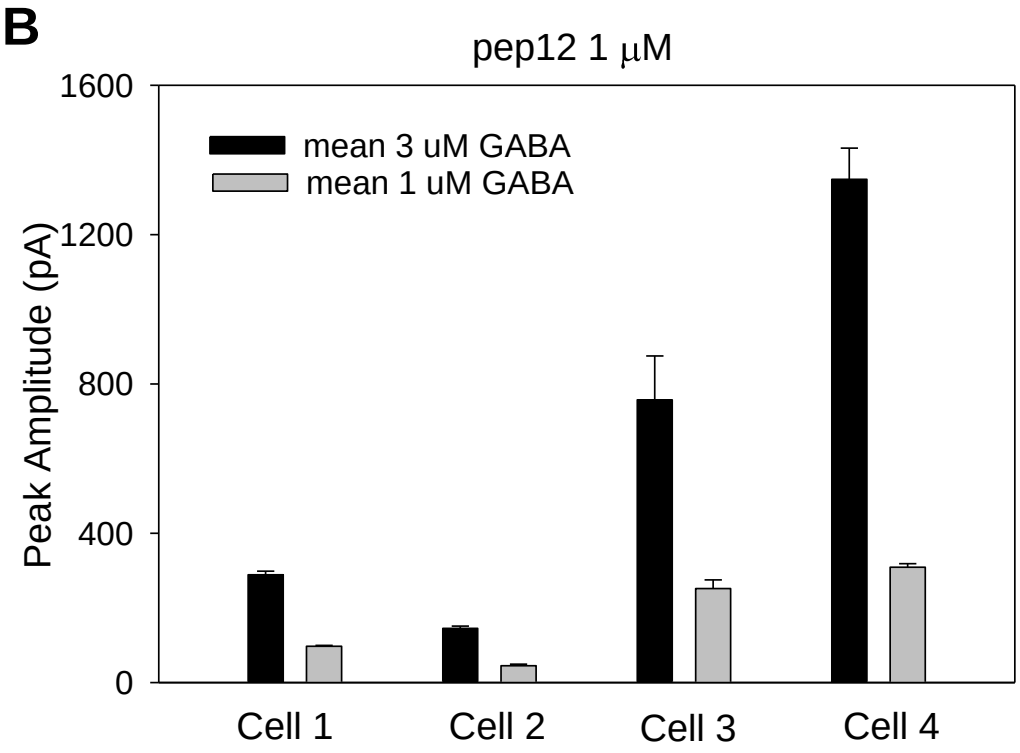
B
pep12 1 μM
mean 3 uM GABA
mean 1 uM GABA
Peak Amplitude (pA)
1600
1200
800
400
0
Cell 1
Cell 2
Cell 3
Cell 4

Electrophysiological (patch-clamp) experiments were performed on the scFv treated neuroblastoma cells. Two concentrations of GABA, 3 µM and 1 µM, were used for testing electrophysiological responses of the cells, with the scFv bound to the $GABA_C$ receptors. These concentrations were chosen based on the dose-response characteristics of GABA. A dose-response curve plots the concentration in molar of GABA *vs.* the peak current at each concentration measured in a whole-cell patch-clamp experiment. Typically concentrations for the GABA dose-response curve are varied between 0.1 - 100 µM. The EC_{50} is the concentration of GABA that produces a response (or current amplitude) that is halfway between baseline and maximum response to GABA. The EC_{50} for GABA is 1-3 µM. Thus, the GABA concentrations of 3 µM and 1 µM lie in the middle of the dynamic range of the dose-response curve for GABA. Mammalian Ringer was continuously perfused into the testing dishes. Each experimental run involved a duration of 40 s. The duration of the application of GABA itself was 4 s; during this 4 s application the medium presented to the cell was only the GABA-supplemented MR. The number of cells tested with a given concentration of a given scFv type was 2-4. The mean peak amplitudes of the responses to 3 µM and 1 µM GABA were plotted as a bar graph. Representative data are shown in Fig. 12, below. This Figure shows peak amplitudes of electrophysiological responses of the neuroblastoma cells to 3 µM (black) and 1 µM (grey) GABA. Results shown in the panel A were obtained from the control (untreated) dish; results in the panel B were obtained on treatment of the cells with 1 µM pep12. As we see from these data, the response to 3 µM GABA was much greater than that to the 1 µM GABA. Note that mean absolute peak amplitudes of the responses differed substantially from cell to cell. The results of the scFv experiments have been summarized in Table 2.

Table 2: **Summary of data obtained in scFv electrophysiological experiments.** Results are shown for all five scFv preparations tested. Three concentrations of each type of scFv were tested, as shown in column 2. Columns 3 and 4 show the average and standard deviations of the peak amplitudes on the electrophysiological response to 1 µM and 3 µM GABA, respectively. Each entry in columns 3 and 4 is the average of 2-4 individual trials from 1-4 cells per scFv type. Column 5 indicates the ratio of the mean current at 1 µM GABA concentration to the mean current at 3 µM GABA concentration. Blank entries in columns 3-4 indicate conditions for which data were not obtained.

1	2	3	4	5
scFv type	scFv conc	1 µM GABA peak current (pA)	3 µM GABA peak current (pA)	Ratio (column 3)/ (column 4)
pep1	untreated	622.69 ± 676.91	1455.19 ± 902.67	0.43
	1 µM	119.93 ± 80.46	1483.86 ± 479.02	0.08
	100 nM	69.625 ± 66.45	945.26 ± 988.05	0.07
	10 nM	348.22 ± 216.89	2556.34 ± 870.88	0.14
pep7	untreated	494.5 ± 108.12	1297.44 ± 383.32	0.38
	1 µM	427.59 ± 284.88	1406.57 ± 716.48	0.3
	100 nM	155.58 ± 37.66	1680.55 ± 1032.11	0.09
	10 nM	-	232.04 ± 213.43	-
pep8	untreated	852.76 ± 419.93	1277.06 ± 598.06	0.67
	1 µM	347.95 ± 179.57	2039.67 ± 763.55	0.17
	100 nM	-	1474.52 ± 328.05	
	10 nM	287.85 ± 309.25	822.17 ± 276.72	0.34
pep11	untreated	70.32 ± 69.04	583.37 ± 69.04	0.12
	1 µM	86.98 ± 19.92	152.99 ± 11.15	0.56
	100 nM	465.99 ± 446.53	-	-
	10 nM	-	-	-
pep12	untreated	177.53 ± 116.69	290.82 ± 154.28	0.61
	1 µM	175.65 ± 115.89	666.11 ± 505.94	0.26
	100 nM	-	979.02 ± 821.77	-
	10 nM	602	662.8 ± 13.86	0.91

In summary, the electrophysiological data described above suggests an essential inertness, i.e., lack of effect, of the scFvs so far tested on the GABA-elicited response of $GABA_C$-expressing neuroblastoma cells. Such inertness is in itself encouraging, as it is likely to be a desirable feature of the ultimately envisioned NNP device. That is, a NNP device based on the scFvs, when eventually used as a therapy, would be expected to preserve the behavior of native receptors in the diseased retina. However, firm conclusion as to whether an scFv-based anchor is electrophysiologically inert will require further investigation using a probe delivery system, where, through electrophysiology and visualization tests, we can verify the interaction of the presented scFv to the receptor-containing surface of the neuroblastoma cell.

4.2 Bead-probe experiments

As described in the Background section, the original plan was to prepare micron-sized silicon surfaces, which could be functionalized with SA and Ni^{2+}/NTA. We could then attach our protein complex of interest to these surfaces through biotin and his6-tags respectively. Such surfaces would then be held at the tip of a suitable micro-manipulator and positioned in close proximity to cells expressing either the $GABA_C$ or the $GABA_A$ receptor. Under patch-clamp recording, we would then test the electrophysiological effect of the binding of the protein complex present on the probe surface to the receptors on the cells. The advantages of this method over the conventional method of perfusing the cells with a solution containing the protein of interest are two-fold. First, this approach would not require perfusion and thus, wastage of test material that was available in limited quantity. Second, being able to stimulate a population of receptors

Fig. 13: Details of experiments performed to address Aim 2.2.
The main questions in Aim 2.2 have been labeled Q1-Q5. These questions were:Q1 and Q2: To determine if individual SA- or Ni^{2+}-beads attached to the tip of a micropipette electrode can bind a NNP based protein complex and subsequently deliver the bound protein complex to the $GABA_C$ receptors on neuroblastoma cells. Q3: To test the binding of the $GABA_C$ Ab-*N*14 and B-domain based NNP on a population of SA-beads. We also tested binding of an effector based muscimol compound (50:50 compound) on SA-beads. Q4: To test the electrophysiological effect of the 50:50 compound (muscimol binding to $GABA_C$ receptors on neuroblastoma cells) using patch-clamp and bead-based microprobes. Q5: To test binding of B-domain and $GABA_C$ Ab-*N*14 based NNP on population of Ni^{2+}-beads. Double labeling was used to confirm binding of both B-domain and $GABA_C$ Ab-*N*14 to Ni^{2+}-beads. As in the previous flowchart, the boxes are numbered 1-8 for easy referencing in the text and the text in the boxes shows, in shorthand form, the protein complexes that were tested in each experiment as well as the type of experiment

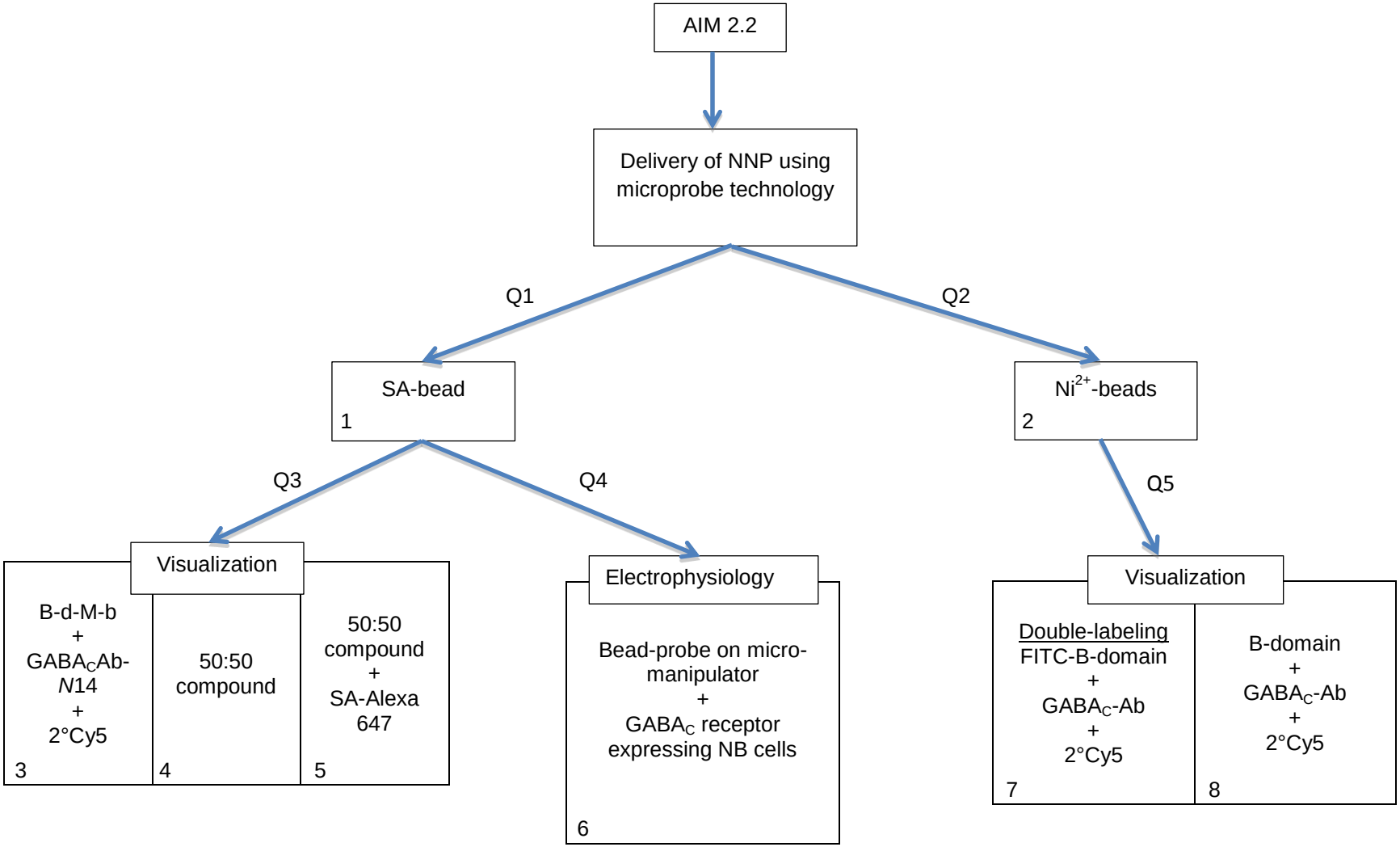
AIM 2.2
Delivery of NNP using microprobe technology
Q1
Q2
SA-bead
1
Ni2+-beads
2
Q3
Q4
Q5
Visualization
B-d-M-b + GABACAb-N14 + 2°Cy5
3
50:50 compound
4
50:50 compound + SA-Alexa 647
5
Electrophysiology
Bead-probe on micro-manipulator + GABAC receptor expressing NB cells
6
Visualization
Double-labeling FITC-B-domain + GABAC-Ab + 2°Cy5
7
B-domain + GABAC-Ab + 2°Cy5
8

using a microprobe system described above would enable us to study interactions on a microscopic and a much more localized scale as compared to the conventional methods. However significant problems in attempting to functionalize macro-silicon surfaces (~5 mm x 5 mm) precluded use of micro-silicon surfaces for any kind of further experiments. To overcome this hurdle, we turned to micron-sized SA (~2.8 µm and ~6 µm diameter) and Ni^{2+} (~10 µm diameter) beads. We were able to capture single beads at the orifice of a hollow glass micro-pipette and have a bead-based probe. In combination with a micro-manipulator with nanometer precision (~40 nm) we were able to stably position the bead in close proximity to $GABA_C$-receptor expressing neuroblastoma cells. The following sections describe the bead-probe experiments in detail. The details of the bead-probe experiments are summarized in the flowchart in Fig. 13.

4.2.1 SA-beads testing with B-domain and $GABA_C$ Ab-*N*14

This experiment addresses Aim 2.2 of this thesis project. SA-beads of diameter 2.8 µm were obtained from Solulink (San Diego, CA). These beads can bind biotinylated protein structures through the biotin-SA interaction.

The main objective of this experiment was to test the binding of the B-d-M-B to the SA-beads (diameter: 2.8 µm, Fig. 13 branches Q1, Q3 - box 3). A specific volume of SA-beads (~10 µl) is first washed in TBST. The protein complex was added to the beads through sequential addition of the individual components. The beads were first blocked with Casein for 30 min, washed twice with TBST and then incubated with 50 nM of B-d-M-B for 1 hour. After three washes with TBST, the beads were then treated with 6.4 nM of the $GABA_C$ Ab-*N*14 and incubated for another hour and then washed with TBST three times. Lastly, the beads were treated with the secondary goat anti-guinea pig antibody

(2°Cy5), which is specific to the $GABA_C$ Ab-*N*14. Thus the protein complex consisted of SA-beads: B-d-M-B: $GABA_C$ Ab-*N*14: 2°Cy5. The negative controls used in this experiment were: the above-mentioned protein complex NC1 - lacking the B-d-M-B, NC2 - lacking the $GABA_C$ Ab-*N*14 and NC3 - lacking both the B-d-M-B and the $GABA_C$ Ab-*N*14.

The beads were suspended in a glass bottom dish, and then imaged under a fluorescence microscope in the Cy5 region (absorption 650 nm and 670 nm). The results are shown in Fig. 14. Panel A depicts the sample dish. Panels B, C and D are respectively NC1, NC2 and NC3 as described above. The images were analyzed by selecting ROIs in the fluorescent images. In each ROI, the maximum pixel value was taken. For each image, the mean and SDs are shown in Fig. 14E. The four bars are labeled as the sample, NC1, NC2 and NC3. Each bar is the mean ± SD of the maximum pixel value from the 4-6 ROIs from a single image. The mean ± SD were 28 ± 1.63 (sample), 17.75 ± 0.96 (NC1), 20.5 ± 1.73 (NC2) and 18.25 ± 0.5 (NC3). From the plot, we can see that the sample bar was larger than all the control bars. A t-test done on the means and SDs between the sample and each of the controls yielded a P-value far less than 0.0001, which showed that there is a significant difference between the samples and each of the controls. This is evidence that the B-d-M-B binds robustly to the SA-beads.

Fig. 14: **Results of the binding of the B-d-M-B and the $GABA_C$ Ab-*N*14 to the SA-beads**.

Panel A is the sample preparation containing the B-d-M-B, $GABA_C$ Ab-*N*14 and the 2°Cy5. The negative controls were; Panel B – the protein complex containing the $GABA_C$ Ab-*N*14 and the 2°Cy5 only (NC1), Panel C - the protein complex containing the B-d-M-B and the 2°Cy5 only (NC2) and Panel D - the protein complex containing the 2°Cy5 only (NC3). Panel E is a histogram where each bar is the mean ± SD from four different ROI from the same image (see detailed description in the accompanying text). The labels on the x-axis indicate that the analysis was done from the corresponding labeled fluorescence images. The y-axis is in terms of fluorescence brightness units. The fluorescence intensities determined from the three negative controls, NC1, NC2 and NC3 are significantly lower than that for the sample ($p \ll 0.001$).

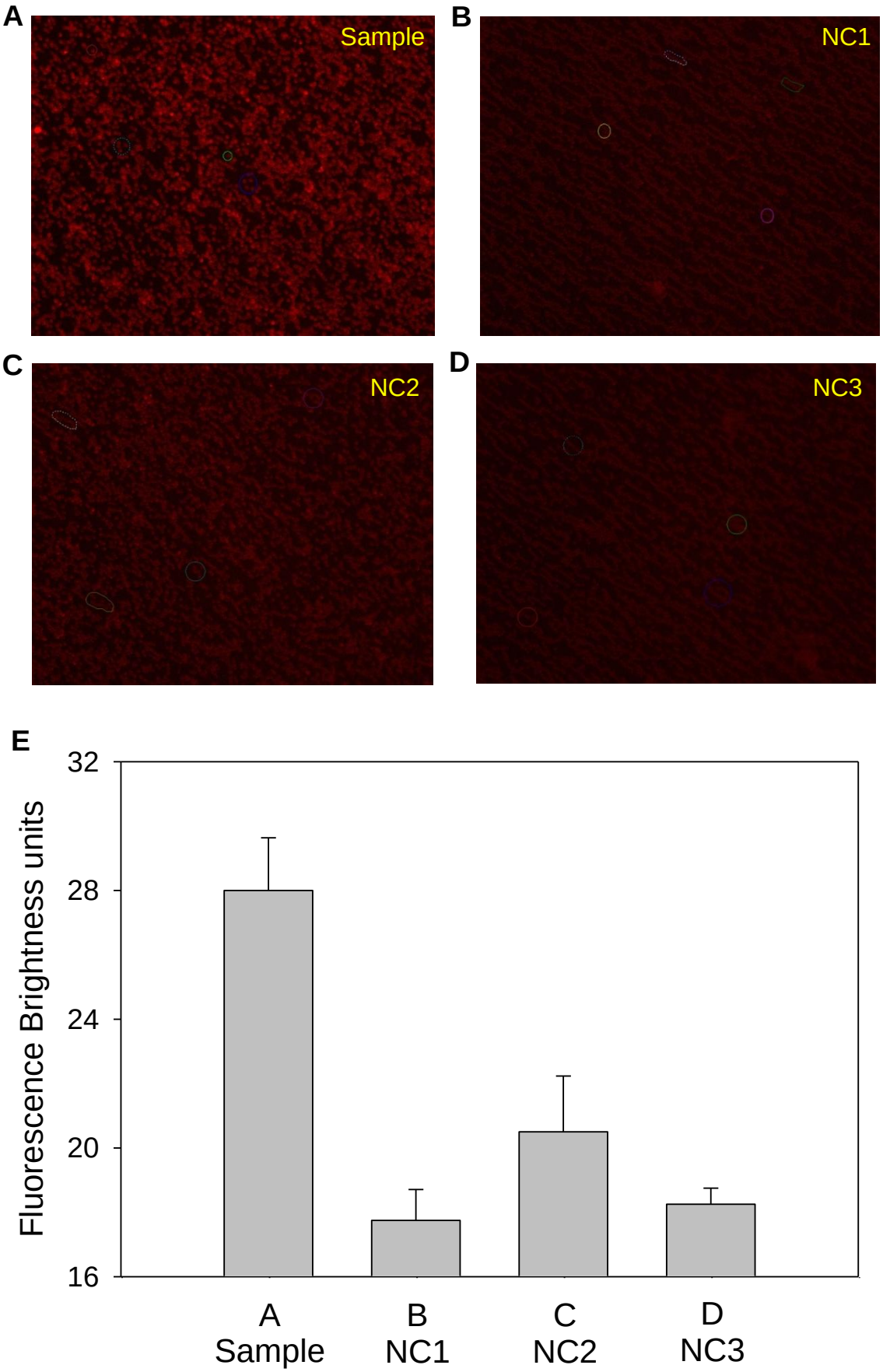
A
Sample
B
NC1
C
NC2
D
NC3
E
Fluorescence Brightness units
32
28
24
20
16
A
Sample
B
NC1
C
NC2
D
NC3

4.2.2 SA-bead with the 50:50 compound

Our colleagues Drs. Ian Tomlinson and Sandra Rosenthal (Vanderbilt University) provided us with a compound, which is a Quantum dot (Qdots) 605 preparation that has multiple (~150) PEG3400 chains. Half of the chains are terminated with biotin and the other half by muscimol and this compound has been referred to earlier as the 50:50 compound.

In the overall goal of this study, we are interested in studying the electrophysiological effect of applying a test protein to $GABA_C$-receptors present on neuroblastoma cells. A potentially useful way of studying such an effect would be if the bead-probe attached protein of interest has $GABA_C$ receptor agonist (effector) at its terminating end. In such a case, application of the probe (or bringing the probe in contact with the cell surface) to the cell could enable the interaction between the effector and the $GABA_C$ receptor. Such an interaction could open the ligand gated chloride channels of the $GABA_C$ receptors, thus resulting in an inward current into the cell, which would be recorded by the patch-clamp. The 50:50 compound described above contains ~75 muscimol-terminated chains. Muscimol is a $GABA_C$ receptor agonist, and we reasoned that having such muscimol-terminated chains bound on the surface of the bead could enable us to study the electrophysiological effect of the interaction between muscimol and the $GABA_C$ receptors.

The aim of this experiment was to test the binding of 50:50 to SA-beads. The biotin-terminated chains present on the 50:50 compound should be able to bind to the SA-beads through the SA-biotin interaction. The presence of the 50:50 compound on the SA-beads was measured in the confocal microscope through the fluorescence of the Qdots present in the 50:50 compound. (Fig. 13 - box 4).

In this experiment, each sample used 10 µl of SA-bead solution; in all, four sample tubes were prepared. Each tube was first treated with the blocking agent casein for one hour. Two samples (duplicates) were then treated with 20 nM of 250 µl 50:50 compound for an hour. The two negative controls (duplicates) were allowed to incubate in 250 µl TBST. At the end of the 1-hr incubation, all tubes were washed with 1 ml TBST. 100 µl of the bead solution was then put on a glass bottom dish and then imaged in the confocal microscope. The results of this experiment have been summarized in Fig. 15.

Fig. 15A and 15C show the sample fluorescence and brightfield images respectively whereas Fig. 15B and 15D show the negative control fluorescence and brightfield images respectively. At the Qdot imaging conditions on the microscope, the negative controls showed considerable autofluorescence (Fig. 15B). Both of the duplicate negative controls showed robust autofluorescence. However, the samples, which were treated with the 50:50 compound, showed brighter fluorescence as shown in representative image Fig. 15A. The images were analyzed by selecting ROIs in the fluorescent images. Two images were taken from each dish. In each image, 4-6 ROIs were selected. In each ROI, the maximum pixel value was taken. For each image, the mean and SDs are shown in Fig. 15E. The four bar stacks are the four dishes. They have been labeled as the sample and control. For each dish, two images were taken, represented by the black and grey bars. Each bar is the mean and SD of the maximum pixel value from the 4-6 ROIs. From the plot, we can see that the mean brightness of the samples exceeds those of the controls.

Fig. 15: **Interaction of the 50:50 compound with SA beads**.
The SA-beads were treated with the 50:50 compound which has biotin terminated chains that enables attachment to the SA-beads. The 50:50 compound is a Qdot compound and the fluorescence in this figure is due to the Qdots. Panels A and B are fluorescence images from the sample (SA-beads-50:50 compound) and control (untreated SA-beads) dishes respectively obtained from the confocal microscope. Panels C and D respectively are the corresponding sample and control brightfield images. Panel E is a histogram of the ROIs analyzed from several images and dishes. Each bar stack represents images obtained from one dish. For each dish, 2-3 images were analyzed which are represented by a different colored bar in each image stack. Each bar is the mean ± SD of the maximum pixel value obtained from 4-6 ROI from a single image. A *t*-test performed on the means revealed a significant difference between the means of the sample and control dishes ($P << 0.001$)

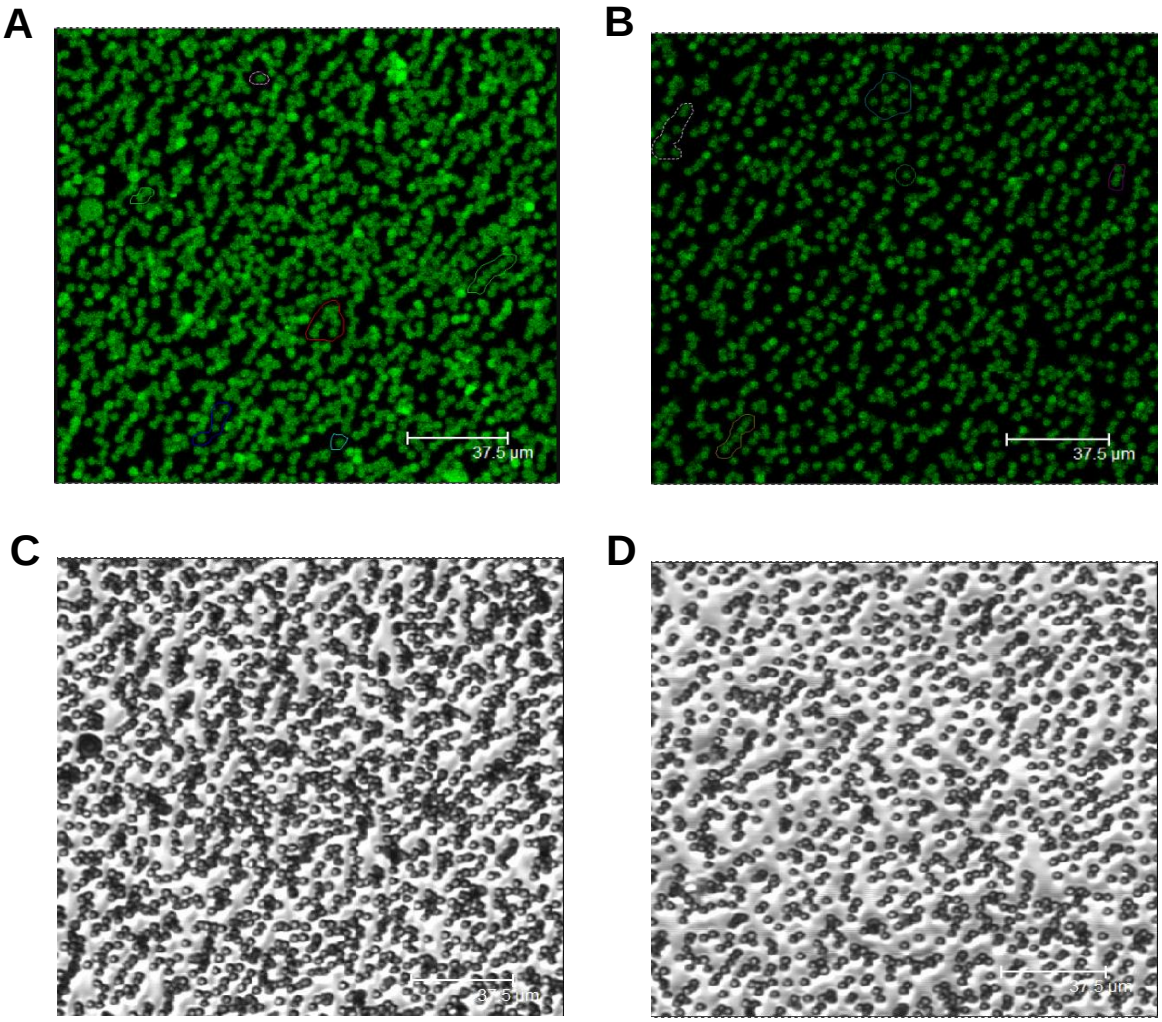
A
B
C
D
37.5 µm
37.5 µm
37.5 µm
37.5 µm

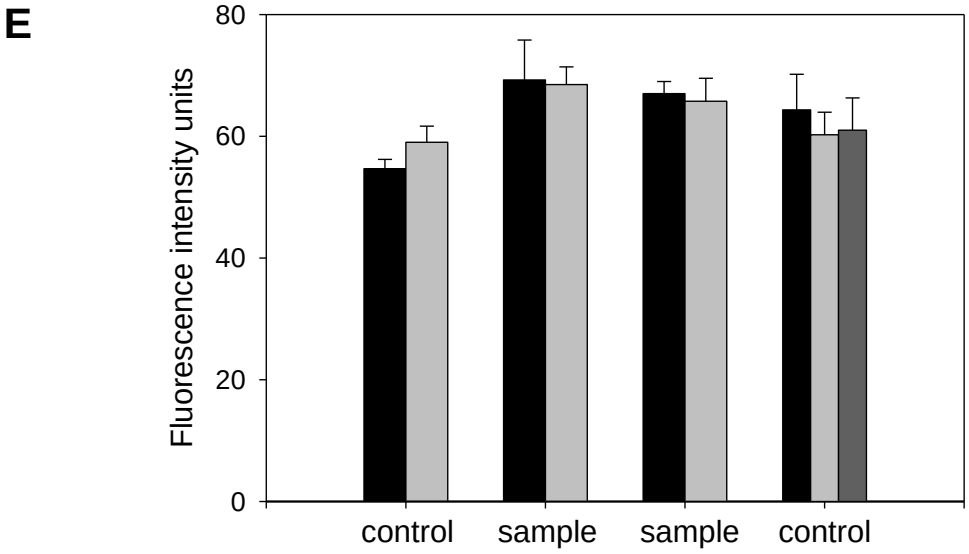
E
Fluorescence intensity units
0
20
40
60
80
control
sample
sample
control

A *t*-test done on the means and SDs of the all the sample and control values (the duplicates were averaged together) yielded a P<<0.001, which showed that there is a significant difference between the samples and controls. Thus, in spite of the problem of autofluorescence in the negative control these results indicate that the 50:50 compound binds to the SA-beads in a robust fashion.

4.2.3 SA-bead with the 50:50 compound and SA-Alexa-647

In the previous experiment of Section 4.2.2, we had attempted to bind the 50:50 compound to the SA-beads. The fluorescence imaging was done on a confocal microscope. However, in the confocal microscope, the SA-beads have a problem of autofluorescence at all detection wavelengths (see Fig. 15). In spite of the autofluorescence problem, data analysis revealed that the SA-bead sample with the 50:50 compound attached was still significantly brighter than the control SA-beads that were not treated with the 50:50 compound. However, preliminary visualization study done on the raw SA-beads in a light microscope revealed that the beads do not autofluoresce only in the Cy5 region (~647 nm detection wavelength).

To overcome the problem of autofluorescence, and to take advantage of the lack of autofluorescence in the Cy5 region on the light microscope, we used another approach. In the previous experiment, the molar concentration of the 50:50 compound that we used was ~5 fold the molar biotin binding capacity of the given concentration of the SA-beads. However, there are ~75 biotin chains per Qdot in the 50:50 compound. Thus, effectively, the molar concentration of the 50:50 compound was ~280 fold the molar concentration of the biotin binding sites present on the specific concentration of

the beads. Thus, ideally, there should be a large number of biotin-terminated chains on the Qdots in the 50:50 compound that do not have attached SA and are available for binding. We decided to take advantage of these potentially unbound biotin chains, by attaching a fluorophore SA-Alexa 647. Thus the aim of this experiment was to test the binding of the 50:50 compound to the SA-beads using a SA-Alexa-647 fluorophore (Fig 7- box 5). We used two dilutions of the SA-Alexa 647; 1/500 and 1/100. Before starting the experiment, the beads were blocked with casein for 1 hour. After the blocking step, two vials of SA-beads (10 µl bead solution per sample) were incubated with 20 nM of the 50:50 compound for 1 hour. The two controls were simply incubated for 1 hour in TBST. After the incubation, the two samples and two controls were washed 3 times with 1 ml TBST. Two dilutions of the SA-Alexa 647 were then added to the samples and controls. Thus in all, we had 4 vials. The first two vials were the samples with the 50:50 compound and two dilutions of the SA-Alexa 647 (1/100 and 1/500). Vials 3 and 4 were the controls which lacked the 50:50 compound, but had the two dilutions of the SA-Alexa 647; 1/100 and 1/500 respectively. After 1 hr of incubation with the SA-Alexa 647, the beads were washed 3 times with 1 ml TBST. From each vial, 100 µl of bead solution was then put in a glass bottom dish and imaged under a light microscope. Fig. 16 shows results of the experiment. The left images, as labeled in panel A are the sample brightfield and fluorescence images. The SA-Alexa 647 dilution in this Figure is 1/500. The fluorescence values of the sample at the two dilutions were generally similar, which meant that saturation of the SA-Alexa 647 was achieved. On the other hand, the controls which lacked the 50:50 compound were completely dark (the control with the SA-Alexa 647 dilution 1/500 shown in the right images of panel A).

Fig. 16: **Results of SA-bead functionalized with 50:50 compound and SA-Alexa 647**
Panel A illustrates the brightfield images (top two images) and the corresponding fluorescence images (bottom two panels). The left two images are the sample (SA-beads, 50:50 compound and SA-Alexa 647) and the right two images are the controls (SA-beads and SA-Alexa 647), as indicated by the labels. Panel B is the histogram obtained from analyzing the means ± SDs of 6 ROIs in the fluorescent images (indicated by the colored areas superimposed on the images). The y-axis is expressed in terms of fluorescence brightness units. A *t*-test done on the means and SDs of the sample *vs.* the control yielded a significant difference ($P << 0.001$) which indicated a strong binding of the 50:50 compound to the SA-beads

A

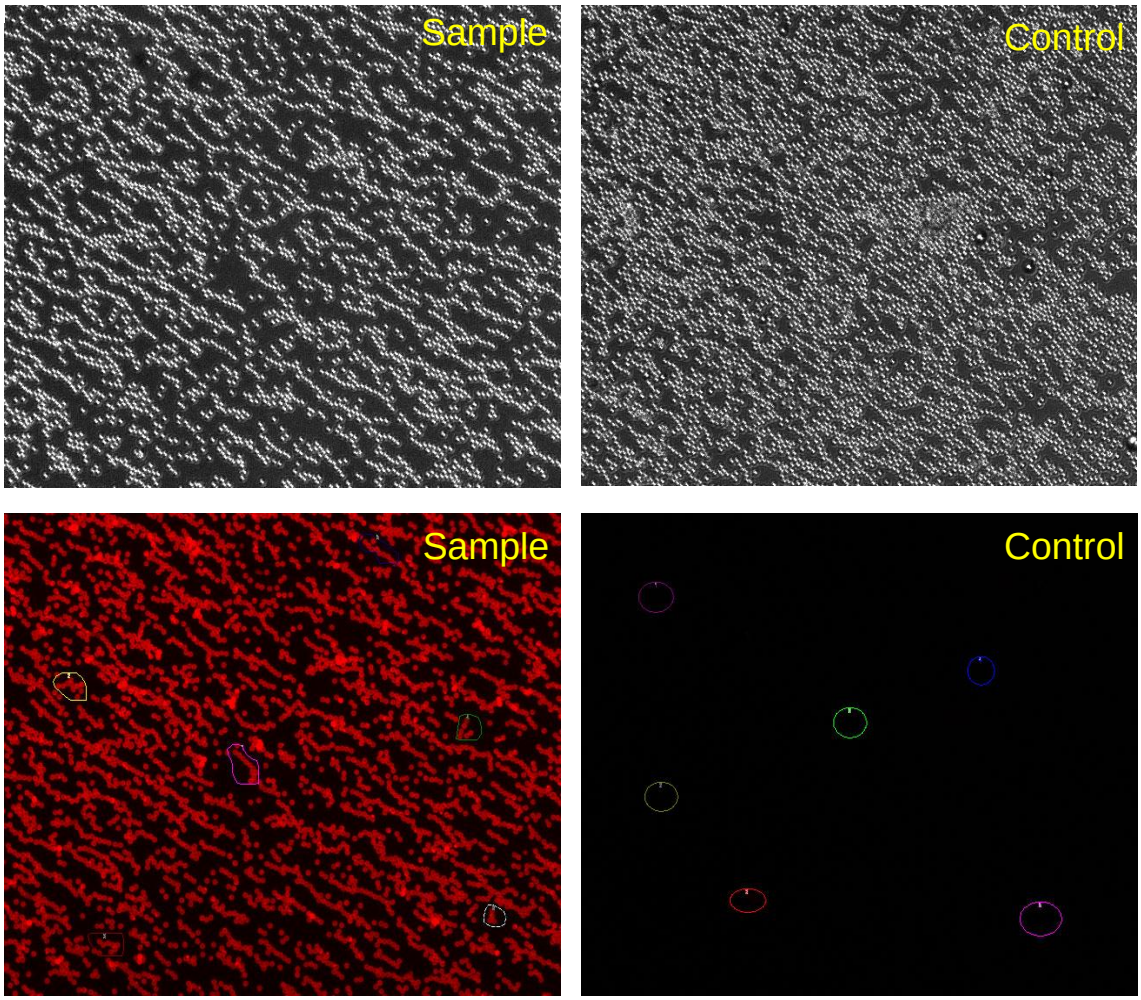
Sample
Control
Sample
Control

B

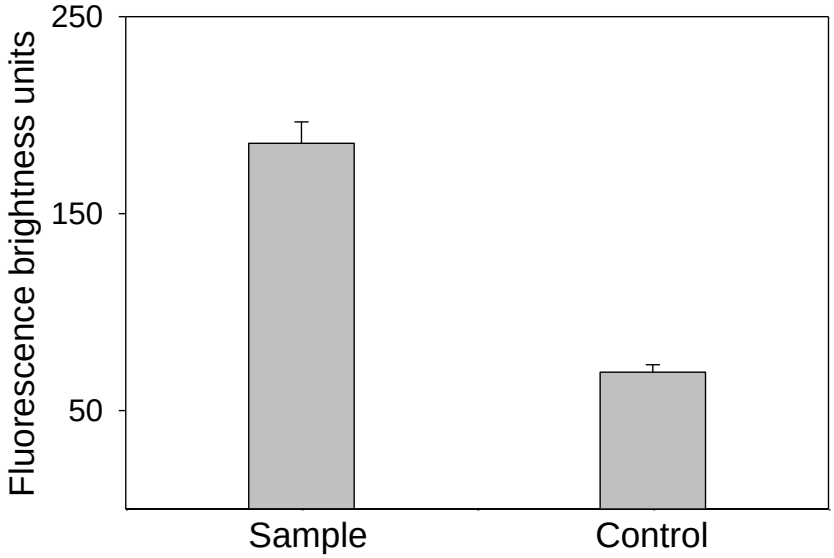
250
150
50
Fluorescence brightness units
Sample
Control

The fluorescent images were analyzed using the ROI method as described above. In this case, 6 ROI were selected from each image and the mean and SD of the maximum pixel value of each ROI was plotted in panel B. The sample and the control bars are labeled as such in panel B. A t-test performed on the means and SD yielded a P-value << 0.001, which indicated a significant difference between the sample and the control. This is conclusive evidence that the 50:50 compound binds robustly to the SA-beads. This also serves as a confirmation of the results obtained in the previous experiment, which had the problems of SA-bead autofluorescence on the confocal microscope. The fact that we saw a significant difference in the fluorescence between the sample and the control in the previous experiment can be attributed to the binding of the 50:50 compound to the SA-beads.

Another interesting facet of this experiment is that the 50:50 compound seems to serve as a robust ‘linker’ component, in that it can use some of its biotin chains to attach to the SA-beads, and other chains can be used to attach other SA-based components downstream. This makes the Qdot based 50:50 compound a very interesting compound in view if its flexibility of being able to use its biotin terminated chains for two distinct purposes and thus acting as a linker.

4.2.4 Bead-probe electrophysiology with the 50:50 compound

The experiment in this section addresses Aim 2.2 of the study. The primary objective here was to determine if the muscimol terminated PEG3400 chains present on the 50:50 compound attached to the bead, can bind to the $GABA_C$ receptors present on the cells, and in doing so, elicit a electrophysiological response as determined from a patch-clamp experiment (Fig 7, branch Q4 - box 6).

The 50:50 compound also has muscimol-terminated chains, which can activate $GABA_C$ receptors. The next step was to attach the 50:50 compound to the SA-beads and in a patch-clamp setup, attach a single bead to the tip of a micropipette and present it to $GABA_C$ receptor expressing neuroblastoma cells. An important requirement of this approach is that, when the bead touches the cell, we need a large number of muscimol molecules to activate a significant number of $GABA_C$ receptors, such that a measurable current is elicited. We can confirm activation of the receptors by the bead-attached protein only when there is a significant (well above noise level) measurable current. For these purposes, we obtained larger 7.9 µm SA-beads from Bang's Labs (Fisher, IN). The advantage of the 7.9 µm beads is that the larger surface area might bind more molecules of the 50:50 compound. The larger surface area might be able in turn to activate a significant number of $GABA_C$ receptors present on neuroblastoma cells in a probe-electrophysiology experiment. This might enable us to see electrophysiological activation of the $GABA_C$ receptors by the muscimol present on the 50:50 compound bound to the beads, leading to a measurable inward current. We tested the new 7.9 µm in an experiment similar to section 4.2.3 above and obtained identical results (results not shown), showing robust binding of the 50:50 compound to the 7.9 µm beads.

The 7.9 µm SA-beads were first functionalized with the 50:50 compound. A small volume (~5 µl) of functionalized bead solution was added to the dish containing the $GABA_C$ expressing neuroblastoma cells. Using a glass micropipette attached to a micro-manipulator, a single bead was held to the tip of the micropipette using gentle suction. After picking up the bead, a cell was patch clamped and held at -60 mV. Two concentrations of GABA (3 µM and 1 µM) were applied to the cell and the response measured. After the initial control measurements, where the currents were allowed to stabilize, the bead-attached probe was then brought close to the cells, and contact achieved. Again, the aim here was to determine if the binding of the muscimol present on the bead to the $GABA_C$ receptor on the patch-clamped neuroblastoma cells, has any electrophysiological effect in the absence or presence of test GABA solutions.

Fig. 17 shows the result of this experiment. All of the waveforms shown in Fig. 17A are current responses to 1 µM GABA from a cell under patch-clamp. The order of application of GABA in the above Figure is black, red, green and blue. The black and red waveforms are the control GABA responses. These waveforms were the application of GABA prior to the bead touching the cell. After these two applications of GABA, the bead was brought in proximity to the neuroblastoma cell and allowed to touch the cell. The touching of the functionalized bead to the cell itself did not elicit any current. However, post-bead treatment, the 1 µM applied GABA gave rise to the currents depicted by the green and blue waveforms. As we can see, post-bead GABA treatment gave rise to currents that are ~1.5 times the pre-bead GABA treatment. However, after the bead was withdrawn from the cell, the current did not recover to the pre-bead treatment levels

(data not shown). Rather the current remained at the higher value at all the subsequent GABA applications.

Experiments done on other cells, however, did not show such a dramatic effect. In one cell (Fig. 17B shown), there was no change in the current pre- and post-bead treatment. In Fig. 17B, the pre-bead application responses are shown in red and blue (in that sequence), while the post-bead responses are shown in green and black (in that sequence). Here as illustrated, there was no change in the current before and after the application of the bead.

The bead application was done on multiple cells (8-10 cells). Control beads (untreated beads) tended to show a variation in responses similar to those depicted in Fig. 17A and B. Thus, the increase in responses as shown in Fig. 17A after the bead application was also seen in some cells in the control experiments. The change (or increase) in current after bead application did not seem to follow a pattern, in that, some cells showed an increase in response, where as other cells did not. This seemingly arbitrary effect was true for control as well as the functionalized beads.

Fig. 17: **Typical responses of $GABA_C$ receptor expressing neuroblastoma cells to 1 µM GABA, before and after 50:50 compound functionalized SA-bead treatment.**
Panels A and B are responses of two different cells to functionalized bead treatment. The different colors indicate the sequence in which the GABA was applied. Black and red waveforms show the GABA responses prior to the application of the bead to the cell (in that sequence). Green and blue waveforms were the responses to GABA application after the bead was applied (touching) the cell. The duration of application of the 1 µM GABA is indicated by the rectangular wave above plots. Panel A describes a cell where there was an increase in the GABA response after the application of the bead (the green and blue waveforms as compared to the black and red). Panel B describes a cell where there was no difference in the waveforms obtained before *vs.* after bead application

A

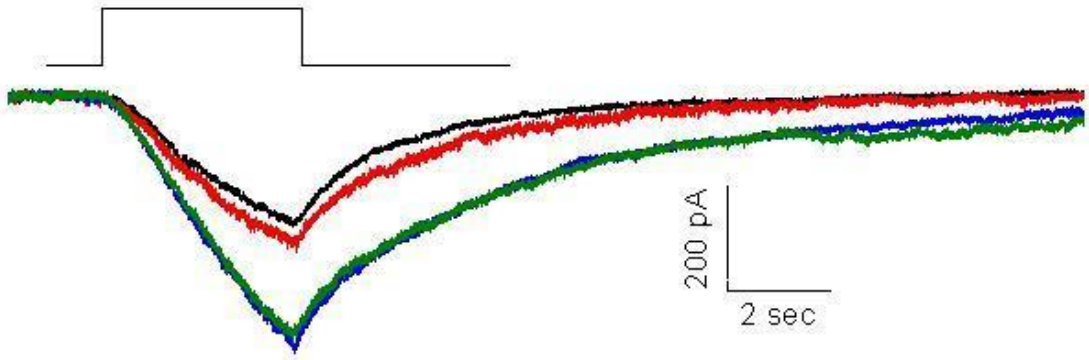

B

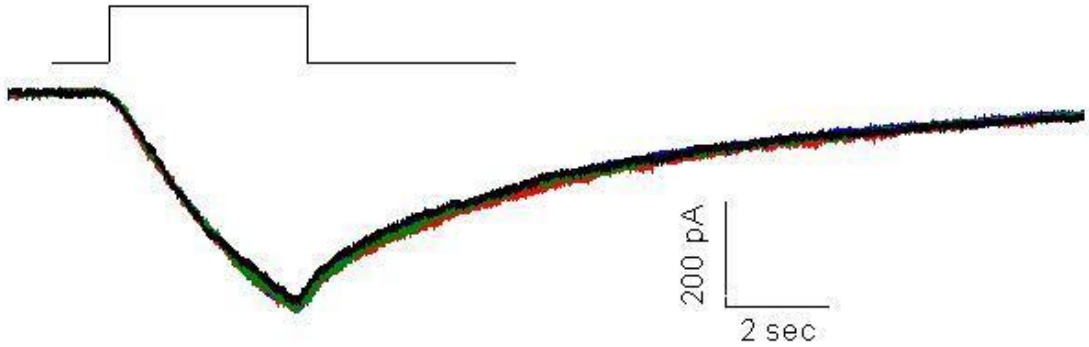

4.3 Ni^{2+}-bead experiments

Nickel coated beads were obtained from Millipore Inc. (Billerica, MA). These beads are ~10 µm in diameter. They have an outer coating of Ni^{2+} ions, which can bind his6 tagged proteins, like the protein B-domain (in the case of the SA-beads, once the SA-biotin bond is formed, it cannot be disrupted). The advantage of using the Ni^{2+}-beads over SA-beads is that the binding of the Ni^{2+}-his6-tag is reversible. Addition of imidazole can disrupt the Ni^{2+}-his6-tag bond, thus releasing the protein. Thus, a Ni^{2+}-bead preparation can be used for delivering a protein structure to the $GABA_C$ receptors expressed on the neuroblastoma cells. Individual protein structure functionalized Ni^{2+}-beads could then be attached to the tip of glass micro-pipettes and with the help of the micro-manipulator, presented to $GABA_C$ Ab-*N*14 receptors present on the surface of neuroblastoma cells.

Before attaching the Ni^{2+}-beads to the probes, we needed to test the ability of the Ni^{2+}-beads to bind our protein of interest. Experiments similar to the ones done in section 4.2 with the SA-beads were done, where, through fluorescence visualization, we demonstrated the binding of the B-domain-$GABA_C$ Ab-*N*14 based protein complex and the 50:50 compound to the SA-beads. In the experiments described in this section (addressing Aim 2.2), we have demonstrated the binding and dissociation through imidazole, of the B-domain-$GABA_C$ Ab-*N*14 based protein complex to the Ni^{2+}-beads (Fig. 13, branch Q5 – box 8).

Fig. 18: **Functionalization of the Ni^{2+}-beads with the protein complex.**
The results of Ni^{2+}-beads treated with the protein complex consisting of B-domain, $GABA_C$ Ab-*N*14 and 2°Cy5, pre-imidazole treatment are shown here. Panels A and B respectively, show brightfield and fluorescence images of the sample which contains the complete protein complex described above. Panels C and D are images taken from the negative controls which lacked only the B-domain, Panels E and F lacked only the $GABA_C$ Ab-*N*14 and Panels G and H lacked both the B-domain and the $GABA_C$ Ab-*N*14. Panel B (the sample) is visually brighter and has more fluorescent beads as compared to the rest of the controls in Panels B, D, F and H.

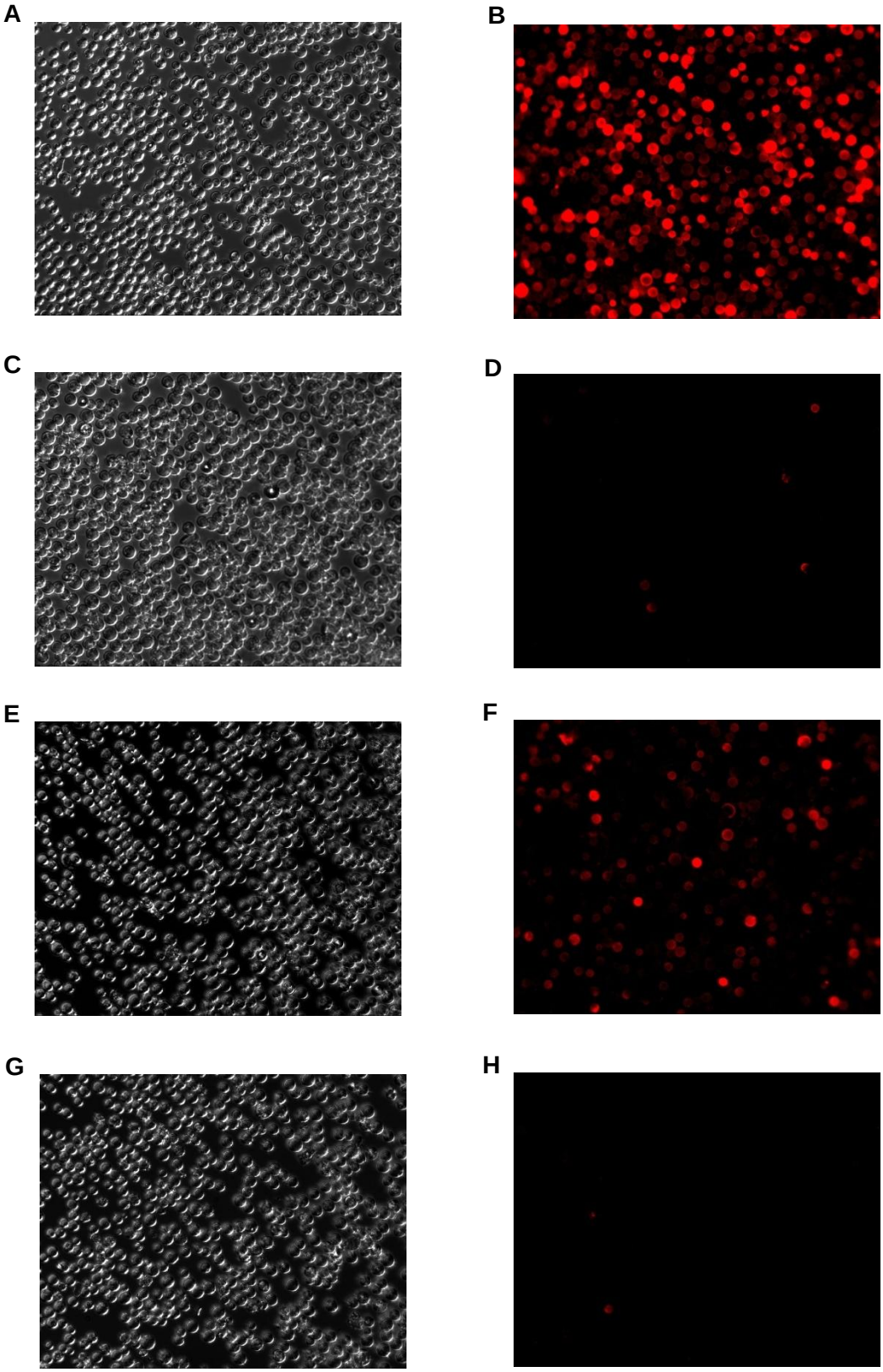
A
B
C
D
E
F
G
H

4.3.1 Ni^{2+}-bead visualization

The main objective of this experiment was to determine whether a protein complex consisting of B-domain and $GABA_C$ Ab-*N*14 could bind to and dissociate from the Ni^{2+}-beads, as analyzed by fluorescence visualization of the beads.

The B-domain has a his6-tag, which can bind to the Ni^{2+}-beads. Thus the protein structure that was attached to the Ni^{2+}-bead consisted of Ni^{2+}-beads: B-domain: $GABA_C$ Ab-*N*14: 2°Cy5. Similar to experiments described in section 4.2, the protein structure, starting with the B-domain, was sequentially attached to the beads. Prior to protein attachment, the beads were blocked with Casein to prevent non-specific binding. Three negative controls were used in this experiment. The first control lacked the only the B-domain, the second control lacked only the $GABA_C$ Ab-*N*14 and the last control lacked both the B-domain and the $GABA_C$ Ab-*N*14. The sample and the controls were then treated with the 2°Cy5 (which is specific to the $GABA_C$ Ab-*N*14). Images were acquired after the sequential treatment of all the components of the protein complex. The beads were then incubated with imidazole, to investigate if there is a change in fluorescence intensity post-imidazole treatment corresponding to the disruption of the his6-tag of the B-domain from the Ni^{2+}-beads, and thus the removal of the protein complex.

Fig. 18 illustrates the results of this experiment pre-imidazole treatment. Panels A, C, E and G are brightfield images and B, D, F and H are the corresponding fluorescence images. The sample (Panels A and B), containing the complete protein complex described above showed robust fluorescence as seen in Panel B. The negative controls which lacked the B-domain are shown in Panels C and D. The second negative

control lacking the $GABA_C$ Ab-*N*14 is shown in Panels E and F and the final control lacking both the B-domain and the $GABA_C$ Ab-*N*14 is shown in Panels G and H. Panels D and H show negligible fluorescence corresponding to the inability of the $GABA_C$ Ab-*N*14 and the 2°Cy5 to bind to the beads in the absence of the B-domain. However the control lacking the $GABA_C$ Ab-*N*14 as depicted in Panel F did show fluorescence. This means that the 2°Cy5 is binding to the B-domain in the absence of the $GABA_C$ Ab-*N*14. It is well known that the B-domain can bind all IgG antibodies. The $GABA_C$ Ab-*N*14 and the 2°Cy5 are both IgG antibodies. So the 2°Cy5 is capable of binding to the B-domain in the absence of the $GABA_C$ Ab-*N*14. Thus the non-zero fluorescence of Panel F is not an unexpected result.

Fig. 19 depicts the result of the experiment post-imidazole treatment. Panel I shows the sample. Panels J, K and L are the negative controls lacking the only the B-domain, only $GABA_C$ Ab-*N*14 and both B-domain and $GABA_C$ Ab-*N*14 respectively. For I and K, treatment of imidazole diminished, but did not completely eliminate the fluorescence. Again, the fluorescence in J and L was almost negligible, similar to the pre-imidazole images. A different method was used for analyzing the images from Fig. 18 and 13. The ROI method used in previous SA-bead experiment was not used in the current experiment because of the presence of both brightly and dimly fluorescing beads in both the samples and controls in both, Fig. 18 and Fig. 19. In the current experiment, each fluorescence image was divided into 9 equal sub-images by a 3x3 grid. Care was taken to select images that had a uniform and visually similar bead population. This was done to ensure that a difference in the number of beads present in a single image did

Fig. 19: Results of imidazole treatment on Ni^{2+}-beads functionalized with the protein complex.

Shown here are the results of the beads functionalized with the protein complex (B-domain: $GABA_C$ Ab-*N*14: 2°Cy5) post-imidazole treatment. As in fig. 12, Panel I shows the sample which contains the complete protein complex described above. Panels J, K and L are the fluorescent images taken from the negative controls which lacked only the B-domain, only the $GABA_C$ Ab-*N*14 and both the B-domain and the $GABA_C$ Ab-*N*14 respectively. There was a substantial reduction in fluorescence in Panels I and K as compared to the corresponding panels in fig. 12. Panels J and L remained dark similar to the corresponding panels in fig. 12. Panel M plots the histograms from Panels A-L. Each bar is the mean ± SD from 9 equally divided regions (sub-images) from the corresponding image, as indicated by the labels below the bars. The black and grey bars are histograms of images pre-imidazole treatment and post-imidazole treatment respectively.

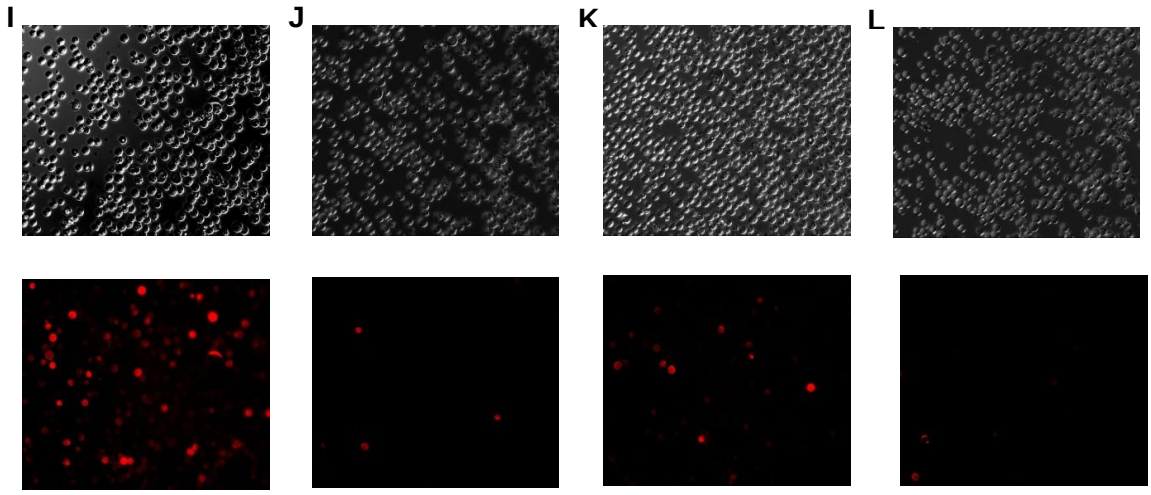
I
J
K
L

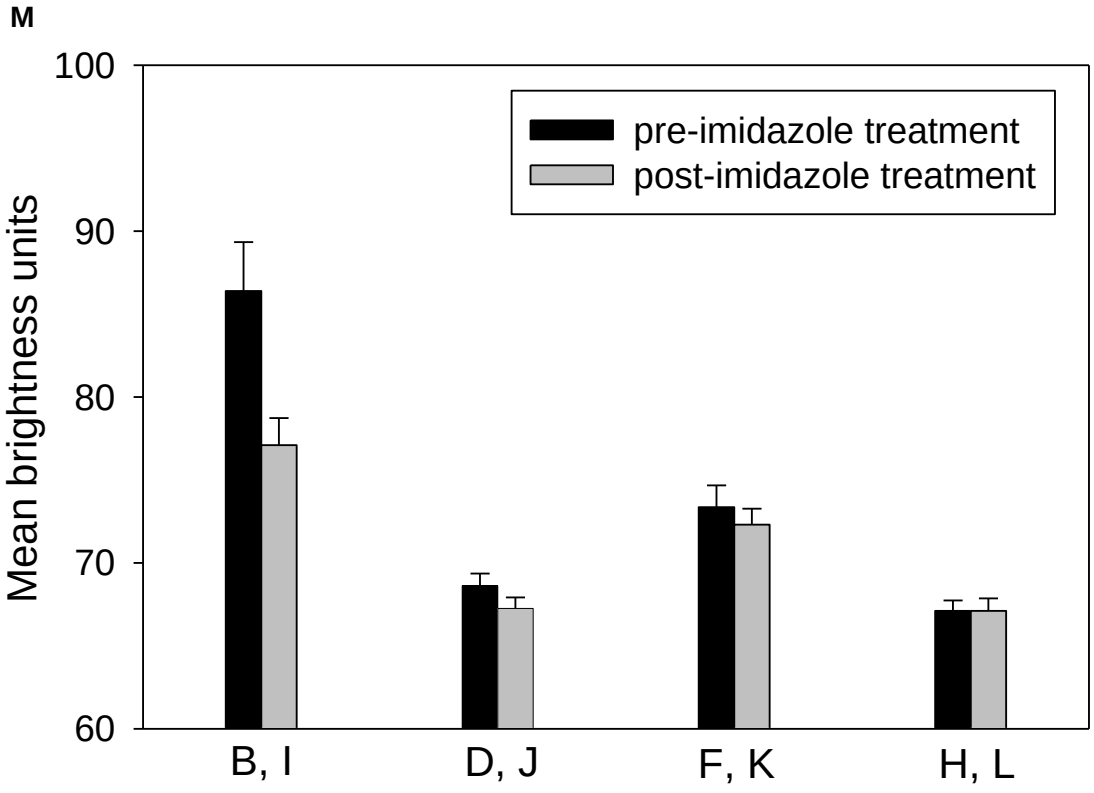
M
Mean brightness units
100
90
80
70
60
pre-imidazole treatment
post-imidazole treatment
B, I
D, J
F, K
H, L

not skew the data, since different beads had different levels of fluorescence brightness. Due to the limitations of the image acquisition and analysis program, the grid was unable to cover the entire image. However, the areas not covered by the grid were marginal and thus ignored. The average brightness value from each of the 9 sub-images was noted. Thus, for each image, a mean ± SD of the average brightness from the 9 sub-images was obtained and plotted in Panel M of Fig. 19. The labels below each black and grey bar identify the corresponding image Panels from which the data was obtained using the above described 9 sub-image method. The black bars were the mean ± SDs obtained from the pre-imidazole treatment images from Fig. 18 (Panels B, D, F and H) and the grey bars were obtained from the post-imidazole treatment images from Fig. 19 (Panels I-L). This histogram illustrates that there was a significant difference in the sample (Bar B) and the negative controls (Bars D, F and H) with $P << 0.0001$. In the post-imidazole treatment bars (grey bars), the sample bar (Bar I) was significantly lower than the corresponding pre-imidazole sample Bar B ($P << 0.0001$). However, there was no significant difference between the control bars pre and post-imidazole (Bars D, J; F, K and H, L).

This experiment showed that we can functionalize and dissociate the protein complex from the Ni^{2+}-beads by the addition of imidazole. The ultimate aim is to capture individual functionalized beads at the tip of hollow glass micropipettes. Such a Ni^{2+}-based microprobe will be then be advanced close to the surface of $GABA_C$ receptors expressing neuroblastoma cell with the aid of a micromanipulator (similar to the SA-bead-probe experiments). The bead present at the tip of the probe will then be treated with imidazole to release the protein complex in the vicinity of the cell. After a brief

incubation time, the cell will be investigated under a microscope for fluorescence (2°Cy5) resulting from the binding of the $GABA_C$ Ab-*N*14 that is part of the dissociated protein complex, to the $GABA_C$ receptors present on the cell. However, before we can move to the Ni^{2+}-based microprobe experiment, we need to determine the concentration of protein present on a single bead. If the amount of fluorescently labeled protein complex present on a single bead were tiny, we would not be able to detect the presence of the protein complex bound to the $GABA_C$ receptors on the targeted cell because of the weak fluorescence signal. Thus, we needed to determine the optimum conditions, in terms of the amount of protein complex present on a single bead that could yield a detectable signal when the protein complex is dissociated from the bead onto the targeted neuroblastoma cell. To achieve this, we needed to first functionalize a population of beads with the protein complex, and then dissociate the protein complex from the beads. This dissociated protein complex could then be incubated with the cells, to determine if the complex that has been dissociated from the beads is capable of binding to the $GABA_C$ receptors on the neuroblastoma cells.

4.3.2 Cell double-labeling experiment

The rationale for carrying out this experiment is to determine optimum conditions for attaching and releasing a protein complex containing the $GABA_C$ Ab-*N*14 and the B-domain from the Ni^{2+}-beads. The design of this type of experiment was to attach the protein complex to the Ni^{2+}-beads through the his6-tag of the B-domain. The protein complex would then be released from the beads with the addition of imidazole, in the vicinity of the $GABA_C$-receptors expressing neuroblastoma cells. The complex, which has a 2°Cy5 directed against the $GABA_C$ Ab-*N*14 antibody, would then be allowed to

bind to the $GABA_C$ receptors on the cells. To obtain the optimum conditions, it was desirable to vary the concentrations of the $GABA_C$ Ab-*N*14 so as to obtain a bright fluorescence signal due to the binding of the released complex onto the cells.

The positive control used in this experiment was the $GABA_C$ Ab-*N*14 and a 2°FITC (directed against the primary antibody) attached to the neuroblastoma cells. This control has been used in previous experiments (Section 4.1.2) and has shown robust fluorescence. The main sample in this experiment is; neuroblastoma cells: $GABA_C$ Ab-*N*14: B-d-M-B: 2°Cy5 directed against $GABA_C$ Ab-*N*14. The drawback of this complex is that the 2°Cy5 binds to the $GABA_C$ Ab-*N*14 and not to the B-d-M-B. We sought to obtain evidence of the binding of the B-d-M-B to the $GABA_C$ Ab-*N*14. For this reason, we decided in this experiment to double-stain the protein complex. For staining the B-d-M-B, we used streptavidin-Dylight 488 (SA-Dylight, Pierce, Rockford, IL), which fluoresces in the FITC wavelength region. Thus, from this sample, we would have evidence of the binding of the B-d-M-B (SA-dylight) as well as the $GABA_C$ Ab-*N*14 (2°Cy5). (For the previous Ni^{2+}-bead experiments, we used B-domain as the scaffold protein and not the B-d-M-B). The original plan was to use just the B-domain, similar to the Ni^{2+}-bead experiments. Previously, in cell labeling experiments (Section 4.1.3), a MAL-Alexa attached to the cysteine of the B-domain was used as a fluorescent label for the B-domain. However, use of the MAL-Alexa did not yield a conclusive fluorescence reporting signal from the B-domain. To overcome this problem, we used the B-d-M-B to which we could attach the SA-dylight 488 though the Biotin-SA interaction). Thus the sample complex was; Nb cells: $GABA_C$ Ab-*N*14: B-d-M-B: 2°Cy5 against $GABA_C$ Ab-*N*14: SA-Dylight 488 coupled to the biotin of the B-d-M-B.

Another positive control was the protein complex which consisted of the $GABA_C$ Ab-*N*14 and the 2°Cy5. Two negative controls were used, one which contained the B-d-M-B and the SA-dylight 488 and lacked the $GABA_C$ Ab-*N*14, and one which contained only the 2°Cy5 and lacked both the B-d-M-B and the $GABA_C$ Ab-*N*14.

The results are shown in Fig. 20. The positive control consisting of the $GABA_C$ Ab-*N*14 and the 2°FITC showed robust fluorescence at the wavelength settings appropriate for FITC (Panel A). The two negative controls, described above were completely dark (Panel C depicts the negative control which only had the 2°Cy5). The other positive control consisting of the $GABA_C$ Ab-*N*14 and the 2°Cy5 did show bright fluorescence at the wavelength settings appropriate for Cy5, but it was not as bright as the positive control with the 2°FITC. The main sample that was double- labeled (see above) showed bright fluorescence for the 2°Cy5 (Panel B) (similar to the positive control with the $GABA_C$ Ab-*N*14 and the 2°Cy5). However, the fluorescence as reported from the SA-dylight 488 was barely detectable (Panel D).

The lack of robust fluorescence of the SA-dylight in the double-labeled sample leads to two distinct possibilities. The first possibility is that there is not enough B-d-M-B bound to the $GABA_C$ Ab-*N*14. The second possibility is that the presence of the 2°Cy5 is somehow hampering the binding of the SA-dylight 488 to the B-domain. One possible experiment to test the second possibility is an experiment where we repeat the double-labeled sample from this experiment, and have two additional samples where we

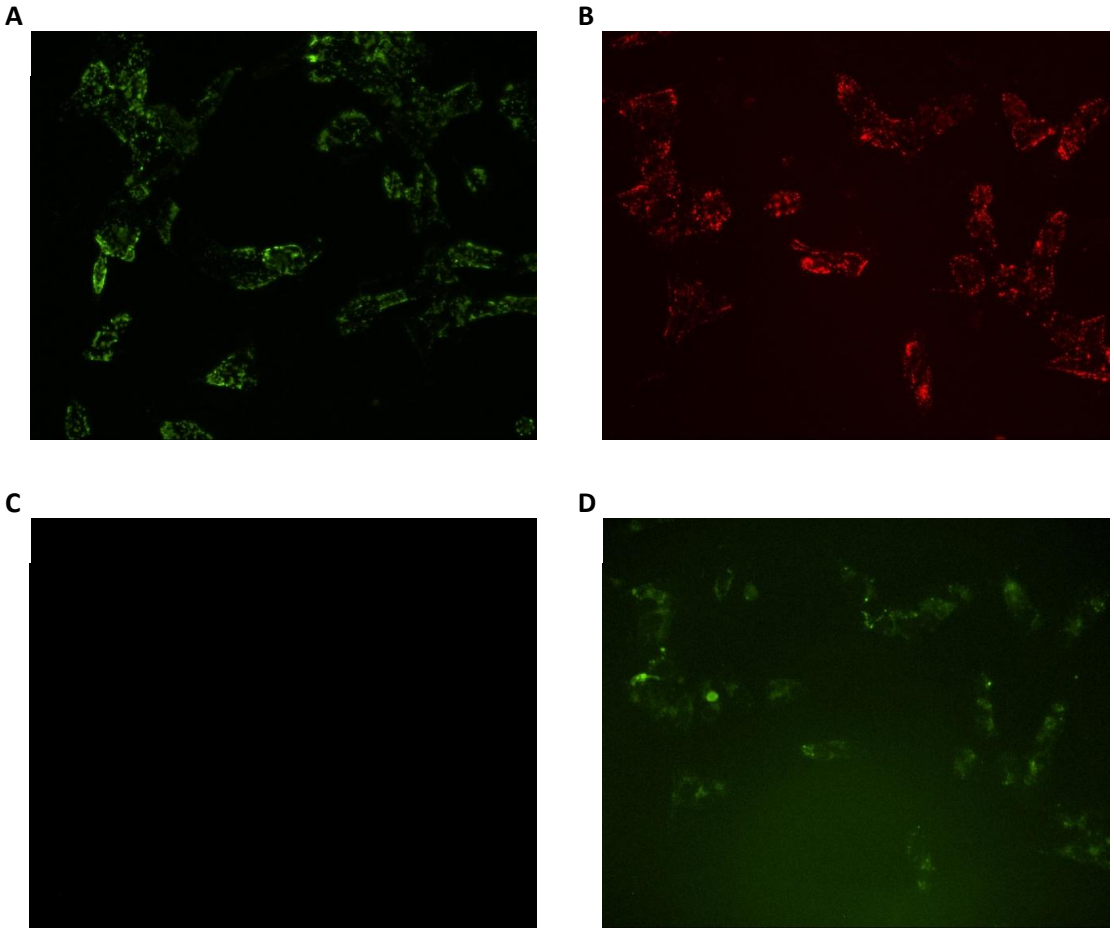

Fig. 20: **Results of the cell double labeling experiment.**

In this experiment, the neuroblastoma cells were double-labeled with a protein complex containing the $GABA_C$ Ab-*N*14 with a 2°Cy5 label and the B-d-M-B with a SA-dylight 488 label. Panel A is the positive control consisting of the $GABA_C$ Ab-*N*14 and the 2°FITC. Panel C is the negative control containing only the 2°Cy5. Panel B and D are the samples containing the $GABA_C$ Ab-*N*14 labeled with the 2°Cy5 and the B-d-M-B labeled with the SA-dylight respectively. Both the positive control in Panel A and the double-labeled sample ($GABA_C$ Ab-*N*14 and 2°Cy5) in Panel B showed robust fluorescence which was indicative of the strong binding of the $GABA_C$ Ab-*N*14 antibody to the $GABA_C$ receptors on the neuroblastoma cells. However, Panel D which shows the fluorescence due to the SA-dylight 488 attached to the B-d-M-B, showed much lower fluorescence as compared to the Panels A and B.

separately label the complex only with the SA-dylight or only with the 2°Cy5. In the absence of the 2°Cy5, the SA-dylight could bind strongly to the B-d-M-B and yield a robust fluorescence signal. However, if the presence of the 2°Cy5 is not hampering the binding of the SA-dylight to the B-d-M-b, then (as mentioned in the first possibility where there is a low amount of bound B-d-M-b) in a single labeling experiment, the protein complex ($GABA_C$ Ab-*N*14: B-d-M-B) which is labeled with just the SA-dylight should show negligible fluorescence, similar to that of the double labeled sample (Fig. 20, Panel D) from the current experiment. The main aim of carrying out the cell-double labeling experiment described above (Section 4.3.2) is to obtain optimum conditions for attaching the protein complex on the Ni^{2+}-beads. On the Ni^{2+}-beads, the sequence in which the protein complex is attached is different from that in the Nb-cell experiments. In the Ni^{2+}-bead experiments, the B-domain attaches to the Ni^{2+}-beads first and then the $GABA_C$ Ab-*N*14 attaches to the B-domain. Thus, to demonstrate binding of the protein complex to the Ni^{2+}-beads, we need fluorescence reporting from the 2°Cy5 attached to the $GABA_C$ Ab-*N*14. In the cells, this sequence is reversed, in that the $GABA_C$ Ab-*N*14 attaches to the cells first, and then the B-domain is added. Thus, for the Ni^{2+}-beads, the 2°Cy5, which is specific to the $GABA_C$ Ab-*N*14, is an important component and was hence used in the double-labeled sample in the current experiment. However, in the neuroblastoma cell experiments, we cannot use just the 2°Cy5 (which binds to the $GABA_C$ Ab-*N*14), because then we do not have any fluorescence reporting from the B-domain, and thus there is no evidence of the binding of the B-domain to the $GABA_C$ Ab-*N*14 on the cells. This led us to use the SA-Dylight 488 (for which we had to use the B-d-M-B, instead of just the B-domain), which attaches to the biotin of the B-d-M-B and thus enables fluorescence reporting from the B-d-M-B. Thus, the problem is that we need to

use the 2°Cy5 for the Ni^{2+}-bead experiment and the SA-dylight 488 for the cell experiment.

A critical experiment in this overall plan is to vary the concentration of the $GABA_C$ Ab-*N*14 in the protein complex. This will assist us in obtaining a fluorescence gradient curve that will enable us to determine the optimum concentration of the $GABA_C$ Ab-*N*14 that will yield robust fluorescence on the cells. However, unless we have direct evidence of the presence of the B-domain on the complex (which the 2°Cy5 will not give, but the SA-dylight 488 might), we cannot say anything conclusive about the results of this proposed next experiment. Once we get the optimum concentration of the $GABA_C$ Ab-*N*14 needed to get good binding of the protein complex onto the $GABA_C$ receptors on the cells, we can use that concentration of the $GABA_C$ Ab-*N*14 along with the B-domain to attach the protein complex on the Ni^{2+}-beads.

4.3.3 Varying the concentration of the $GABA_C$ Ab-*N*14 in a cell labeling experiment

The aim of this experiment was to determine if a change in the concentration of the $GABA_C$ Ab-*N*14 influences the binding of the protein complex containing the $GABA_C$ Ab-*N*14, B-domain and SA-Alexa to the neuroblastoma cells.

In the previous experiments, we have shown that the protein complex containing the $GABA_C$ Ab-*N*14, B-d-M-B and 2°Cy5 can bind to the $GABA_C$ receptor-expressing neuroblastoma cells. The 2°Cy5 binds to the $GABA_C$ Ab-*N*14. To obtain evidence of the presence of the B-d-M-B on the cells, we had double-labeled the complex with SA-

Dylight 488, which binds to the biotin on the B-d-M-B. However, we observed that the fluorescence of the SA-Dylight 488 was very low, to the point of being almost negligible.

In the current experiment, we labeled the protein complex containing the $GABA_C$ Ab-*N*14 and B-d-M-B with SA-Alexa 647 (excitation wavelength: 647 nm, emission wavelength: 690 nm). It was preferable to use the SA-Alexa 647 rather than the SA-Dylight 488, because eventually, we would be binding the protein complex to the beads, and the beads tend to autofluoresce at 488 nm wavelength and not at 647 nm wavelength. Thus, the protein complex in this experiment consisted of; neuroblastoma cells: $GABA_C$ Ab-*N*14: B-d-M-B: SA-Alexa 647

In this experiment, we varied the concentrations of the $GABA_C$ Ab-*N*14. In previous experiments, we have used dilutions of 1/1000. In this experiment, 3 dilutions were used; 1/100, 1/1000 and 1/10,000 (the reason for using these three dilutions was to establish a type of bracketing, or arrive at a range where presumably 1/100 dilution would completely saturate the $GABA_C$ receptors and hence yield the highest fluorescence intensity and the 1/10,000 would yield low fluorescence intensity, closer to background. This would also enable us to arrive at an optimum concentration of the $GABA_C$ Ab-*N*14 that would yield a quantitatively conclusive experimental result). This corresponded to concentrations of 1.6 nM, 16 nM and 0.16 nM of the $GABA_C$ Ab-*N*14 respectively.

Overall, six dishes of $GABA_C$-receptor expressing neuroblastoma cells were used in the experiment. The first dish was a positive control that contained only the $GABA_C$ Ab-*N*14 (1/100 dilution) and the 2°FITC. The next three dishes were the above-mentioned protein complex with the three different dilutions (1/100, 1/1000 and

1/10,000) of the $GABA_C$ Ab-*N*14. The other two dishes were negative controls. One of the negative controls was the protein complex lacking only the B-d-M-B, and the other negative control lacking the only the $GABA_C$ Ab-*N*14.

Fig. 21 shows results of this experiment. Panel A is the positive control ($GABA_C$ Ab-*N*14: 2°FITC). Panels B, C and D are the samples containing the complete protein complex described above, with $GABA_C$ Ab-*N*14 dilutions of 1/100, 1/1000 and 1/10,000 respectively. Panels E and F are the negative controls containing the protein complex that lacked only the B-d-M-B and only the $GABA_C$ Ab-*N*14 respectively. As seen in the Figure the positive control (panel A) showed bright fluorescence. The sample containing the lowest $GABA_C$ Ab-*N*14 dilution (Panel B: 1/100) showed negligible fluorescence. The sample containing the $GABA_C$ Ab-*N*14 at 1/1000 dilution (Panel C) showed higher fluorescence than both Panel B ($GABA_C$ Ab-*N*14: 1/100) and Panel D ($GABA_C$ Ab-*N*14: 1/10,000). The negative control lacking the B-d-M-B (Panel E) showed negligible fluorescence, whereas the other negative control lacking only the $GABA_C$ Ab-*N*14 showed dim fluorescence.

Thus the 1/1000 dilution of the $GABA_C$ Ab-*N*14 yields the brightest fluorescence results. However, the brightness of the SA-Alexa 647 is much lesser than the positive control 2°FITC. This is because for the SA-Alexa 647, there is one Alexa 647 molecule per SA, and one SA binds to one biotin on the B-d-M-B. On the other hand, there are multiple FITC molecules per secondary antibody and multiple secondary antibodies bind to a single copy of the primary $GABA_C$ Ab-*N*14. In case of the positive control, there is a great amount of amplification taking place with respect to the fluorescence brightness. Thus, the reduced fluorescence brightness of the SA-Alexa 647 as compared to the 2°FITC is not a surprising result by itself.

Fig. 21: Varying the concentration of the $GABA_C$ Ab-*N*14 in a neuroblastoma cell labeling experiment

The protein complex used in this experiment was the $GABA_C$ Ab-*N*14, B-d-M-B and SA-dylight 647. Three dilutions of the $GABA_C$ Ab-*N*14 were used; 1/100, 1/1000 and 1/10,000. Panel A is the positive control which contains the $GABA_C$ Ab-*N*14 and 2°FITC. Panels B, C and D are the samples containing the complete protein complex with $GABA_C$ Ab-*N*14 dilutions of 1/100, 1/1000 and 1/10,000 respectively. Panels E and F are the negative controls containing the protein complex that lacked only the B-d-M-B and only the $GABA_C$ Ab-*N*14 respectively. Panel C which had the primary antibody dilution of 1/1000 showed brighter fluorescence as compared to 1/1000 and 1/10,000. However, only a few cells had detectable fluorescence (those cells are shown in Panel C). In all cases, the samples were much lower in brightness compared to the positive controls.

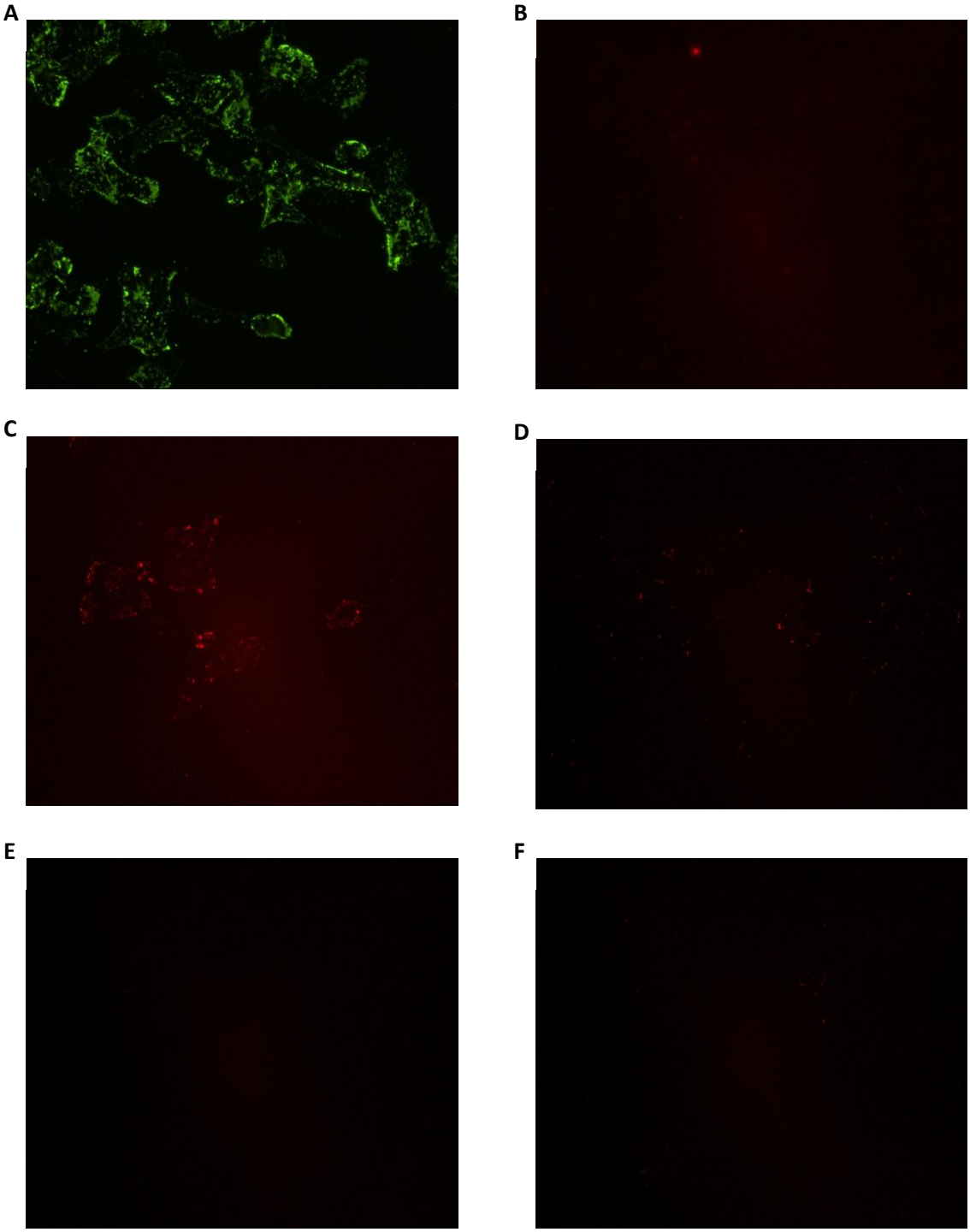
A
B
C
D
E
F

4.3.4 FITC-B-domain experiments

Our colleague, Dr. Nasser Qtaishat has prepared a B-domain that has been pre-labeled with FITC. FITC molecules (potentially 4-6) can be conjugated to lysine residues on the B-domain, yielding a stable and highly fluorescent FITC-labeled B-domain. There are many advantages to having such a preparation. As noted earlier in this thesis project (Sec. 4.3.2) it is highly desirable to have both the B-domain and the $GABA_C$ Ab-*N*14 labeled (in a protein complex containing the B-domain: $GABA_C$ Ab-*N*14). This is because, when the protein complex containing the B-domain and the $GABA_C$ Ab-*N*14 binds to the Ni^{2+}-beads, the B-domain attaches to the Ni^{2+} on the beads followed by the $GABA_C$ Ab-*N*14. However, when this protein complex is eluted from the beads onto the cells, the sequence in which the complex binds to the cells is reversed (the $GABA_C$ Ab-*N*14 attaches to the $GABA_C$ receptors on the neuroblastoma cells, followed by the B-domain) to sequence in which the complex binds to the Ni^{2+}-beads. Having a B-domain that is pre-labeled with the FITC would be a good solution to the problem of achieving double-labeling. In such a scenario, we would have the FITC-B-domain and the $GABA_C$ Ab-*N*14 labeled with a 2°Cy5. This would enable us to have evidence of the presence of both the B-domain and the $GABA_C$ Ab-*N*14 when the complex is eluted from the Ni^{2+}-beads onto the neuroblastoma cells. Thus the objective of this experiment was to achieve double labeling of the protein complex by using the FITC-B-domain and the $GABA_C$ Ab-*N*14 labeled with the 2°Cy5 (Fig. 13, branch Q5 – box 7).

For testing the FITC-B-domain, two experiments were attempted. The first experiment was the attachment of the complex (FITC-B-domain: $GABA_C$ Ab-*N*14: 2°Cy5) to the Ni^{2+}-beads. The results of this experiment are shown in Fig. 22. The second experiment was the attachment of the protein complex ($GABA_C$ Ab-*N*14: 2°Cy5: FITC-B-

domain) to the $GABA_C$ receptors on the neuroblastoma cells. The results are shown in Fig: 17.

As seen in Fig. 22, the beads which were incubated with the complete protein complex (FITC-B-domain: $GABA_C$ Ab-*N*14: 2°Cy5) showed robust fluorescence in the FITC region, due to the presence of the FITC-B-domain (Panel A). However, there was negligible fluorescence on the beads in the Cy5 region (Panel B). In the control that lacked only the $GABA_C$ Ab-*N*14, again there was robust fluorescence on the FITC region (Panel C), and as expected negligible fluorescence in the Cy5 region, because the 2°Cy5 cannot bind to the beads in the absence of the $GABA_C$ Ab-*N*14 (Panel D). In the negative control that lacked the FITC-B-domain, there was negligible fluorescence in both the FITC (Panel E) and the Cy5 region (Panel F). These results indicate that the FITC-B-domain can bind robustly to the Ni^{2+}-beads. However, the negligible fluorescence due to the 2°Cy5 in the sample (Panel B) seems to indicate that the $GABA_C$ Ab-*N*14 and hence the 2°Cy5 in unable to bind to the FITC-B-domain. The images were analyzed using the ROI procedure described above, where 6 regions were selected. The mean and SD of the maximum pixel value (in terms of fluorescence brightness units) from the 6 ROI were plotted in Panel G as shown. The label for each bar indicates the corresponding Panel number as depicted (Panels A-F). A *t*-test performed on the plotted mean and SDs yielded a significant difference between Panel A and Panels B, D-F. There was a significant difference between Panel C and Panels A-B, D-F. The presence of the $GABA_C$ Ab-*N*14 and the 2°Cy5 on Panel A, in addition to the FITC-B-domain does yield a significant difference than Panel C, which has only the FITC-B-domain and the 2°Cy5, but lacks the $GABA_C$ Ab-*N*14.

Fig. 22: Functionalization of the Ni^{2+}-beads with a double-labeled protein complex. The protein complex used here was the FITC-B-domain, $GABA_C$ Ab-*N*14 and 2°Cy5. The Panels on the left side (A, C, E and G) depict fluorescence in the FITC wavelength region (due to the FITC-B-domain) and those on the right (B, D, F and H) show fluorescence in the Cy5 region (due to the 2°Cy5). Panels A and B are the samples which depict the Ni-beads functionalized with the complete protein complex (FITC-B-domain: $GABA_C$ Ab-*N*14: 2°Cy5). Panel C and D are the controls which lacked only the $GABA_C$ Ab-*N*14 and Panel E and F are the negative controls which lacked only the FITC-B-domain. Panel G: Means ± SD of the maximum pixel value from ROI analysis of each image. The letter below each bar identifies the corresponding image that was analyzed to yield the bars. From Panel G, we see that Panels A and C, which were treated with the FITC-B-domain show significantly brighter fluorescence as compared to the other panels which were close to the background level. This is indicative of strong binding of the FITC-B-domain and inability of the $GABA_C$ Ab-*N*14 to bind to the beads

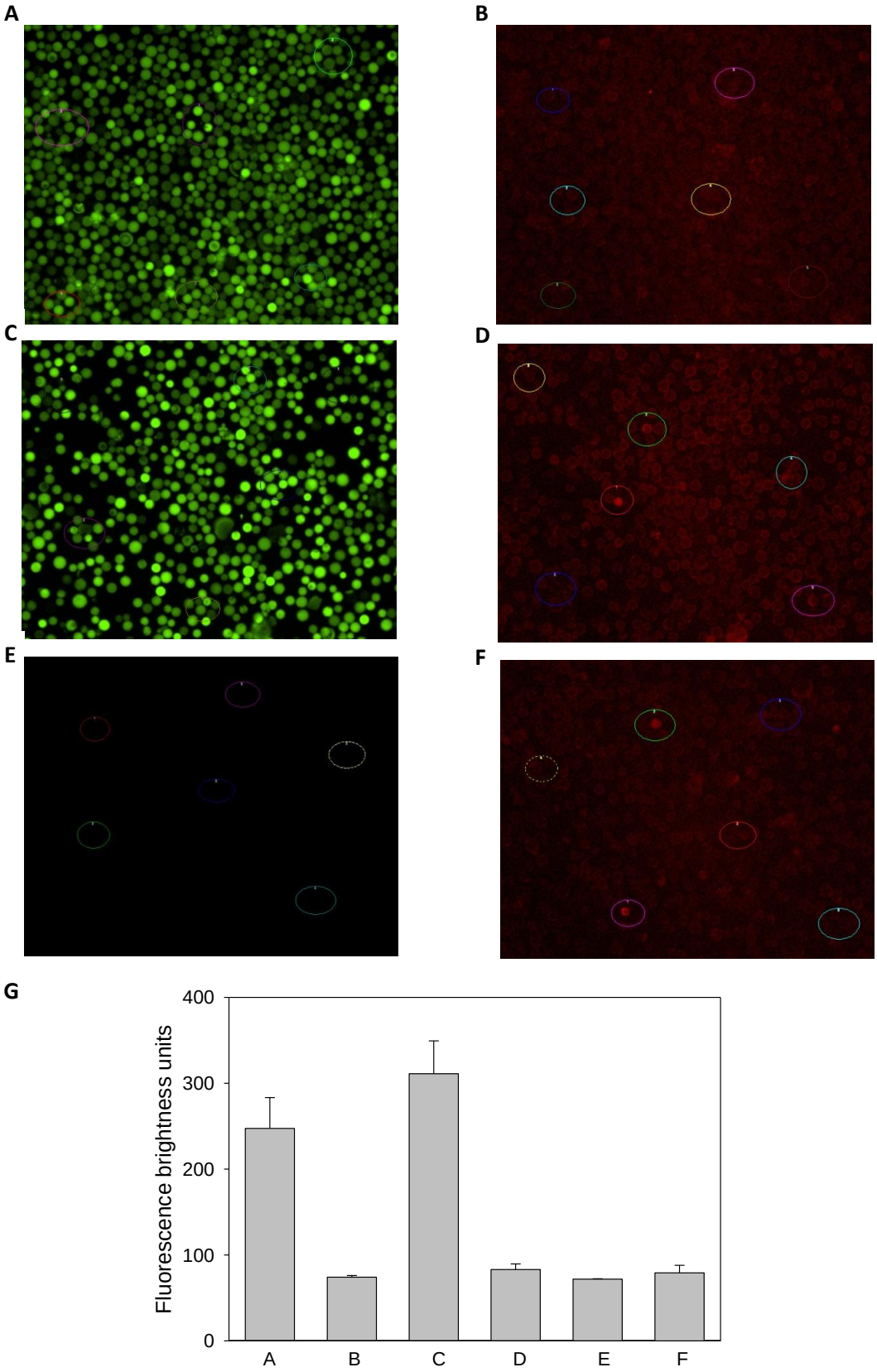
A
B
C
D
E
F
G
Fluorescence brightness units
400
300
200
100
0
A
B
C
D
E
F

The results of the binding of the FITC-B-domain based protein complex ($GABA_C$ Ab-*N*14: 2°Cy5: FITC-B-domain) on the $GABA_C$ receptors on the neuroblastoma cells are summarized in Fig. 23. Panels A and B are the positive control which contain only the $GABA_C$ Ab-*N*14 and 2°Cy5. As seen in panel A, there is robust fluorescence due to the 2°Cy5. At the same time, in spite of the absence of the FITC-B-domain on the positive control, we do see dim fluorescence in the FITC region, as seen in panel B. Panels C and D are the sample containing the complete protein complex; $GABA_C$ Ab-*N*14: 2°Cy5: FITC-B-domain. Similar to Panels A and B, we see robust fluorescence in Panel C due to the 2°Cy5 (Panel C) and some fluorescence due to the FITC-B-domain (Panel D). Panels E and F are the negative controls which contain only the 2°Cy5. As expected, in the case of the negative control, there is negligible fluorescence in both the 2°Cy5 and FITC region. From Panels C and D, we find that the cells are fluorescing in both the 2°Cy5 and the FITC regions, as expected. However, in the sample, which lacks the FITC-B-domain, we still see fluorescence in the FITC region. The reason for this might be the that there is cross-talk in the fluorescence between the 2°Cy5 and the FITC wavelengths (in a fluorescent microscope, there could be cross-talk between fluorescent dyes where excitation light of a particular wavelength might in some cases excite a fluorophore of a different wavelength; in this case, light in the FITC region is exciting the 2°Cy5 in the double-labeling experiment) causing the cells to fluoresce in the FITC region even where there is no FITC-B-domain in the positive control. Thus, the FITC fluorescence we see in the sample (Panel D) might also be due to the fluorescence leakage from the 2°Cy5 to the FITC region. These results indicate that the $GABA_C$ Ab-*N*14 and the 2°Cy5 bind to the cells, but the FITC-B-domain is unable to bind to the

Fig. 23: **Results of the FITC-B-domain neuroblastoma cell double-labeling experiment.**
The protein complex used in this experiment was the $GABA_C$ Ab-*N*14, FITC-B-domain and 2°Cy5. Left panels (A, C and E) depict the fluorescence due to the 2°Cy5; right panels (B, D and F) are the fluorescence results due to the FITC-B-domain. Panels A and B: positive controls that contained the $GABA_C$ Ab-*N*14 and the 2°Cy5. Panels C and D: samples containing the $GABA_C$ Ab-*N*14: FITC-B-domain: 2°Cy5. Panels E and F: negative controls which contain only the 2°Cy5.

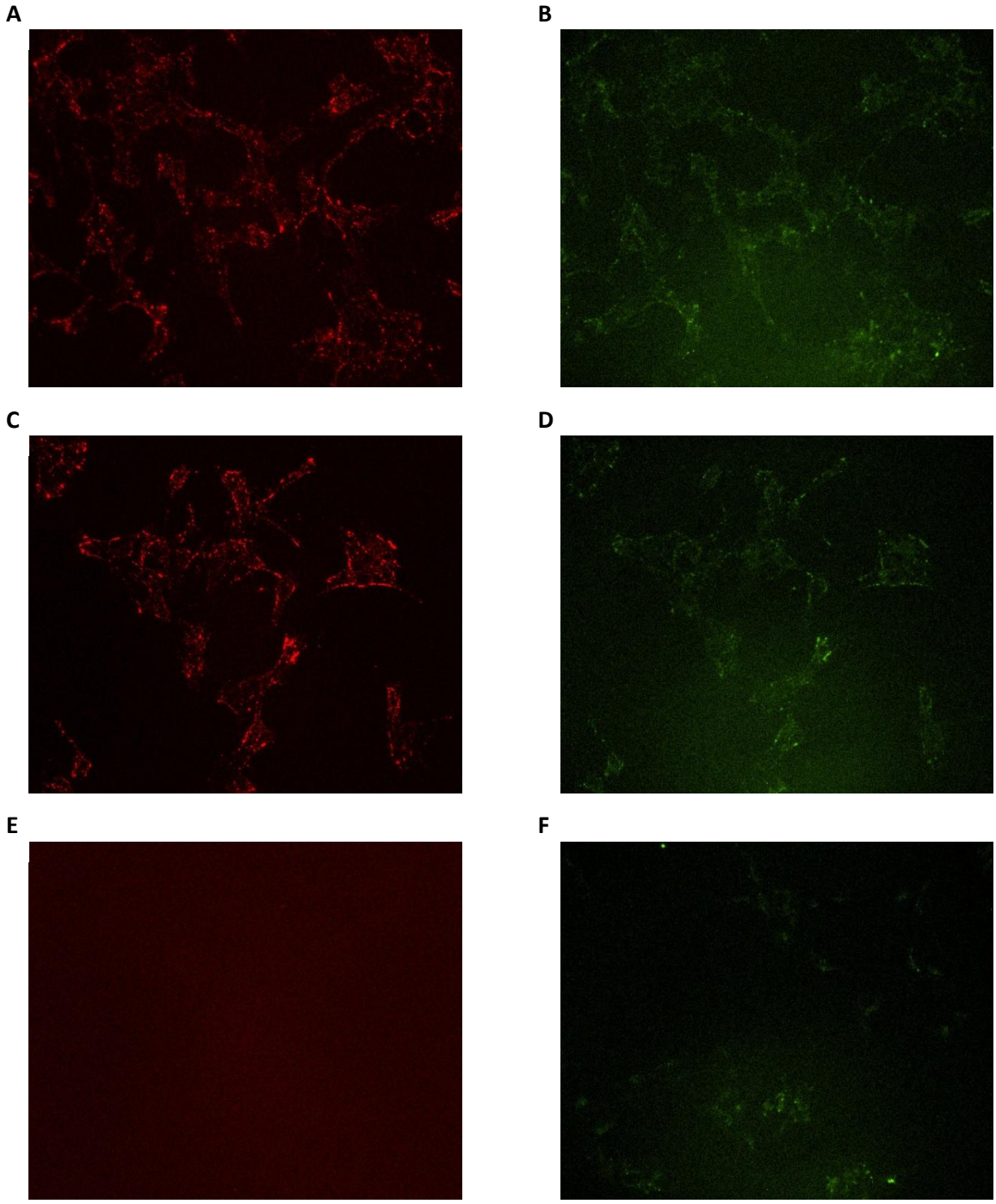
A
B
C
D
E
F

$GABA_C$ Ab-*N*14. This result is consistent with the result from the Ni^{2+}-bead experiment where the $GABA_C$ Ab-*N*14 and the FITC-B-domain are unable to bind to each other.

To summarize these experiments, we do not see evidence of the binding of the $GABA_C$ Ab-*N*14 to the FITC-B-domain either on the Ni^{2+}-beads or on the neuroblastoma cells. In the bead preparation, this is in contrast to results of previous experiments, where we have demonstrated the binding of the $GABA_C$ Ab-*N*14 bound to the non-FITC-labeled B-domain that is attached through the his-tag to the Ni^{2+}-beads (see above, Sec. 4.3.1). This result seems to indicate that the presence of multiple copies of FITC molecules on the B-domain might be sterically hindering or completely blocking the binding of the $GABA_C$ Ab-*N*14 to the B-domain and subsequent binding of the complex onto the beads.

This conclusion is further evidenced in the neuroblastoma cell experiments, where the binding of the FITC-B-domain to the $GABA_C$ Ab-*N*14 that bound to the $GABA_C$ receptors on the cells does not yield any desired fluorescence in the FITC region. The fact that we can see fluorescence due to the 2°Cy5 confirms that the $GABA_C$ Ab-*N*14 is bound to the $GABA_C$ receptors on the neuroblastoma cells. These two experimental results seem to indicate that the FITC-B-domain does not bind to the $GABA_C$ Ab-*N*14.

One important aspect of the Ni^{2+}-beads protein complex experiments is the desirability to obtain quantitative information about the molar concentration of the his6-tagged B-domain that attaches to the population of beads, or the molar concentration of the B-domain present on a single bead. Using the FITC-B-domain, we were able to obtain the molar concentration of B-domain present on a single Ni^{2+}-bead.

In this experiment, the population of beads (10 µl bead solution) were first treated with the fixed concentration of FITC-B-domain that has been used in the previous experiments (62.5 nM). This fluorescence of the starting concentration was measured in a plate reader (TECAN). After the 4-hour incubation at room temperature, the solution containing the FITC-B-domain was collected prior to the washing of the beads. The fluorescence of the supernatant was then measured post-incubation. The fluorescence measurement obtained post-incubation was approximately half of that obtained pre-incubation. This indicates that only half of the FITC-B-domain presented to the population of beads actually bound to the beads. Thus, 31.1 nM of the FITC-B-domain was able to bind to the beads.

However, in a typical experiment, the beads go through a series of washes (4-6 washes per experiment). During the washes, there could be a loss of beads, or tiny loss of the attached protein complex from the beads. The objective here was to determine the amount of protein present on the population of beads, after the beads go through a series of steps and washes, thus simulating the conditions of a typical bead-protein binding experiment. Thus, after the FITC-B-domain treatment, the beads were then washed three times, then treated with the $GABA_C$ Ab-*N*14, washed three times again, and then treated with the 2°Cy5. Thus, the beads went through the same sequence of steps as in the visualization experiments. After the 2°Cy5 treatment, the beads were treated with 500 mM imidazole, to allow the removal of the complex from the beads. This imidazole wash was collected and analyzed in the TECAN for the FITC fluorescence. The fluorescence measurement obtained was ~ 1/3 of the post-FITC-B-domain-incubation measurement done at the beginning of the experiment (~1/3 of 31.1 nM, i.e. ~10 nM). Thus, we were able to elute 10 nM of the protein complex from the Ni^{2+}-beads

at the end of the experiment. Assuming that all of the protein complex is eluted from the beads, we can say that there is 10.1 nm present on the population of beads at the end of the experiment. We then counted the number of beads present in 10 µl of bead solution. There are ~ 4 x 10^6 beads in 10 µl of bead solution. So according to the calculations, there is ~ 2.5 x 10^{-15} M protein per bead or 2.5 x 10^{-18} moles of the protein complex per bead. Using Avogadro's constant, there are 1.5 x 10^6 molecules of FITC-B-domain per Ni^{2+}-bead. This number looks favorable in comparison to the number of receptors present on the surface of a single cell (in the range of 10^5 – 10^6). Thus the number of copies of the protein complex compared favorably with the number of receptors per cell. With the current individual protein binding efficiency of a single bead, we should be able to stimulate enough $GABA_C$ receptors to see a substantial electric signal in electrophysiology experiments

4.4 Testing binding of the protein complex to mouse isolated retinal slices (slice-protein complex experiments)

In previous experiments, we were unable to demonstrate the binding of NNP protein structures to $GABA_C$ receptors expressing neuroblastoma cells (Sec. 4.3.2, 4.3.3, 4.3.4). An important objective of this project was to test the binding of the NNP based protein complexes on target native extracellular membrane receptors in the retina. The receptors being targeted in the current study are the $GABA_A$ and the $GABA_C$ receptors. For the $GABA_C$ receptors, two representative cell systems are being used; a $GABA_C$ receptor expressing neuroblastoma mammalian cell system and a $GABA_C$ receptor expressing xenopus oocyte system (being used by our colleagues in the lab).

In experiments utilizing the protein complex containing both, the $GABA_C$ Ab-*N*14 and B-domain performed on $GABA_C$ receptor expressing neuroblastoma cells, we were unable to demonstrate binding of the protein complex to the receptors, in either visualization or electrophysiology studies. However, our colleagues have been able to demonstrate binding of the above-mentioned protein complex to $GABA_C$-expressing oocytes in visualization studies. The binding of the protein complex has also been confirmed in oocytes expressing the $GABA_A$ receptors. In this case, a commercially available $GABA_A$-Ab has been used in conjunction with the B-domain. However, we currently do not have a stable neuroblastoma cell-like mammalian cell line that can express the $GABA_A$ receptors. So it was not possible to test the binding of the protein complex containing the $GABA_A$-Ab and the B-domain in the neuroblastoma cells.

The main objective of this experiments briefly described in this section, was to be able to bind NNPs to target extracellular membrane receptors in the retina (Fig. 24). In the following experiments, we have used mouse retinal slices as a test system. Such a system is a highly physiologically relevant and, as compared with previously used systems (neuroblastoma cells, oocytes), has a close correspondence with the ultimate target of the therapeutic device being developed in the project. If the binding of the protein complex to the $GABA_A$ receptors could be confirmed on a retinal slice preparation, it would be an important step that demonstrates the workability of a protein complex containing the $GABA_A$-Ab and B-domain.

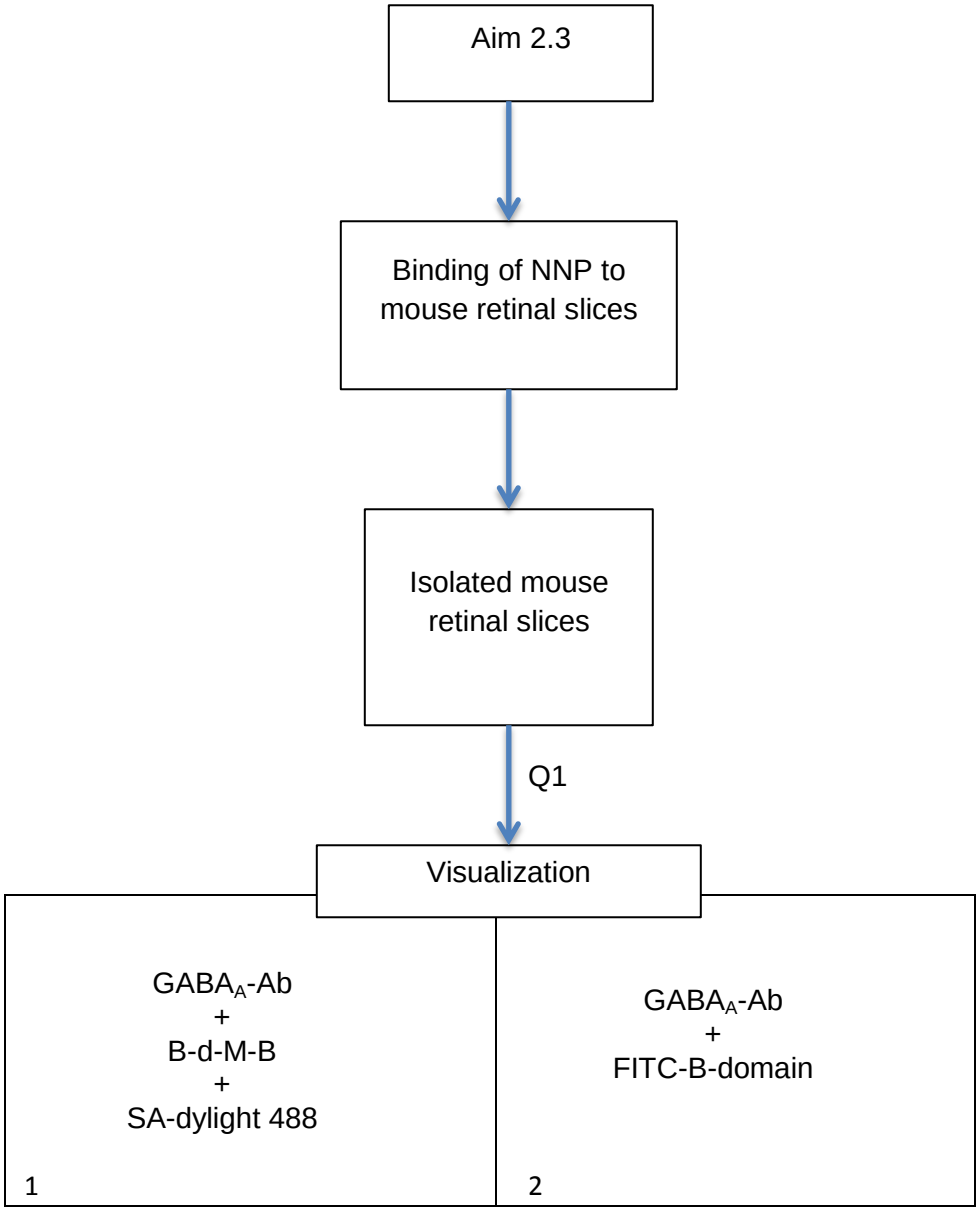

Fig. 24: Description of Aim 2.3
This flowchart describes Aim 2.3 of the NNP project. The question addressed in Aim 2.3 is Q1: To test the binding of the GABA$_A$-Ab and B-domain (two variations; B-d-M-B and FITC-B-domain) on isolated retinal slices on native GABA$_A$-Ab receptors on the retina.

In experiments conducted on the retinal slices, the $GABA_A$-Ab and a 2°FITC specific to the $GABA_A$-Ab were used. This preparation has been tested previously (experiments not described in the thesis) and shows excellent fluorescence. Two preparations of the B-domain were tested; the B-d-M-B with the SA-dylight 488 (Fig. 24 – box 1) and the FITC-B-domain (Fig. 24 – box 2). Thus the preparations used in this slice-protein complex experiment were: 1) Slice: $GABA_A$-Ab: 2°FITC (positive control), 2) Slice: $GABA_A$-Ab: B-d-M-B: SA-dylight 488, 3) Slice: $GABA_A$-Ab: FITC-B-domain, 4) Slice: B-d-M-B: SA-dylight 488 (negative control), 5) Slice: $GABA_A$-Ab: SA-dylight 488 (negative control), 6) Slice: FITC-B-domain (negative control).

The above-mentioned experiment was performed twice. In the first instance, the positive control showed good fluorescence in the photoreceptor layer, outer plexiform layer (the layer containing dendrites of bipolar cells and horizontal cells) and the inner plexiform layer (axons of the bipolar cells, dendrites of ganglion cells). The sample (2) described above containing the $GABA_A$-Ab: B-d-M-B and SA-dylight 488 exhibited bright fluorescence in the same areas as the positive control mentioned above. The sample (3) containing the $GABA_A$-Ab and FITC-B-domain however displayed bright fluorescence in the inner nuclear layer (layer containing the cell bodies of bipolar, horizontal and amacrine cells) and the ganglion cell layer (layer containing the ganglion cell bodies). The negative controls were comparatively dark in all the layers of the retina.

Before repeating of the above experiment, new retinal slices were prepared. Prior to conducting the complete experiment, the new slices were tested in a control experiment in which only the positive control (1) described above was compared

between the two batches of slices. Both the slice batches displayed similar fluorescence in the positive control, thus confirming the workability of the new slice batch.

The above slice-protein complex experiment was repeated in exactly the same way as described above with the same samples and controls. However, as opposed to the earlier slice-protein complex experiment, the current experiment produced different results. In this experiment all the retinal slices, including the samples and the controls exhibited similar fluorescence, i.e., the negative controls tended to autofluoresce, i.e., as in the earlier experiment, the samples were not brighter than the controls. This was a surprising result, since the new batch of slides demonstrated good workability as shown in the control experiment and the current slice-protein complex experiment was performed in exactly the same way as described above. These differences in results could be attributed to a number of reasons, including a problem with the slices themselves; it is possible that the slicing procedure somehow affected the health of slices. However, we know that the control experiment with only the positive control worked well. Thus, it could be possible that the new slices might be working well with the preparation containing only the $GABA_A$-Ab and 2°FITC. However, with an extra step with the addition of B-d-M-B or FITC-B-domain is affected somehow due to the state or conformation of the receptors on the new batch of slices that prevents the B-d-M-B or FITC-B-domain from effectively binding to the $GABA_A$-Ab. Another problem could be with the B-domain preparations (repeated freezing and thawing of a tube that is more than 6 months old), or with a possible problem in the activity of the SA-Dylight 488 used. Troubleshooting the experiment would involve testing all of the above hypothesis in a

step-by-step procedure to arrive at a suitable conclusion on the differences seen in the two repeat experiments described above.

5. CONCLUSIONS AND DISCUSSION

The overall goal of our laboratory is the development of light-sensitive molecular structures that have specificity for $GABA_C$ and $GABA_A$ receptors and in response to light, are capable of modifying the activity of those receptors. As part of the broad research program of the lab, my role has been to assemble and test these molecular structures (specifically the anchor and scaffolding protein) in binding studies through visualization and electrophysiology experiments. Aim 2.1 of Part 2 of my thesis was the assembly and testing of the molecular structures *in-vitro*. With regard to Aim 2.1, we have shown that the protein complex consisting of the B-domain and the $GABA_C$ Ab-*N*14 can be formed in-vitro on Ni^{2+}-coated 96-well plates. A sub-aim of Aim 2.1 was to demonstrate the binding of the above-mentioned protein complex to $GABA_C$ receptor-expressing neuroblastoma cells. However, in our experiments, we did not find sufficient evidence that the protein complex was binding to the cells (Sections 4.1.2, 4.3.2, 4.3.3, 4.3.4). The two core components of the protein complex were the $GABA_C$ Ab-*N*14 and B-domain (by itself, or in the form of B-d-M-B, or FITC-B-domain). In all cases, through the positive control ($GABA_C$ Ab-*N*14 and a secondary fluorescent antibody), we confirmed the binding of the $GABA_C$ Ab-*N*14 to the $GABA_C$ receptors on the neuroblastoma cells. However, in none of the experiments described above, either in single- or double-labeling experiments, did we get any conclusive evidence that the B-domain (in its several forms) was attached to the $GABA_C$ Ab-*N*14 bound to the receptors on the cells. In previous experiments, our colleagues in the lab have demonstrated the binding of the $GABA_C$ Ab-*N*14 with the B-domain (in the *Xenopus* oocyte system and other studies in the lab). There are two possibilities that could explain the negative results. One could be that the binding of the $GABA_C$ Ab-*N*14 on the $GABA_C$ receptors on the neuroblastoma

cells is somehow suppressing the binding of the B-domain to the antibody, either through steric hindrance or the inaccessibility of the Fc region of the $GABA_C$ Ab-*N*14 (see Background) by the B-domain, when the antibody is bound to the neuroblastoma cells. The problems faced with the neuroblastoma cell system were a major hurdle that affected both Aim 2.1 and Aim 2.2 of this thesis project.

Aim 2.2 was to develop a probe delivery system that can deliver minute amounts of the protein complex to cells expressing the $GABA_C$-receptors. Due to significant hurdles (see Background) we used SA and Ni^{2+}-beads. Individual beads were attached to the tip of micro-pipettes and with the help of a micro-manipulator and positioned in close proximity to the cell surface. In experiments described in the results section (Sec. 4.2.2, 4.2.3,) we demonstrated the binding of a protein complex consisting of the $GABA_C$ Ab-*N*14, B-domain and a protein complex consisting of the 50:50 compound to the SA-beads. The 50:50 compound was especially interesting because it has several PEG3400 chains with terminating muscimol, which is a $GABA_C$ receptor agonist. In probe experiments, a population of SA-beads were functionalized with the 50:50 compound and a single bead held at the tip of the probe was presented to $GABA_C$-receptor expressing cells. Again, in this experiment, the result was inconclusive, because we saw several instance where there was a change in the amplitude of the GABA current post-bead application (after the bead touched the cell), and other instances in which there was no effect on the GABA current post-bead application. Again, there are two possibilities on why we are not seeing a robust response on bead application. The first possibility is that the number of terminating muscimol molecules present on a single bead are not enough to elicit a significant (above background) current from the cell. The

second possibility concerns the curvature of the bead surface that comes in contact with the cell surface. Since the beads are spheres, the surface area of bead that comes in contact with the cell surface is effectively much smaller than the overall surface area of the bead itself. Thus effectively, only a small patch of the bead surface is actually able to stimulate (assuming all the muscimols present in the contacted bead patch bind to all the receptors present under the patch of cell membrane being contacted) the cell membrane. One way to overcome these hurdles is to design or micro-machine a silicon probe with a concave tip surface that resembles the natural curvature of the cell. The dimension of the probe tip would be large enough to cover as large a cell area as possible, at the same time leaving room for the patch clamp electrode needed for recording currents.

In the experiments with the Ni^{2+}-beads, the aim was to stimulate cells with a protein complex that remains attached to the beads, similar to the SA-bead experiments, or to deposit the protein complex onto the neuroblastoma cells, by using imidazole to achieve dissociation of the protein complex from the beads. In the deposition type of experiments, the protein complex would have a fluorescence tag that would allow visualization of the protein complex on the cell. Two hurdles prevented us from performing these experiments. The first hurdle was the lack of evidence of the binding of the protein complex to the neuroblastoma cells (see results section). In all the above described experiments, we did not observe robust binding of the protein complex containing the $GABA_C$ Ab-*N*14 antibody and B-domain to the $GABA_C$ receptors expressed on the neuroblastoma cells. The main objective of the Ni^{2+}-bead based probe experiments was to attach the above mentioned protein complex having a fluorescence

tag to a population of Ni^{2+}-beads. The next step was to hold a single bead at the tip of a micropipette and then approach the cell using a micromanipulator. Once the bead is within touching distance above the cell, we would be adding a tiny amount of imidazole. This would release the protein complex from the bead (as evidenced from experiments in Sec. 4.3.1) and on the cell. The protein complex would then be allowed to incubate for a certain amount of time (~1 hr) on the cell. We would then look at the cell under a fluorescence microscope for evidence of binding. Based on the results described in Sec 4.3.2, 4.3.3, 4.3.4 there was a slim chance that we would see binding of the protein complex released from the bead on the neuroblastoma cell. Another hurdle we faced was in other experiments (not described in this study) in which the neuroblastoma cells were allowed to incubate in three concentrations of imidazole (100 mM, 250 nM and 500 mM) to test if a prolonged exposure to imidazole affects the health of the cells. In all experiments involving the Ni^{2+}-coated ELISA plates and the Ni^{2+}-beads, 500 mM of imidazole was used to detach the protein from the plates and beads. We observed that after 1 hour (which is the amount of time a protein complex would be incubated with the cells), at all the concentrations the cells were completely dead. For the 500 mM concentration cell dish, the cells were dead within 15 min, while it took longer for the other concentrations. But at the end of 1 hr, all the cells incubated in the three concentrations of imidazole were dead. These results precluded any bead-probe deposition experiments that were planned with the Ni^{2+}-beads.

As described previously, the NNPs are being developed as a novel therapy for restoring sight in the millions of people affected by photoreceptor degenerative diseases like AMD. AMD, which primarily targets the rod and cone photoreceptors of the retina

and leads to deterioration and dysfunction of these cells, is a leading cause of vision loss in senior citizens. As yet, there do not exist therapies that can substantially repair/restore vision lost in this disease. The overall aim of the project to which I contributed, is to bypass the blinding effect of photoreceptor degeneration in AMD by designing/constructing molecular structures that, in light-dependent fashion, can activate remaining healthy, non-photoreceptor nerve cells in the retina. The approach investigated in our project differed from an electronic approach being used by other investigators, in which remaining healthy retinal cells are stimulated by electrical pulses in light-dependent fashion (Bach *et al*., 2010, Loudin *et al*., 2007, Chow *et al*., 2004) or by expressing channelrhodopsins (a non-native, photosensitive ion channel) in retinal cells (Doroudchi *et al*., 2011, Berndt *et al*., 2011). We are currently using $GABA_C$ receptors as the model system for our study, and the work described in this project is focused on the development and testing of $GABA_C$-reactive anchoring complexes that will form a part of the desired overall NNP structure. In addition to advancing progress on the preparation and study of these anchoring components, the present thesis research will facilitate further studies in this area, include expansion of the relevant technologies to other types of postsynaptic membrane receptors. We anticipate that this future work will employ a similar strategy of using anchoring protein complexes of the types I researched for my thesis project. While the molecular/chemical approaches we are pursuing are at present at an early stage of development, we believe that this molecular approach is a logical and promising avenue that can potentially lead to repairing/restoring vision loss in AMD and related photoreceptor degenerative diseases.

An important objective of this project was the development of a microprobe system that will allow the focal delivery of minute quantities of the protein complex to target $GABA_C$ receptor expressing neuroblastoma cells. In addition to approaches described earlier in the Background section, including functionalized AFM tips (Allen *et al*., 2003; Zlatanova *et al*., 2000; Janshoff *et al*., 2000; Hugel and Seitz, 2001, Schmitt *et al*., 2000), Ni^{2+}/NTA functionalized silica surfaces (Kang *et al*, 2007) and functionalized carbon nanotubes (Liu *et al*., 2009), other approaches include a combined optical electrical approach (LeChasseur *et al*., 2011). In this approach, the investigators developed a dual-core fiberoptics-based microprobe that has an optical core for fluorescence visualization and an electrolyte-filled hollow core for extracellular patch-clamp recording. Other probe-like approaches include the Biacore system developed by GE Healthcare and Octet Red system developed by Fortebio. Both these systems use label-free detection techniques for studying biomolecular interactions. These systems use a cylindrical probe (~500-600 µm diameter) that can attach proteins and using an optical analysis technique, detect and measure protein-protein interactions. However, none of these systems are able to study, in real time, the effect of the biomolecular interaction between proteins and receptors present on cell surfaces under electrophysiological recording on live cells, in the way that we have envisioned in this project.

With the current hurdles being faced in the development of a microprobe delivery system, using a different approach, like micro-machining custom electrodes with a concave surface to increase the number of receptors being activated and thus elicit a measurable current, as described above is potentially an encouraging avenue. That,

along with perfecting techniques that enable functionalizing of raw silicon surfaces with SA or Ni^{2+}/ NTA to enable attachment of NNP components to the surfaces is an important step towards the development of a workable microprobe system. We anticipate that such a system, by enabling several types of electrophysiological and visualization studies of receptor-ligand interactions in this type of preparation will represent a significant engineering achievement and have high impact in the field of neuroscience/neural engineering. My thesis project thus has helped to lay the foundation for studying, at a highly focal level, physiologically relevant interactions of target surface receptors with active ligands and will also make important contributions towards the overall lab program by facilitating development of NNP structures and nanoscale actuation devices as possible future therapies for photoreceptor degenerative diseases.

6. REFERENCES

1. Albrecht, B.E., Breitenbach, U., Stühmer, T., Harvey, R.J., Darlison, M.G. (1997). In situ hybridization and reverse transcription--polymerase chain reaction studies on the expression of the $GABA_C$ receptor rho1- and rho2-subunit genes in avian and rat brain. *Eur J Neurosci* **9**: 2414-22.
2. Allen, S., Rigby-Singleton, S.M., Harris, H., Davies, M.C., O'Shea, P. (2003). Measuring and visualizing single molecular interactions in biology. *Biochem Soc Trans*. **31**: 1052-7.
3. Amin, J. & Weiss, D.S. (1996). Insights into the activation mechanism of rho1 GABA receptors obtained by coexpression of wild type and activation-impaired subunits. *Proc Biol Sci* **263**: 273-82.
4. Arenkiel, B.R., Peca, J., Davison, I.G., Feliciano, C., Deisseroth, K., Augustine, G.J., Ehlers, M.D., Feng, G. (2007). In vivo light-induced activation of neural circuitry in transgenic mice expressing channelrhodopsin-2. *Neuron*. **54(2)**: 205
5. Bach, M., Wilke, M., Wilhelm, B., Zrenner, E., Wilke, R. (2010). Basic quantitative assessment of visual performance in patients with very low vision. *Invest Ophthalmol Vis Sci.* **51(2)**: 1255-60.
6. Bain, C.D. & Whitesides, G.M. (1988). Molecular-Level Control over Surface Order in Self-Assembled Monolayer Films of Thiols on Gold. *Science*. **240**: 62-63.
7. Banghart, M., Borges, K., Isacoff, E., Trauner, D., Kramer, R.H. (2004). Light-activated ion channels for remote control of neuronal firing. *Nat Neurosci*. **12**: 1381-6

8. Berndt, A., Schoenenberger, P., Mattis, J., Tye, K.M., Deisseroth, K., Hegemann, P., Oertner, T.G. (2011). High-efficiency channelrhodopsins for fast neuronal stimulation at low light levels. *Proc Natl Acad Sci U S A.* **108(18)**: 7595-600.
9. Berndt, A., Yizhar, O., Gunaydin, L.A., Hegemann, P., Deisseroth, K. (2009). Bi-stable neural state switches. *Nat Neurosci*. **2**: 229-34
10. Boyle, M.D.P. & Reis, K.J. (1987). Bacterial Fc Receptors. *BioTechnology* **5**: 697-703
11. Braisted, A.C. & Wells, J.A. (1996). Minimizing a binding domain from protein A. *Proc Natl Acad Sci U S A* **93**: 5688-92.
12. Cahalan, M. & Neher, E. (1992). Patch clamp technique; an overview. *Methods Enzymol*. **207**: 3-14.
13. Chow, A.Y., Chow, V.Y., Packo, K.H., Pollack, J.S., Peyman, G.A., Schuchard, R. (2004). The artificial silicon retina microchip for the treatment of vision loss from retinitis pigmentosa. *Arch Ophthalmol.* **122(4)**: 460
14. Dong, C.J., Picaud, S.A., Werblin, F.S. (1994). GABA transporters and $GABA_C$-like receptors on catfish cone- but not rod-driven horizontal cells. *J Neurosci* **14**: 2648-58.
15. Doroudchi, M.M., Greenberg, K.P., Liu, J., Silka, K.A., Boyden, E.S., Lockridge, J.A., Arman, A.C., Janani, R., Boye, S.E., Boye, S.L., Gordon, G.M., Matteo, B.C., Sampath, A.P., Hauswirth, W.W., Horsager, A. (2011). Virally delivered Channelrhodopsin-2 Safely and Effectively Restores Visual Function in Multiple Mouse Models of Blindness. *Mol Ther.* (Epub ahead of print)

16. Duan, C., Meyerhoff, M.E. (1994). Separation-free sandwich enzyme immunoassays using microporous gold electrodes and self-assembled monolayer/immobilized capture antibodies. *Anal Chem.* **66**: 1369-77
17. Enz, R. & Cutting, G.R. (1999). $GABA_C$ receptor rho subunits are heterogeneously expressed in the human CNS and form homo- and heterooligomers with distinct physical properties. *Eur J Neurosci* **11**: 41-50.
18. Fine, S. L., Berger, J.W., Maureen, G.M., Allen, C.H. (2000). Age-related macular degeneration. *Drug Therapy.* **342(7)**: 483-92.
19. Finlayson, P.G. & Iezzi, R. (2010). Glutamate stimulation of retinal ganglion cells in normal and s334ter-4 rat retinas: a candidate for a neurotransmitter-based retinal prosthesis. *Invest Ophthalmol Vis Sci.* **51(7)**: 3619-28.
20. Giessibl, G.J. (2003). Advances in atomic force microscopy. *Rev. Mod. Phys.* **75**: 949-983.
21. Gorostiza, P., Volgraf, M., Numano, R., Szobota, S., Trauner, D., Isacoff, E.Y. (2007). Mechanisms of photoswitch conjugation and light activation of an ionotropic glutamate receptor. *Proc Natl Acad Sci U S A*.**104**: 10865-70
22. Gorostiza, P. & Isacoff, E.Y. (2008). Nanoengineering ion channels for optical control. *Physiology (Bethesda).* **23**: 238-47
23. Gussin, H.A., Khasawneh, F.T., Xie, A., Qian, H., Le Brenton, G.C., Pepperberg, D.R. (2008). Characterization of a Novel Polyclonal Anti Human ρ1 $GABA_C$ Antibody. *Invest. Ophthalmol. Vis. Sci.* **49**: e-abstract 1288
24. Hamill, O.P., Marty, A., Neher, E., Sakmann, B., Sigworth, F.J. (1981). Improved patch-clamp techniques for high-resolution current recording from cells and cell-free membrane patches. *Pflugers Arch*. **391**: 85-100.

25. Hinterdorfer, P., Baumgartner, W., Gruber, H.J., Schilcher, K., Schindler, H. (1996). Detection and localization of individual antibody-antigen recognition events by atomic force microscopy. *Proc Natl Acad Sci U S A* **93**: 3477-81.

26. Hugel, T. & Seitz, M. (2001). The Study of Molecular Interactions by AFM Force Spectroscopy. *Macromol. Rapid Commun*. **22**: 989–1016.

27. Hughes, T.E., Carey, R.G., Vitorica, J., de Blas, A.L., Karten, H.J. (1989) Immunohistochemical localization of $GABA_A$ receptors in the retina of the new world primate Saimiri sciureus. *Vis. Neurosci.* **2(6)**: 565-81

28. Hughes, T.E., Grunert, U., Karten, H.J. (1991). $GABA_A$ receptors in the retina of the cat: an immunohistochemical study of wholemounts, sectons, and dissociated cells. *Vis. Neurosci*. **6(3)**: 229-38

29. Humayun, M.S., Dorn, J.D., Ahuja, A.K., Caspi, A., Filley, E., Dagnelie, G., Salzmann, J., Santos, A., Duncan, J., daCruz, L., Mohand-Said, S., Eliott, D., McMahon, M.J., Greenberg, R.J. (2009). Preliminary 6 month results from the Argus II epiretinal prosthesis feasibility study. *Conf Proc IEEE Eng Med Biol Soc*. **2009**: 4566-8

30. Humayun, M.S., de Juan, E. Jr, Dagnelie, G., Greenberg, R.J., Propst, R.H., Phillips, D.H. (1996). Visual perception elicited by electrical stimulation of retina in blind humans. *Arch Ophthalmol* **114(1)**; 40-6.

31. Janshoff, A., Neitzert, M., Oberdörfer, Y., Fuchs, H. (2000). Force Spectroscopy of Molecular Systems-Single Molecule Spectroscopy of Polymers and Biomolecules. *Angew Chem Int Ed Engl.* **39**: 3212-3237

32. Jurkat-Rott, K. & Lehmann-Horn, F. (2004). The patch clamp technique in ion channel research. *Curr Pharm Biotechnol.* **5**: 387-95

33. Kaneda, M., Mochizuki, M., Aoki, K., Kaneko, A. (1997). Modulation of GABAC response by Ca^{2+} and other divalent cations in horizontal cells of the catfish retina. *J Gen Physiol.* **110**: 741-7.

34. Kang, E., Park, J.W., McClellan, S.J., Kim, J.M., Holland, D.P., Lee, G.U., Franses, E.I., Park, K., Thompson, D.H. (2007). Specific adsorption of histidine-tagged proteins on silica surfaces modified with Ni^{2+}/NTA-derivatized poly(ethylene glycol). *Langmuir* **23**: 6281-8.

35. Kim, H., Kang, D.Y., Goh, H.J., Oh, B.K., Singh, R.P., Oh, S.M., Choi, J.W. (2008). Analysis of direct immobilized recombinant protein G on a gold surface. *Ultramicroscopy.* **108**: 1152-6.

36. Lagali, P.S., Balya, D., Awatramani, G.B., Münch, T.A., Kim, D.S., Busskamp, V., Cepko, C.L., Roska, B. (2008). Light-activated channels targeted to ON bipolar cells restore visual function in retinal degeneration. *Nat Neurosci.* **11**: 667-75

37. LeChasseur, Y., Dufour, S., Lavertu, G., Bories, C., Deschênes, M., Vallée, R., De Koninck, Y. (2011). A microprobe for parallel optical and electrical recordings from single neurons in vivo. *Nat Methods*. **8(4)**: 319-25

38. Liu, Y., Li, Y., Wu, Z.Q., Yan, X.P. (2009). Fabrication and characterization of hexahistidine-tagged protein functionalized multi-walled carbon nanotubes for selective solid-phase extraction of Cu^{2+} and Ni^{2+}. Talanta; **79(5)**: 1464-7

39. Loudin, J.D., Simanovskii, D.M., Vijayraghavan, K., Sramek, C.K., Butterwick, A.F., Huie, P., McLean, G.Y., Palanker, D.V. (2007). Optoelectronic retinal prosthesis: system design and performance. *Journal of Neural Engineering* **4:** S72—S84.

40. Lukasiewicz, P.D. (2005). Synaptic mechanisms that shape visual signaling at the inner retina. *Prog Brain Res* **147**: 205-18.

41. MacLaren, R.E., Pearson, R.A., MacNeil, A., Douglas, R.H., Salt, T.E., Akimoto, M., Swaroop, A., Sowden, J.C., Ali, R.R. (2006). Retinal repair by transplantation of photoreceptor precursors. *Nature*. **444**: 203-7

42. McKernan, R.M. and Whiting, P. J. (1996). Which $GABA_A$-receptor subtypes really occur in the brain. *Trends Neurosci*. **19**: 139-143

43. Nagel, G., Szellas, T., Huhn, W., Kateriya, S., Adeishvili, N., Berthold, P., Ollig, D., Hegemann, P., Bamberg, E. (2003). Channelrhodopsin-2, a directly light-gated cation-selective membrane channel. *Proc Natl Acad Sci U S A*. **100**: 13940-5

44. Neher, E. & Sakmann, B. (1976). Single-channel currents recorded from membrane of denervated frog muscle fibres. *Nature*. **260**: 799-802

45. Nilsson, B., Moks, T., Jansson, B., Abrahmsén, L., Elmblad, A., Holmgren, E., Henrichson, C., Jones, T.A., Uhlén, M. (1987). A synthetic IgG-binding domain based on staphylococcal protein A. *Protein Eng* **1**: 107-13.

46. Nord, K., Gunneriusson, E., Ringdahl, J., Ståhl, S., Uhlén, M., Nygren, P.A. (1997). Binding proteins selected from combinatorial libraries of an alpha-helical bacterial receptor domain. *Nat Biotechnol* **15**: 772-7.

47. Noy, A., Frisbie, C.D., Rozsnyai, L.F., Wrighton, M.S., Lieber, C.M. (1995). Chemical Force Microscopy: Exploiting Chemically-Modified Tips To Quantify Adhesion, Friction, and Functional Group Distributions in Molecular Assemblies. *J. Am. Chem. Soc*. **117**: 7943–7951.

48. Noy, A., Sanders, C.H., Vezenov, D.V., Wong, S.S., Lieber, C.M. (1998). Chemically-Sensitive Imaging in Tapping Mode by Chemical Force Microscopy: Relationship between Phase Lag and Adhesion. *Langmuir* 14: 1508–1511.

49. Nygren, P.A. & Skerra, A. (2004). Binding proteins from alternative scaffolds. *J Immunol Methods* 290: 3-28.

50. Palanker D., Vankov, A., Huie, P., Baccus., S. (2005). Design of a high-resolution optoelectronic retinal prosthesis. *J. Neural Engg*. **2**: S105-S120

51. Picaud, S., Pattnaik, B., Hicks, D., Forster, V., Fontaine, V., Sahel, J., Dreyfus, H. (1998). $GABA_A$ and GABAC receptors in adult porcine cones: evidence from a photoreceptor-glia co-culture model. *J Physiol* **513**: 33-42.

52. Qian, H. & Dowling, J.E. (1993). Novel GABA responses from rod-driven retinal horizontal cells. *Nature* **361**: 162-4.

53. Qian, H. & Dowling. J.E. (1995). $GABA_A$ and $GABA_C$ receptors on hybrid bass retinal bipolar cells. *J Neurophysiol* **74**: 1920-8.

54. Qian, H., Li, L., Chappell, R.L., Ripps, H. (1997). GABA receptors of bipolar cells from the skate retina: actions of zinc on GABA-mediated membrane currents. *J Neurophysio*l **78**: 2402-12.

55. Rizzo, J.F. 3rd, Wyatt, J., Loewenstein, J., Kelly, S., Shire, D. (2003). Perceptual efficacy of electrical stimulation of human retina with a microelectrode array during short-term surgical trials. *Invest Ophthalmol Vis Sci.* **44(12)**: 5362-9.

56. Schmitt, L., Ludwig, M., Gaub, H.E., Tampé, R. (2000). A metal-chelating microscopy tip as a new toolbox for single-molecule experiments by atomic force microscopy. *Biophys J.* **78**: 3275-85.

57. Sivilotti, L. & Nistri, A. (1991). GABA receptor mechanisms in the central nervous system. *Prog Neurobiol*. **36**: 35-92.

58. Szobota, S., Gorostiza, P., Del Bene, F., Wyart, C., Fortin, D.L., Kolstad, K.D., Tulyathan, O., Volgraf, M., Numano, R., Aaron, H.L., Scott, E.K., Kramer, R.H., Flannery, J., Baier, H., Trauner, D., Isacoff, E.Y. (2007). Remote control of neuronal activity with a light-gated glutamate receptor. *Neuron*. **54**: 535-45.

59. Uhlén, M., Forsberg, G., Moks, T., Hartmanis, M., Nilsson, B. (1992). Fusion proteins in biotechnology. *Curr Opin Biotechnol* **3**: 363-9.

60. Van der Vegte, E.W. & Hadziioannou, G. (1997). Scanning Force Microscopy with Chemical Specificity: An Extensive Study of Chemically Specific Tip−Surface Interactions and the Chemical Imaging of Surface Functional Groups. *Langmuir* **13**: 4357–4368.

61. Vardi, N. and Sterling, P. (1994). Subcellular localization of GABAA receptor in bipolar cells in macaque and human retina. *Vision Res*. **34(10)**: 1235-46

62. Volgraf, M., Gorostiza, P., Numano, R., Kramer, R.H., Isacoff, E.Y., Trauner, D. (2006). Allosteric control of an ionotropic glutamate receptor with an optical switch. *Nat Chem Biol.* **2**: 47-52.

63. Wang, H., Peca, J., Matsuzaki, M., Matsuzaki, K., Noguchi, J., Qiu, .L, Wang, D., Zhang, F., Boyden, E., Deisseroth, K., Kasai, H., Hall, W.C., Feng, G., Augustine, G.J. (2007). High-speed mapping of synaptic connectivity using photostimulation in Channelrhodopsin-2 transgenic mice. *Proc Natl Acad Sci U S A.* **104(19)**: 8143-8.

64. Wong, K.Y. & Dowling, J.E. (2005). Retinal bipolar cell input mechanisms in giant danio. III. ON-OFF bipolar cells and their color-opponent mechanisms. *J Biol Rhythms* **22**: 400-10.

65. Wong, S.S., Joselevich, E., Woolley, A.T., Cheung, C.L., Lieber, C.M. (1998). Covalently functionalized nanotubes as nanometre-sized probes in chemistry and biology. *Nature* **394**: 52-5

66. Young, B.A. and Chu, D. (1990). Distribution of $GABA_A$ and $GABA_B$ receptors in the mammalian brain. *Drug Dev. Res.* **21**: 161-167

67. Zarbin, M.A. (2004). Current concepts in the pathogenesis of age-related macular degeneration. *Arch Ophthalmol Soc.* **122(4)**: 598-614

68. Zhao, S., Cunha, C., Zhang, F., Liu, Q., Gloss, B., Deisseroth, K., Augustine, G.J., Feng, G. (2008). Improved expression of halorhodopsin for light-induced silencing of neuronal activity. *Brain Cell Biol.* **36**: 141-54

69. Zhang, J. & Slaughter, M.M. (1995). Preferential suppression of the ON pathway by $GABA_C$ receptors in the amphibian retina. *J Neurophysiol* **74**: 1583-92.

70. Zlatanova, J., Lindsay, S.M., Leuba, S.H. (2000). Single molecule force spectroscopy in biology using the atomic force microscope. *Prog Biophys Mol Biol*. **74**: 37-61

VITA

Ambarish S. Pawar

Education:
University of Illinois at Chicago
Ph.D in Bioengineering, 2011

University of Illinois at Chicago
Masters in Bioengineering, 2005

University of Mumbai, India
Bachelors in Instrumentation Engineering, 2003

Grants and other Academic Honors/Awards

- Deiss Provost Award received in 2010 from the UIC graduate college that recognizes outstanding graduate researchers.
- Research Project Grant received in 2009 from the Illinois Society for Prevention of Blindness (ISPB). This grant supported the purchase of supplies required for my research.
- Student stipend award received in 2009 from the Midwest Eye Banks. This award supported my annual stipend as a Graduate research assistant.
- Grant-in-Aid of Research received in 2005 from Sigma Xi, a national scientific society.
- Travel Grants received in 2006 and 2007 from the UIC Graduate College and the UIC Graduate Students Council. These grants supported travel to the 2006 and 2007 Annual Meetings of the Association for research in Vision and Ophthalmology (ARVO)
- Recommended by the Department of Education of the University of Mumbai for National Merit Scholarship (1997)

Publications:

- Roitberg B.Z., Mangubat E., Sugaya K., Thulborne K., Ramaswamy S., Evans M., Pawar A., Konecny T., Kordower J.H., Emborg M.E. Pilot study of transplantation of human neural stem cells (hNSCs) neurospheres into a non human primate model of stroke. J. Neurosurg. 2006 Jul; 105(1): 96-102
- Pawar A. S., Qtaishat N. M., Little D. M., Pepperberg D. R., Recovery of Rod Photoresponses in ABCR-Deficient Mice. Invest. Ophthalmol. Vis. Sci. 2008 49: 2743-2755.

Abstracts:

- Roitberg B.Z., Mangubat E., Sugaya K., Thulborne K., Ramaswamy S., Evans M., Pawar A., Konecny T., Kordower J.H., Emborg M.E. Pilot study of transplantation of human neural stem cells (hNSCs) neurospheres into a non human primate model of stroke. 11th Annual Meeting of the American Society for Neurotransplantation and Repair, Clearwater, Fl. Exp. Neurol. 187: 217.
- Evans M., Pawar A., Chen E-Y., Kordower J.H., Emborg M.E. Administration of MPTP to GFAP-knock out mice. Annual Meeting of the Society for Neuroscience, 2004, San Diego, CA.

- Pawar A. S., Qtaishat N. M., Pepperberg D.R. Photoreceptor Recovery in abcr-/- and Wildtype Mice Following Weak Bleaching of Rhodopsin. Invest. Ophthalmol. Vis. Sci. 2006 47: E-Abstract 4736
- Pawar A. S., Qtaishat N. M., Pepperberg D. R., Initial Recovery Kinetics of Post-Bleach Photoreceptor Responses in abcr-/- Mice. Invest. Ophthalmol. Vis. Sci. 2007 48: E-Abstract 608.
- Koduvayur S.P., Memic A., Kierny M., Gussin H. A., Feng F., Pawar A. S., Pepperberg D.R., Kay B.K. Selection and characterization of affinity reagents for GABA receptors in the retina. 5th ESF/ Affinomics Workshop of Affinity Proteomics, Alpbach, Austria, March 14-16, 2011.

Characterization and Development of potential molecular therapies for retinal photoreceptor disease.

Ambarish S. Pawar, M.S.
Department of Bioengineering
University of Illinois at Chicago
Chicago, Illinois (2011)

Dissertation Chairperson: David R. Pepperberg

The overall goal of this project is twofold; understanding the pathology of photoreceptor disease, and development of novel molecular therapies for treatment of retinal photoreceptor disease.

Part I of my thesis project has involved study of dark-adaptation in a mouse strain lacking the photoreceptor protein known as ABCR protein (*abcr-/-* mouse). The ABCR protein is present along the periphery of rod outer segment discs in the retinal rod photoreceptors and plays an important role in dark-adaptation. Impairment in the activity of the ABCR protein has been associated with Stargardt disease in humans. A 1999 study by Weng *et al*. observed significantly slower recovery of the ERG a-wave amplitude in *abcr-/-* mice as compared to wildtype mice, indicating slowed dark-adaptation in the *abcr-/-* mice following ~45% rhodopsin bleaching. In our study, where we compared dark-adaptation between the *abcr-/-* and wildtype mice at much lower bleach levels, we observed a significantly *faster* dark-adaptation in the *abcr-/-* mice as compared to wildtype, a result different from the Weng *et al.* (1999) finding. Based on this result, we hypothesized that the primary physiological role of the ABCR protein is to promote clearance, from the disc, of *minute, residual amounts* of all-*trans* retinal, a rhodopsin bleaching product, that other mechanisms, such as thermal diffusion across the disc membrane, cannot achieve.

Photoreceptor degenerative diseases such as age-related macular degeneration (AMD) lead to the loss of functional photoreceptors, and subsequently the loss of vision. However, other cells types in the retina are believed in many cases to remain intact and functional despite the loss of the photoreceptors. Part II of my thesis concerns development of molecular structures that are responsive to light and can interface with postsynaptic membrane receptors of specific types of remaining healthy retinal cells, to “bypass” the degenerated native photoreceptors and restore vision in patients affected by AMD. Through electrophysiology and visualization experiments, we have demonstrated the binding of individual components of the molecular structures *in vitro*. We have also developed a novel functionalized microprobe delivery system that can focally and efficiently deliver candidate test structures to receptors expressed on mammalian cells.